The Dissertation Committee for Inti Antonio Nicolas Sodemann Villadiego certifies that this is the approved version of the following dissertation:

The fractional quantum Hall regime in graphene

Committee:

Allan H. MacDonald, Supervisor

Sanjay Banerjee

Alexander A. Demkov

Gregory A. Fiete

Qian Niu

Emanuel Tutuc

Zhen Yao

The fractional quantum Hall regime in graphene

by

Inti Antonio Nicolas Sodemann Villadiego, B.PHY.; M.S.

DISSERTATION

Presented to the Faculty of the Graduate School of

The University of Texas at Austin

in Partial Fulfillment

of the Requirements

for the Degree of

DOCTOR OF PHILOSOPHY

THE UNIVERSITY OF TEXAS AT AUSTIN

August 2014

A mi familia.

Acknowledgments

I wish to thank several people for their support throughout my time in Texas.

I want to thank Allan. He has been a great mentor and a friend. Physicists as clever, dedicated, and with such kind touch to interact with others, as Allan are rare. I am extremely happy that life has given me a chance to come to Austin to learn from him.

It has been great to interact with many members in our Group, Department, and University: Yasufumi Araki, Rafi Bistritzer, Hua Chen, Ashley da Silva, Karin Everschor-Sitte, Gregory Fiete, Hsian-Hsuan Hung, Jeil Jung, Guru Khalsa, Xiao Li, Michael Marder, Maria Moura, Qian Niu, Matthias Sitte, Heidi Seinige, Daniel Tennant, Dagim Tilahun, John Tolsma, James Wang-Kong Tse, Ming Xie, and Fan Zhang. I wish to specially thank Dima Pesin, Rohit Hegde, Insun Jo, Juan Pedraza, Walter Tangarife and Fengcheng Wu, for numerous valuable discussions and interactions.

I want to thank my teachers in Austin: Professors Duane Dicus, Jacques Distler, Gregory Fiete, Austin Gleeson, Allan H. MacDonald, Qian Niu, Peter Riley, Lorenzo Sadun, E. C. George Sudarshan, and Steven Weinberg. I want to thank Professors Sanjay Banerjee, Alexander Demkov, Gregory Fiete, Qian Niu, Emanuel Tutuc, and Zhen Yao, for their assistance in these final steps

leading to graduation.

I would like to thank members of our Staff: Becky Drake, Matt Ervin, Annie Harding, and Michele Landfield, for their continued support and assistance.

An finally, I want to thank Ariette: my love and best friend.

The fractional quantum Hall regime in graphene

Publication No. _____

Inti Antonio Nicolas Sodemann Villadiego, Ph.D.
The University of Texas at Austin, 2014

Supervisor: Allan H. MacDonald

In the first part of this work, we describe a theory of the ground states and charge gaps in the fractional quantum Hall states of graphene. The theory relies on knowledge of these properties for filling fractions smaller than one. Then, by the application of two mapping rules, one is able to obtain these properties for fractional quantum Hall states at arbitrary fillings, by conceiving the quantum Hall ferromagnets as *vacua* on which correlated electrons or correlated holes are added. The predicted charge gaps and phase transitions between different fractional quantum Hall states are in good agreement with recent experiments.

In the second part, we investigate the low energy theory for the neutral Landau level of bilayer graphene. We closely analyze the way different terms in the Hamiltonian transform under the action of particle-hole conjugation symmetries, and identify several terms that are relevant in explaining the lack of such symmetry in experiments. Combining an accurate parametrization

of the electronic structure of bilayer graphene with a systematic account of the impact of screening we are able to explain the absence of particle-hole symmetry reported in recent experiments. We also study the energetics of fractional quantum Hall states with coherence between $n = 0$ and $n = 1$ cyclotron quantum numbers, and obtain a general formula to map the two-point correlation function from their well-known counterparts made from only $n = 0$ quantum numbers. Bilayer graphene has the potential for realizing these states which have no analogue in other two-dimensional electron systems such as Gallium Arsenide. We apply this formula to describe the properties of the $n = 0/n = 1$ coherent Laughlin state which displays nematic correlations.

Table of Contents

[1]This chapter is based on Ref. [68], all authors in this reference contributed equally to this work.

[2]This Appendix is based on Ref. [68], all authors in this reference contributed equally to this work.

List of Figures

Chapter 1

Introduction

In this document I will describe theories of the quantum Hall regime in monolayer and bilayer graphene and their connection to experiments. Chapters 2 and 3 elaborate and expand the results described in this publication [68].

Chapter 2 attempts to present a general theory for multicomponent fractional quantum Hall states without explicit connection to any particular material system, but relying chiefly on the general assumption that the incompressible liquids are ground states of a repulsive interaction with a strong hard-core or on-site energy cost. The fermions making up the liquid are conceived as having some internal degrees of freedom and their interaction to be invariant under global unitary transformations of these internal flavors. In addition we could have some weak symmetry breaking terms. The purpose of this general construction is to provide a theory that could cover systems, other than monalyer graphene, that would share these characteristics.

Chapter 3 follows closely Ref. [68] and applies the theory described in Chapter 2 to the specific case of monolayer graphene. In particular, we provide a series of direct comparisons with the beautiful measurements performed in these works [20, 21], which have been a source of motivation and inspiration

for our work.

In chapter 4 we discuss the construction of low energy theories for bilayer graphene. The landscape of experimental observations that has been reported so far is quite rich [5, 39, 40, 44, 49]. We focus on understanding one specific aspect: the absence of particle-hole symmetry reported in Ref. [40]. We first underscore that particle-hole symmetry is expected in the convetional models of bilayer graphene and that it cannot be destroyed simply by the presence of a magnetic field. We then make use of recent density-functional theory estimations of the explicit particle-hole symmetry breaking terms in the Hamiltonian to predict the charge gaps at integer fillings. We will find that accounting for screening is crucial in understanding the absence of particle-hole symmetry in Ref. [40]. The reason is that the terms that attempt to restore particle-hole symmetry arise from exchange interactions with the negative energy sea. However, the substantial screening of Coulomb interactions in bilayer graphene reduce these terms in comparison to the explicit single-particle terms that break this symmetry. As a consequence the system behaves as if the symmetry is explicitly broken.

Finally in chapter 5 we put aside the details of the microscopic Hamiltonian to investigate a novel possibility offered by bilayer graphene: FQH states with coherence between the $n = 0$ and $n = 1$ cyclotron quantum numbers. This possibility arises from their near degeneracy in the neutral Landau level. These states are interesting because in addition to its quantum Hall characteristics they display ferroelectric and nematic behavior.

I have not included an introduction to the general physics of the quantum Hall effect. Many excellent reviews and textbooks cover this subject. A wonderful introduction that help me much in learning the subject is the one written by Allan [46]. Very insightful discussions are also provided in the different chapters of this early book [27].

I have not included thorough descriptions of monolayer and bilayer graphene either but have included brief mentions of the specific properties that are relevant for our purposes. This review article [10] provides a comprehensive introduction to various aspects of graphene.

Chapter 2

SU(N) fractional quantum Hall states

The fractional quantum Hall effect (FQHE) is a transport anomaly that occurs whenever a two-dimensional electron system (2DES) in a strong perpendicular magnetic field has a gap for charged excitations at a fractional value of the Landau level (LL) filling factor. Gaps at fractional filling factors can only be produced by electron-electron interactions. The FQHE has therefore been a rich playground for the study of strongly correlated phases of the electron liquid, hosting a variety of exotic phenomena including fractional and non-Abelian quasiparticle statistics [54] and electron-hole pair superfluidity [18].

The integer and fractional quantum Hall effects differ in a manner analogous to that in which a paramagnet in a magnetic field differs from a ferromagnet. In the former the order is *imprinted* by an external field which polarizes the spin of the electrons, whereas in the second the order arises "spontaneously" from interactions. In the integer Hall phases the order is *imprinted* by the external field coupling to the orbital motion of the electrons, whereas in the fractional quantum Hall phase the order is "spontaneously" arising from the interactions. The external magnetic field is not a sufficient cause for the

fractional quantum Hall order. The latter is evident from the fact Wigner crystal type states instead of fractional quantum Hall liquids are also possible in strong magnetic fields.

However, integer quantum Hall phases can also arise spontaneously as a consequence of interactions and are known as integer quantum Hall ferromagnets. They arise when different internal degrees of freedom are nearly degenerate in a single Landau level.

2.1 SU(N) fractional quantum Hall states

Let us imagine electrons whose orbital wavefunction is constrained to be in the Lowest Landau Level (LLL), but posses N internal discrete degrees of freedom or flavors, and let us imagine that their interactions are independent of such flavors. Their Hamiltonian is simply,

$$H = P_{LLL} \sum_{i<j} v(r_i - r_j) P_{LLL} = \frac{1}{2} \sum v(m_1, m_2; m_2', m_1') c^\dagger_{m_1,\sigma_1} c^\dagger_{m_2,\sigma_2} c_{m_2',\sigma_2} c_{m_1',\sigma_1}, \tag{2.1}$$

where m are intra-Landau level guiding center labels and σ labels the N internal degrees of freedom. This Hamiltonian is endowed with a SU(N) symmetry associated with global unitary transformations in the flavor space. As a result there appear a set of operators that commute with the Hamiltonian and with each other which serve as labels for the eigenstates. In particular the number of particles in any of the flavors are good quantum number. Additionally the

eigenstates would appear in SU(N) multiplets, namely subspaces that have the same energy and that are "irreducible" under the action of SU(N). Another way of saying this is that there exist $N-1$ additional good quantum which correspond to a set of independent Casimir operators of SU(N) and which serve to Label its irreducible representations.

The ground state of the system thus belongs to an irreducible representation of SU(N). The irreducible representations of a system of N_e electrons, with internal SU(N) symmetry can be labeled by a set of non-decreasing numbers $n_1 \geq n_2 \geq \cdots n_N \geq 0$, satisfying the constraint $N_e = \sum_i n_i$. And one can define an associated SU(N) magnetization vector specifying the partial filling of each flavor $(\nu_1, \cdots, \nu_N)$, such that $\nu_i = n_i/N_\phi$, with the total filling factor being $\nu = \sum_i \nu_i$, and N_ϕ being the total number of flux quanta.

It has been known for a long time that when the system has a total filling factor which is an integer, $\nu = \{0, 1, \cdots, N\}$, the Slater determinants that have maximal polarization are exact many body eigenstates of the Hamiltonian in Eq. (2.12). These states are known by the name of "Quantum Hall Ferromagnets". This conclusion simply follows from the fact that the Hilbert space has a single maximally polarized state at integer filling fractions. These states typically are the ground states of repulsive interactions, and in particular they have been shown to be the ground states of the Coulomb interaction in exact diagonalization studiess.

The fact that ground states at the integers are maximally polarized can be viewed as a type of many-body Hunds' rule. Essentially, the Pauli exclusion

principle will gurantee the existence of zeroes of the many body wavefunction whenever any two particles that have the same SU(N) flavor coincide spatially. Therefore electrons try to "pile up" into as little flavors as possible in order to create as many of these zeroes as they can in order to minimize their repulsive energy, whereby forming a state with largest possible SU(N) magnetization.

I will next demonstrate a property of quantum Hall ferromagnets which has been used by several authors in the past, but which I have never seen stated in a completely explicit fashion. The property is that quantum Hall ferromagnets serve as *perfect vacua* on top of which strongly correlated phases can be constructed just in the same manner as they can be constructed on top of the completely empty LLL.

Imagine a many-body eigenstate filling F flavors ($F < N$), which would describe a strongly correlated multicomponent fractional quantum Hall state. This state would belong to an SU(N) representation with $N - F$ completely empty components an would thus have an SU(N) polarization vector of the form,

$$\vec{\nu} = (\nu_1, \cdots, \nu_F, 0, \cdots, 0). \tag{2.2}$$

This state can be created on top of vacuum by the action of creation operators and have an expansion in Slater determinants of the form,

$$|\Psi_{\vec{\nu}}\rangle = \sum_{M_{n_1}\cdots M_{n_F}} C[M_{n_1},\cdots,M_{n_F}] \left(\prod_{m\in M_{n_1}} c^\dagger_{m,1}\right)\cdots\left(\prod_{m\in M_{n_F}} c^\dagger_{m,F}\right)|\Phi_0\rangle, \tag{2.3}$$

where M_n denotes a set of labels for guiding center states with n elements, and $C[M_{n_1},\cdots,M_{n_F}]$ is the probability amplitude of the corresponding Slater determinant in which those states are filled. Now, we could instead construct this state on top of a quantum Hall ferromagnet which completely fills some of the flavors that are left empty in the correlated state. This quantum Hall ferromagnet would serve as a vacuum, in which N_1 flavors are completely filled ($N_1 \leq N - F$), and let us call it $|\Phi_{N_1}\rangle$. It can be shown that if the initial correlated initial $|\Psi_{\vec{\nu}}\rangle$ is an exact eigenstate, the new state $|\Psi^1_{\vec{\nu}'}\rangle$ is also a many body eigenstate:

$$|\Psi^1_{\vec{\nu}'}\rangle = \sum_{M_{n_1}\cdots M_{n_F}} C[M_{n_1},\cdots,M_{n_F}] \left(\prod_{m\in M_{n_1}} c^\dagger_{m,1}\right)\cdots\left(\prod_{m\in M_{n_F}} c^\dagger_{m,F}\right)|\Phi_{N_v}\rangle. \tag{2.4}$$

The new state will have a different SU(N) magnetization vector given by:

$$\vec{\nu}' = (1,\ldots,1,\nu_1,\ldots,\nu_F,0,\ldots,0), \tag{2.5}$$

and a larger total filling $\nu' = \nu + N_1$, which is the sum of the filling of the original correlated state and that of the ferromagnet that serves as vacuum. In other words, we have an exact way to construct correlated states of higher

density, from correlated states of lower density, by combining them with quantum Hall ferromagnets. The energies of both states can be shown to be related in a simple fashion:

$$E[\Psi^1_{\vec{\nu}'}] = E[\Psi_{\vec{\nu}}] + E[\Phi_{N_1}] + \frac{\nu N_\phi N_1}{2\pi l^2} \int d^2 r v(r), \tag{2.6}$$

where the last term is simply the classical Hartree potential arising from the repulsion between the correlated part of liquid and the quantum Hall ferromagnet part, and would be absent if there is a neutralizing background. Therefore, for the Coulomb interaction the energy of the ferromagnet and the correlated liquid would simply add up:

$$E[\Psi^1_{\vec{\nu}'}] = E[\Psi_{\vec{\nu}}] + E[\Phi_{N_1}]. \tag{2.7}$$

But this is not the end of the story. So far we have constructed correlated states by adding correlated *particles* to the ferromagnets. It is possible to perform a similar construction by removing particles on a correlated fashion from the ferromagnets, in other words by adding correlated *holes*. This is possible because in addition to a global particle-hole symmetry, the interaction in Eq. (2.12) possesses additional restricted particle-hole symmetries in which only some of the flavors are particle-hole conjugated, when acting on the subspace of functions on which only those flavors are occupied.

More explicitly, consider the quantum Hall ferromagnet in which all of the flavors involved in making the correlated state $|\Psi_{\vec{\nu}}\rangle$ of Eq. (2.3), are

completely filled. This ferromagnet has therefore F completely filled flavors and let us denote by $|\Phi_F\rangle$. It follows that the following state of correlated holes is an exact eigenstate provided the original correlated state is too:

$$|\Psi^2_{\vec{\nu}'}\rangle = \sum_{M_{n_1}\cdots M_{n_F}} C[M_{n_1},\cdots,M_{n_F}] \left(\prod_{m\in M_{n_1}} c_{m,1}\right)\cdots\left(\prod_{m\in M_{n_F}} c_{m,F}\right)|\Phi_F\rangle. \tag{2.8}$$

This new state will have a SU(4) magnetization vector:

$$\vec{\nu}' = (1-\nu_F,\cdots,1-\nu_1,0,\cdots,0), \tag{2.9}$$

and its total filling factor is $\nu' = F-\nu$, and it will have higher density than the original state if $\nu < F/2$. The energy of this state also has a simple relation to that of the original correlated state and can be obtained from it by applying a particle-hole transformation restricted to the F flavors involved:

$$E[\Psi^2_{\vec{\nu}'}] = E[\Psi_{\vec{\nu}}] + N_\phi(F-\nu)\left[\frac{F}{2\pi l^2}\int d^2r v(r) - \int \frac{d^2q}{(2\pi)^2} v(q)|F(q)|^2\right], \tag{2.10}$$

where $|F(q)|^2 = exp(-q^2l^2/2)$ is the squared density form factor of the LLL, and the Hartree piece would be absent if there would be a neutralizing background and only the exchange potential would be left:

$$E[\Psi^2_{\vec{\nu}'}] = E[\Psi_{\vec{\nu}}] - N_\phi(F/2-\nu)\int \frac{d^2q}{(2\pi)^2} v(q)|F(q)|^2, \tag{2.11}$$

for Coulomb interaction $\int \frac{d^2q}{(2\pi)^2} v(q)|F(q)|^2 = \sqrt{\pi/2}e^2/\epsilon l$.

In summary, we have described two rules to construct correlated states on top of quantum Hall ferromagnets, provided we know how to construct them on top of the original vacuum.

2.2 SU(N) V_0 Hard-core model

An important observation made in the early days of the FQHE by Haldane [26] was that the Laughlin wavefunction at $\nu = 1/3$ [43] is the exact ground state of a short-ranged interaction potential in which only the V_1 Haldane pseudopotential is finite and positive [27]. Moreover, for spinless fermions, the Laughlin state is the highest density state that remains a zero energy state for such model, implying the existence of discontinuity in chemical potential at $\nu = 1/3$ and hence the presence of a charge gap.

A by-product of Haldane's argument is that the Laughlin wavefunction *cannot* be an exact eigenstate of the full Coulomb interaction. This is because the Coulomb interaction has finite Haldane pseudopotentials of higher angular momentum, which when viewed as perturbations added to the V_1 hard-core model, will necesarily induce mixing with excited non-zero energy eigenstates of the V_1 model. In these states particles have a finite probability amplitude of being in pairs of relative angular momentum $m = 1$, which are completely absent in the Laughlin state.

This is however not a problem. Numerical studies have overwhelm-

ingly demonstrated that the true ground state of the Coulomb interaction is extremely well described by the Laughlin wavefunction, and in particular, that the adiabatic "turning on" of higher angular momentum pseudopotentials added to the Hard-core model do not meet an intermediate phase transition [28]. In other words the two wavefunctions, namely the true Coulomb ground state and Laughlin's, are two representatives of the same phase of the strongly correlated fractional quantum Hall liquid. The Laughlin state can be thought of as the *ideal* representative of such phase [46].

The lesson from this is that Hard-core models serve to define the *idealized* fractional quantum Hall states. They are also useful in discriminating what is the relevant low-energy physics. We will find useful in our study of the SU(N) quantum Hall states to consider the V_0 hard-core model, in which only the $m = 0$ relative angular momentum is energetically penalized [68]. The interaction for such model can be written as:

$$H = V_0 \sum_{i<j} 4\pi l^2 P_{LLL} \delta(r_i - r_j) P_{LLL} = V_0 \sum_{i<j} P^0_{ij}. \tag{2.12}$$

where P^0_{ij} is the projector of two-particles into a state of zero relative angular momentum contained in the LLL.

For $V_0 > 0$ the Hamiltoninan is a positive definite operator, and hence the lowest energy eigenstates cannot have negative energies. In the symmetric gauge, the zero energy eigenstates of the model can be written generally as a

product of the Vandermonde determinant and an $SU(N)$ bosonic wavefunction [47, 78],

$$\Psi = \prod_{i<j}(z_i - z_j)\ \Psi^B_{\mathrm{SU(N)}}, \tag{2.13}$$

where $\Psi^B_{\mathrm{SU(N)}}$ is a SU(N) bosonic wavefunction in the lowest Landau level. In other words, the zero energy manifold of the Hard-core model contains all the wavefunctions in which every pair of electrons has zero probablity amplitude to coincide spatially with any other electron. The highest density state that satisfies this constraint is the SU(N) ferromagnetic Vandermonde determinant whose spatial part is:

$$\Psi_{\nu=1} = \prod_{i<j}(z_i - z_j)\ e^{-\frac{|z_i|^2}{4l^2}}. \tag{2.14}$$

This state has total filling $\nu = 1$ and SU(N) polarization $(1, 0, \cdots, 0)$, *i. e.* it is a qunatum Hall ferromagnet. The zero energy manifold of the SU(N) V_0 Hard-core model is highly degenerate. For n fermions and total number of N_ϕ flux quanta, one finds that the total number of many-body zero energy states is:

$$\binom{n - 1 + N(n + 1 - N_\phi)}{n}, \tag{2.15}$$

the number above includes the multiplicity within the SU(N) multiplets, but the number of states is large even after removing such redundancy.

Equation (2.13) makes manifest that it is impossible to construct zero energy states of density higher than $\nu = 1$ for the V_0 model. This is the origin of the incompressibility at the integer fillings for the quantum Hall ferromagnets. The construction of the lowest energy states for $\nu \in [1, 2]$ is achieved by employing the observations made in section 3.1. The two mappings will produce states of equal energy:

$$E = 2V_0(n - N_\phi), \text{ for } n \in [N_\phi + 1, 2N_\phi]. \tag{2.16}$$

Above equation follows from Eq. (2.6), after the following observations: (1) $E[\Psi_\nu] = 0$, because the correlated liquid created on top of the ferromagnet is a zero energy eigenstate of V_0 hard-core model; (2) $E[\Psi_{N_v=1}] = 0$ because the ferromagnet itself is a zero energy eigenstate of V_0 hard-core model; (3) $v(r) = 4\pi l^2 \delta(r)$. The same equation follows from the second mapping, namely from Eq. (2.10) by similar reasonings (note that in Eq.(2.10) ν was referring to the filling of the original correlated state with $\nu \leq 1$, so it must be changed into $\nu \to 2 - \nu$, to denote the filling of the state with $\nu \geq 1$ after the particle-hole conjugation).

This degeneracy obtained from the two mappings emphasizes that there are two competing vacua at any filling factor $\nu \in ([\nu], [\nu] + 1)$: one of them is the quantum Hall ferromagnet with filling $[\nu]$, which sustains a correlated liquid of $N_\phi(\nu - [\nu])$ particles, and the other is the adjacent quantum Hall

ferromagnet at $[\nu]+1$, which sustains a correlated liquid of $N_\phi([\nu]-\nu)$ holes[1]. The energy of the low energy states of the V_0 hard-core model for n particles can be obtained inductively from the previous reasoning using either Eq. (2.6) or Eq. (2.10) and reads as follows:

$$E(n) = 2V_0\ [\nu]\ n - V_0\ [\nu]([\nu]+1)\ N_\phi, \tag{2.17}$$

the chemical potential of the V_0 model has therefore jumps of size $2V_0$, whenever the filling fraction is an integer, indicating the consecutive filling of the different SU(N) flavors:

$$\mu \equiv \frac{dE}{dn} = 2V_0\ [\nu], \tag{2.18}$$

the energy and filling factor are illustrated in fig 2.1. These integer incompressibilities of the hard-core model are analogous to the behavior of a Hubbard model of fermions on a lattice with onsite repulsions, no kinetic energy, and N internal flavors.

I believe equations (2.17) and (2.18) describe exhaustively the lowest energy manifold V_0 SU(N) hard-core model *exactly*, although I have not constructed a rigourous proof thus far. In other words, the entire lowest energy manifold of the hard-core model in the filling factor range $\nu \in ([\nu], [\nu]+1)$ is constructed from these two mappings, one of which adds correlated holes to

[1] $[x]$ denotes the integer part of x.

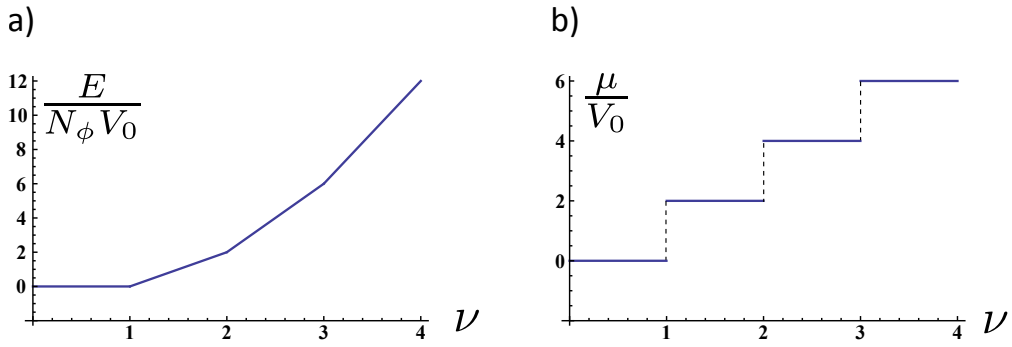

Figure 2.1: Energy (a) and chemical potential (b) of the SU(N) V_0 hardcore model as a function of filling, displaying the cusps and chemical potential jumps associated with the incompressible integer quantum Hall ferromagnets.

the quantum Hall ferromagnets at $\nu = [\nu] + 1$ and the other adds correlated electrons to the quantum Hall ferromagnets at $\nu = [\nu]$, in exactly the same fashion that correlated particles are added to the true vacuum at $\nu = 0$.

2.3 Theory of weakly broken SU(N) FQHE ground states

More realistic repulsive interactions will contain in general finite Haldane pseudopotentials of higher angular momentum, in addition to the V_0 term present in the hard-core model described in the previous section. However, for many repulsive interactions, including the Coulomb potential, the V_0 pseudo-potential is the strongest. This motivates the conjecture that the ground states of a large class of SU(N) invariant repulsive interactions can be well described by states in the lowest energy manifold of the V_0 hard-core model. As previously discussed, except at integer fillings factors, this manifold is in general highly degenrate. Therefore, many states in the manifold might

not be suitable for describing the ground states of a particular interaction. But the conjecture is that at least one of them will have the right type of correlations to optimize the finite repulsive energy created by the higher angular momentum Haldane pseudopotentials.

This conjectures leads to a remarkable conclusion: in order to construct the ground state manifold of an SU(N) repulsive interaction for the entire filling factor range $\nu \in [0, N]$, whose dominant term is the V_0 pseudo-potential, it is only sufficient to construct it for the the filling factor range $\nu \in [0, 1]$. This follows from the fact that given the ground states in the range $\nu \in (0, 1)$, one is able to consruct the lowest energy states in a filling range $\nu \in ([\nu], [\nu] + 1)$ by using the two mappings described in section 3.1, in which one adds either correlated holes to the quantum Hall ferromagnet at $\nu = [\nu] + 1$ or else correlated electrons to the quantum Hall ferromagnet at $\nu = [\nu]$. Since these mappings are believed to exhaust the lowest energy manifold model, they will contain the states that have the right correlations to optimize the repulsive energy of an interaction with finite Haldane pseudopotentials of higher angular momentum.

Let us now consider that the SU(N) symmetry is not exact but weakly broken by an additional Hamiltonian of the form:

$$H_a = \sum_{i<j,\sigma} V_\sigma \, \tau_\sigma^i \, P_0^{ij} \, \tau_\sigma^j - \sum_{i,\sigma} h_\sigma \tau_\sigma^i \tag{2.19}$$

where τ_σ are the $N^2 - 1$ traceless hermitian matrices that generate the SU(N)

Lie algebra, and serve as a basis for the vector space of $N \times N$ traceless hermitian matrices. P_0^{ij} is the projector into the state with zero relative angular momentum for particles i and j, and V_σ are flavor dependenpent Haldane-pseudopotentials. h_σ are the strength of single particle flavor-dependent symmetry breaking terms.

At this point the choice of symmetry breaking Hamiltonian in Eq. (2.19) might appear somewhat arbitrary. The motivation for it, is that it parametrizes a large class of short-ranged symmetry breaking interactions. In particular it contains as a specific case a model for the symmetry breaking interactions that are believed to be relevant in the lowest Landau level of graphene [38]. The single particle term parametrized by h_σ can be thought of as a generalized form of the Zeeman-like term for N flavors. In the case of graphene it can account for the real Zeeman term as well as a sublattice staggered potential. The specific realization of this Hamiltonian for monolayer graphene will be discussed in Chapter 3.

We would like conceptualize the symmetry breaking terms as being weak in comparison to the dominant SU(N) invariant energy scales. In the case of Coulomb interaction this can be explicitly stated as follows: $V_\sigma \ll e^2/\epsilon l$ and $h_\sigma \ll e^2/\epsilon l$. In this case we can pressume that the symmetry breaking terms do not alter the orbital correlations that optimize the SU(N) invariant interaction, but that their role is to pin down the specific SU(N) spinors associated with the flavors that are filled in a particular state. Essentially this same idea underlies the analysis of Ref. [2], where the correlated states of electrons or holes was

added to quantum Hall ferromagnetic state of graphene at neutrality, but the correlated part was assumed to have zero probability amplitude for the spatial coincidence of electrons, which is equivalent to the statement that it is a lowest energy state of the V_0 hard-core model.

Let us then imagine a many-body ground state of the SU(N) repulsion of the form described in Eq. (2.4), whose filling vector is:

$$(1, \ldots, 1, \nu_1, \ldots, \nu_F, 0, \ldots, 0), \tag{2.20}$$

and is therefore made out of a quantum Hall ferromagnet with N_1 complely filled flavors which we call $\{|\chi_1\rangle, \ldots, |\chi_{N_1}\rangle\}$, and a strongly correlated part with fillings $(\nu_1, \ldots, \nu_F)$ and associated spinors $\{|\chi_{N_1+1}\rangle, \ldots, |\chi_{N_1+F}\rangle\}$. The expectation value of H_a in this state takes the form:

$$\frac{\langle H_a \rangle}{N_\phi} = \frac{1}{2}\mathrm{tr}(P_i H_i^{HF}) + \mathrm{tr}(P_f H_i^{HF}) - \frac{1}{2}\sum_\sigma h_\sigma \mathrm{tr}(P_i \tau_\sigma), \tag{2.21}$$

where $P_i = |\chi_1\rangle\langle\chi_1| + \cdots + |\chi_{N_1}\rangle\langle\chi_{N_1}|$ is the projector onto the completely filled flavors of the quantum Hall ferromagnet component, and $P_f = \nu_1|\chi_{N_1+1}\rangle\langle\chi_{N_1+1}| + \cdots + \nu_F|\chi_{N_1+F}\rangle\langle\chi_{N_1+F}|$ is a weighed projector onto fractionally filled spinors of the strongly correlated component. In Eq. (2.21), H_i^{HF} is the anisotropy contribution to the Hartree-Fock quasi-particle Hamiltonian that one would obtain if there were no fractionally occupied components, namely:

$$H_i^{HF} = \sum_\sigma V_\sigma \left[\mathrm{tr}(P_i\tau_\sigma)\tau_\sigma - \tau_\sigma P_i \tau_\sigma\right] - \sum_\sigma h_\sigma \tau_\sigma. \tag{2.22}$$

Equation (2.21) follows from the hard-core assumption, and from the following property of completely filled spinors:

$$\hat{\rho}_m(r)|\Psi\rangle = \frac{1}{2\pi l^2}|\Psi\rangle, \tag{2.23}$$

where $\hat{\rho}_m(r) \equiv \hat{P}_{LLL}(\sum_i \delta(\hat{r}_i - r)|\chi_m\rangle_{ii}\langle\chi_m|)\hat{P}_{LLL}$ is the particle density projected to the m-th completely filled spinor.

Equation (2.21) must then be seen as a variational expression for the anisotropy energy whose variational parameters are the filled spinors. The problem reduces then to minimize this expression with the only constraint of keeping the spinors orthonormalized. An analogous expression can be derived for the states obtained by adding correlated holes to the quantum Hall ferromagnet by applying a global particle-hole conjugation.

2.4 Charge gaps of weakly broken SU(N) FQHE states

One of the necessary ingredients for the existence of the fractional quantum Hall effect is the presence of gap for the charged exciations in the bulk of the correlated liquid [46]. A similar reasoning to that presented in the previous section to obtain the variational estimate of the ground state energy in Eq. (2.21) can also be used to compute the contributions of the anisotropy term in the Hamiltonian H_a to the charge gaps.

Charge gaps are defined as the sum of the energy of the single quasielectron plus the energy of a single quasihole created on top of the incompressible FQH liquid and which are arbitrarily spatially far apart from each other. If we assume that the quasiparticle states in the presence of the symmetry breaking anisotropy Hamiltonian, H_a, evolve *adiabatically* from SU(N) quasiparticle states, then, we can label them with SU(N) quantum numbers. Quasielectron-quasihole pair states can be labeled by integers which specify changes in the occupation numbers for each flavor relative to the incompressible ground state. Let us assume that in creating the quasielectron-quasihole pair a number of particles can flip their occupation numbers from the fractionally filled spinors into the initially un-occupied spinors, as follows:

$$(N_\phi, \ldots, N_\phi, n_1, \ldots, n_F, 0, \ldots, 0) \rightarrow$$
$$(N_\phi, \ldots, N_\phi, n_1 + \delta n_1, \ldots, n_F + \delta n_F, \delta n_{F+1}, \ldots, \delta n_N). \quad (2.24)$$

Because the far distant quasielectron-quasihole pair can be seen as a neutral excitation of the original system, the integers specifying the flavor flips are constrained to satisfy $\delta n_{N_1+1} + \cdots + \delta n_{n_F} + \cdots + \delta n_N = 0$. Let us assume the far distant quasielectron-quasihole pair to be well described by a V_0 hard-core model wavefunction as well. Then in the thermodynamic limit for excitations involving a finite number of flips, i.e. when $\delta n_i \ll N_\phi$, one can use Eq. (2.21) to compute the correction to the energy of the quasielectron-quasihole pair state arising from H_a much in the same way as it is done for the imcompress-

ible ground state itself. Then, it follows that the gap for such excitations is the SU(N) value plus an anisotropy correction arising from H_a given by the expression:

$$\Delta_a = \sum_{j=N_1+1}^{N} \delta n_j \langle \chi_j | H_i^{HF} | \chi_j \rangle. \tag{2.25}$$

Chapter 3

FQHE in monolayer graphene[1]

Since its discovery [71] more than three decades ago, the FQHE has been studied almost exclusively in the two-dimensional electron systems (2DESs) formed near GaAs/AlGaAs heterojunctions. Because of their small Zeeman to cyclotron energy ratio [29], the electron spin degree-of-freedom in the $N = 0$ LL of the GaAs conduction band is often experimentally relevant, endowing the FQHE with ground and quasiparticle states that would not occur in the spinless fermion case [69].

The $N = 0$ LL of monolayer graphene is nearly four-fold degenerate because of the presence of spin and valley degrees of freedom, and is partially occupied over the filling factor range from $\nu = -2$ to $\nu = 2$, opening the door to SU(4) manifestations of the FQHE. However, because graphene sheets on substrates generally have stronger disorder than modulation-doped GaAs/AlGaAs 2DESs, it has until recently not been possible to observe their fractional quantum Hall effects. Recent studies of high-quality graphene samples have started to clear the fog [9, 14, 17, 20–22] however, and a rich picture has emerged with

[1]This chapter is based on Ref. [68], all authors in this reference contributed equally to this work.

it. Experiments indicate that the graphene FQHE is stronger for $0 < |\nu| < 1$ than for $1 < |\nu| < 2$, and that phase transitions between distinct states at the same ν occur as a function of magnetic field strength [20, 21]. In this work we shed light on these trends by using the general variational approach developed in Chapter 2 to the specific case of the Landau level near neutrality of graphene. We will account for the crucial SU(4) symmetry breaking terms that are present in this system. A closely related analysis of the FQH states in graphene can be found in Ref. [2].

We will find that in the absence of symmetry breaking terms the ground state at $|\nu| = 1/3$ is *not* of the simple Laughlin type, as it has been previously assumed in the literature.

3.1 The $N = 0$ Landau level of graphene

Electrons in graphene possess a relativistic dispersion relation at low energies. Low energy excitations appear at two inequivalent crystal momemta at the K and K' points of the reciprocal unit cell. The kinetic energy at these points in the presence of a magnetic field is within the continuum description:

$$H_K = v\sigma \cdot (p + eA/c),\ H_{K'} = v\sigma^T \cdot (p + eA/c), \tag{3.1}$$

where $p = -i\nabla$ is the two-dimensional momentum operator, A vector potential associated with a uniform magnetic field $B = \nabla \times A$, and σ is a Pauli matrix in the honeycomb AB sublattice degree of freedom [10]. The Landau levels of

the relativistic fermions in graphene have energies given by [51],

$$E_N = \frac{v}{l} sign(N)\sqrt{2N}. \tag{3.2}$$

Counting spin, these Landau levels are nearly four-fold degenerate. We are interested here in the Landau level that occurs near neutrality for $N = 0$. The single-particle states in each valley are fully polarized in the subalttice degree-of-freedom, and thus valley and sublattice are locked in the $N = 0$ Landau level of graphene [10].

In the spirit of degenerate perturbation the interaction can be projected into the $N = 0$ LL. It is worth emphasizing that cyclotron energy and long-range part of the Coulomb interaction scale with the same power of the quantizing perpendicular magnetic field, namely $\sqrt{B}$, and there is no analogue of a formal large field limit to justify this projection, as it is the case for Galilean fermions. A parameter controlling the Landau level mixing corrections is thus the effective fine structure constant of graphene [59],

$$\alpha = \frac{e^2}{\epsilon v} \tag{3.3}$$

which is not small for suspended graphene and approximately given by $\alpha \sim 2.2$.

The filling factor of graphene measured from neutrality ranges from $\nu = [-2, 2]$ in the $N = 0$ LL. It is also convenient to define a filling factor measured from the empty $N = 0$ LL, which we denote by $\tilde{\nu} \in [0, 4] = 2 + \nu$.

3.2 Symmetry breaking terms in the $N = 0$ LL

The long range part of the Coulomb interaction is independent of spin and valleys and hence SU(4) invariant. However, it has become clear from experimental [20, 21, 32, 79, 80] and theoretical [2, 4, 31, 34, 37, 38] studies that short-range valley-dependent corrections to the long-range SU(4) symmetric Coulomb interactions play a significant role in determining the ground state of the quantum Hall ferromagnet state realized at neutrality ($\tilde{\nu} = 2$) in graphene. It is natural that these symmetry breaking terms play an important role in the FQH states as well.

The symmetry breaking interactions can be modeled as *zero-range* valley-sublattice dependent interactions. The discrete symmetries of the honeycomb lattice serve to constrain the allowed zero-range symmetry breaking interactions [3]. The projection into the $N = 0$ produces additional simplifications because of the equivalence between sublattice and valley degrees of freedom in such subspace. As a consequence the symmetry breaking interactions reduce to the following [38]:

$$H_a = \sum_{i<j,\sigma} V_\sigma \, \tau_\sigma^i \; P_0^{ij} \tau_\sigma^j - \sum_i h\sigma_z^i \tag{3.4}$$

where τ_σ^i is a Pauli matrix which acts on the valley degree of freedom of particle i, $\sigma = \{x, y, z\}$, σ_z^i is the z-axis Pauli matrix which acts on the spin of particle i, P_0^{ij} projects the pair state of particles i and j onto relative angular momentum 0, and V_σ is a valley-dependent Haldane pseudopotential. Because

conservation of total crystal momentum implies that the number of electrons in each valley is conserved, we have $V_x = V_y \equiv V_\perp$. The system's weakly-broken SU(4) symmetry is therefore characterized by three parameters V_z, $V_\perp$, and by the Zeeman field strength h. The values of V_z and $V_\perp$ are dependent on the component of magnetic field perpendicular to the graphene plane $B_\perp$, whereas the Zeeman strength is determined by the total magnetic field, therefore, their relative strengths can be controlled by tilting the magnetic field away from the 2DES normal. In Eq. (3.4) the z-axis of spin is chosen along the direction of the total magnetic field.

The symmetry breaking interaction parametrized by V_z, preserves the valleys of the scattering electrons at each vertex but it has opposite sign for intra- and inter-valley interactions, it is diagrammatically depicted in Figs. 3.1(a-b). The symmetry breaking interaction parametrized by $V_\perp$ is an inter-valley scattering term, it flips the valleys of the electrons at each vertex, but it does so in a manner that preserves the total number of electrons in each valley. Therefore, it is non-vanishing only when the scattering electrons have opposite valleys and it swaps their valleys after scattering, as it is diagrammatically depicted in Fig. 3.1(c).

In addition to the Zeeman coupling, a single particle valley symmetry breaking term could present. For example a sublattice staggered potential would give rise to a term of the form:

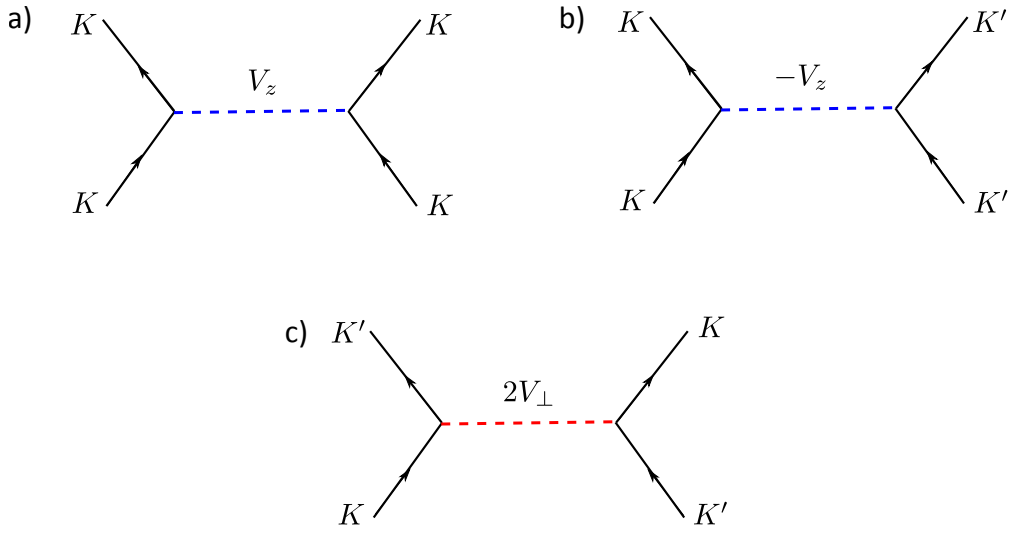

Figure 3.1: Diagramatic depiction of symmetry breaking interactions in the $N = 0$ LL of graphene.

$$\delta H_a = -\sum_i m\tau_z^i. \tag{3.5}$$

A term of this form is ruled out for suspended graphene due to the symmetry between A and B sublattices. However, terms of this sort are expected to arise from the staggered potential created on graphene when it is closely aligned with a boron-nitride substrate [32, 60, 75]. In this work we will focus on understanding the FQH states of suspended graphene, but this term is likely to be crucial in explaining the additional FQH states observed for graphene on boron-nitride [32], as it will become clear in the coming sections.

3.3 Multi-component FQH states in the $N = 0$ LL of graphene

Because of the full particle-hole symmetry of the Hamiltonian describing the $N = 0$ LL of graphene it is sufficient to restrict the contruction to the filling factor range $\tilde{\nu} \in [0, 2]$, and incompressible states in the range $\tilde{\nu} \in [2, 4]$ can then be obtained by applying global particle-hole conjugation. To construct the incompressible sates in the filling factor range $\tilde{\nu} \in [0, 2]$ we apply the formalism discussed in Chapter 2. Let us summarize the procedure for particles with four internal degrees of freedom, which correspond to the spin/valley flavors of the electrons in the $N = 0$ LL of graphene. Consider a multicomponent FQH state with total filling $\tilde{\nu_0} \in (0, 1)$. Then we can construct FQH states using the following two rules:

Map 1 If the state involves three components or less, namely if it has a filling vector $(\nu_1, \nu_2, \nu_3, 0)$, we can construct an associated state by adding the correlated particles to the quantum Hall ferromagnet at $\tilde{\nu}_{FM} = 1$ (as described in Eq. (2.4)), to obtain a state with total filling $\tilde{\nu}_0 + 1$ and filling vector $(1, \nu_1, \nu_2, \nu_3)$. The Coulomb energy per flux quantum of the state obtained from this map is related to the energy per flux quantum of the original state as follows:

$$E_{\tilde{\nu}_0+1} = E_{\tilde{\nu}_0} + E_1, \tag{3.6}$$

where $E_1 = -\sqrt{\pi/2}\ e^2/2\epsilon l$ is the Coulomb energy of the $\tilde{\nu}_{FM} = 1$ ferromagnet.

Map 2 If the state involves two components or less, namely if it has a filling vector $(\nu_1, \nu_2, 0, 0)$, we can construct an associated state by adding the correlated holes to the quantum Hall ferromagnet at $\tilde{\nu}_{FM} = 2$ (as described in Eq. (2.8)), to obtain a state with total filling $2 - \tilde{\nu}_0$ and filling vector $(1 - \nu_2, 1 - \nu_1, 0, 0)$. The Coulomb energy per flux quantum of the state obtained from this map is related to the energy per flux quantum of the original state as follows:

$$E_{2-\tilde{\nu}_0} = E_{\tilde{\nu}_0} + (1 - \tilde{\nu}_0)E_2, \tag{3.7}$$

where $E_2 = 2E_1$ is the Coulomb energy of the $\tilde{\nu}_{FM} = 2$ ferromagnet.

We will focus on the states at $\tilde{\nu} = p/3$, with $p = \{1, 2, 4, 5\}$, which are representative enough to understand the many of the observations reported in Refs. [20, 21].

3.3.1 FQH states at $\tilde{\nu} = 1/3$ and $\tilde{\nu} = 2/3$

The FQH states $\tilde{\nu} = 1/3$ and $\tilde{\nu} = 2/3$ involve only two flavors and are therefore familiar from the studies in the context of gallium arsenide (GaAs) when spin is considered to be an active degree of freedom. We will describe the properties of these states in the absence of symmetry breaking terms and discuss the symmetry breaking in the next sections. We begin by considering

the ground state for $\tilde{\nu} = 1/3$. At this fraction the expected ground state is the SU(4) ferromagnet Laughlin state [43], with filling vector $(1/3, 0, 0, 0)$, and wavefunction,

$$\Psi_{1/3} = \left[\prod_{i<j}(z_i - z_j)^3 \; e^{-\frac{|z_i|^2}{4l^2}}\right]\left[\bigotimes_i |\chi\rangle_i\right]. \tag{3.8}$$

In this state electrons are fully polarized into occupying a single SU(4) spinor which we denote by $|\chi\rangle$. The energy per particle of this state for the Coulomb interaction is $-0.41e^2/\epsilon l$, as determined from exact diagonalization studies [28].

At $\tilde{\nu} = 2/3$, two incompressible states compete in correlation energy. One of them is the single component particle-hole conjugate of the Laughlin state, with filling vector $(2/3, 0, 0, 0)$. The other state is a two-component singlet with filling vector $(1/3, 1/3, 0, 0)$. Exact diagonalization studies have determined that the ground state of the Coulomb interaction for two-component fermions is the singlet with fillings $(1/3, 1/3)$ [12, 13, 55, 72, 76, 77], whose wavefunction is of the form:

$$\Psi_{(1/3,1/3)} = \mathcal{A}_{1\leftrightarrow 2}\left[\Psi^{orb}_{(1/3,1/3)}[\{z_i\}]\bigotimes_{i=1}^{N/2}|\chi_1\rangle_i \bigotimes_{i=N/2+1}^{N}|\chi_2\rangle_i\right]. \tag{3.9}$$

In this state electrons would occupy two of the SU(4) spinors which we denote by $|\chi_1\rangle, |\chi_2\rangle$. $\mathcal{A}_{1\leftrightarrow 2}$ denotes the antisymmetrization between electrons in these two flavors. An explicitly holomorphic form for the orbital part of

this wavefunction analogous to that of the Laughlin state in Eq. (3.8) is unknown. A composite fermion wavefunction for this state can be written, and it is such that the composite fermions experience an effective field with opposite direction to that of the physical field and make a two-component singlet at $\nu = 2$ [33].

Exact diagonalization studies find that the Coulomb energy difference per particle between the two competing states at $\tilde{\nu} = 2/3$ is [12, 13, 55, 72, 76, 77],

$$\frac{E^{Coul}_{(2/3,0,0,0)} - E^{Coul}_{(1/3,1/3,0,0)}}{n} \approx 0.009 \, \frac{e^2}{\epsilon l}. \tag{3.10}$$

Composite Fermion trial wavefunctions significantly underestimate this energy difference to be about $0.0036 e^2/\epsilon l$ [12, 13], although they correctly predict the ground state to be the singlet [76].

3.3.2 FQH states at $\tilde{\nu} = 4/3$ and $\tilde{\nu} = 5/3$

At $\tilde{\nu} = 4/3$, we obtain two competing states with flavor compositions $(1, 1/3, 0, 0)$ and $(2/3, 2/3, 0, 0)$, by applying the two-component particle-hole conjugation to the states $(2/3, 0, 0)$ and $(1/3, 1/3, 0, 0)$ at $\tilde{\nu} = 2/3$ discussed in the previous sections. These two states are well known from work on the FQHE of spinful fermions as well. From Eq. (3.7) it follows that the state with lower Coulomb energy is $(2/3, 2/3, 0, 0)$.

At $\tilde{\nu} = 5/3$ we obtain two states with flavor fillings $(1, 2/3, 0, 0)$ and

$(1, 1/3, 1/3, 0)$. These two states are obtained by constructing the same two-component correlated states $(2/3, 0, 0)$ and $(1/3, 1/3, 0, 0)$ at $\tilde{\nu} = 2/3$, but instead of particles being added to the vacuum the are added to the quantum Hall ferromagnet at $\tilde{\nu} = 1$. Note that the state $(1, 2/3, 0, 0)$ could also be conceptualized as adding a Laughlin state of correlated holes to the quantum hall ferromagnet at $\tilde{\nu} = 2$, with fillings $(1, 1, 0, 0)$. However the state $(1, 1/3, 1/3, 0)$ needs to be thought of as two-component correlated state added to the quantum hall ferromagnet at $\tilde{\nu} = 1$. Figure 3.2 illustrates how the states at $\tilde{\nu} = 4/3$ and $\tilde{\nu} = 5/3$ are related to the states at $\tilde{\nu} = 2/3$.

The appearance of a three-component state at $\tilde{\nu} = 5/3$ demonstrates that there is no reason to anticipate a simple relationship between $\tilde{\nu}$ and $2 - \tilde{\nu}$ states in graphene. The $(1, 1/3, 1/3, 0)$ state has not previously been discussed as a possible ground state of graphene. Interestingly, Eq. (3.6) implies that this state has lower Coulomb energy than the Laughlin state of of holes $(1, 2/3, 0, 0)$, which is believed to be realized in graphene. As we will illustrate later on, this is likely to be the case when the symmetry braking interactions are added.

3.4 FQH phases with SU(4) symmetry breaking interactions

In this section we will consider the effects of the terms that explicitly break the SU(4) spin-valley symmetry in graphene described in Eq. (3.4). We assume that these symmetry breaking terms are not strong enough to alter the Coulomb correlations of the SU(4) model states. Much as in the

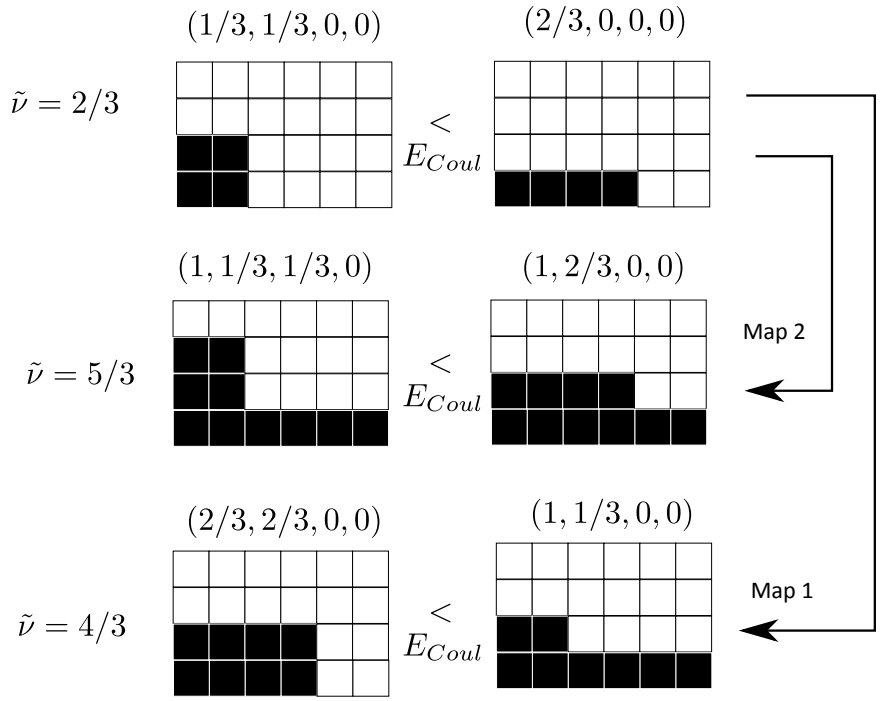

Figure 3.2: $\tilde{\nu} = 5/3$ can be understood as electrons added to $\tilde{\nu} = 1$ ferromagnet. $\tilde{\nu} = 4/3$ can be understood as holes added to $\tilde{\nu} = 2/3$ quantum Hall ferromagnet. The black (white) boxes represent to filled (empty) single-particle states, and thus are the Young tables of the electron (hole) many-body wavefunction.

case of standard magnetic systems, the role of the anisotropy terms is to select the 4-component spinors assigned to wave function components. Since more than one incompressible state might enjoy good Coulomb correlations at a given $\tilde{\nu}$, symmetry breaking terms will also alter the energy balance between these states. This occurs in spite of their smallness compared to the Coulomb energy scale, and the reason for this is that typically the Coulomb energy favors the correlation of a particular state with respect to another one rather weakly as illustrated in Eq.(3.10), thus the symmetry breaking terms

can play a role in deciding which state is favored. Additionally the scaling of the symmetry breaking terms is typically linear with the perpendicular magnetic, $B_\perp$, whereas the Coulomb energies scale as the square root of field $\sqrt{B_\perp}$, therefore the anisotropy energy scales tend to dominate at large fields, whereas Coulomb energy tends to dominate at low fields. This different scaling is the ultimate reason for the observation of phase transitions between different FQH states of graphene [21], in an analogous fashion as the transtions between states of different spin-polarization observed in GaAs [16, 41].

3.4.1 Symmetry breaking at $\tilde{\nu} = 1/3$ and $\tilde{\nu} = 2/3$

The states at $\tilde{\nu} = 1/3$ and $\tilde{\nu} = 2/3$ can be well approximated by zero energy states of the Hard-core model. In other words they are such that there is vanishing probability amplitude for spatial coincidence of fermions. As a consequence they do not experience the short range valley-dependent interactions [2], the only relevant symmetry breaking term is therefore the Zeeman coupling of the electron spin.

At $\tilde{\nu} = 1/3$ we therefore expect the Laughlin state to be fully spin polarized, with a remnant valley SU(2) symmetry of the form:

$$\Psi_{1/3} = \left[\prod_{i<j}(z_i - z_j)^3\right]\left[\bigotimes_i |\uparrow\rangle_i \otimes (u_K|K\rangle + v_{K'}|K'\rangle)_i\right], \tag{3.11}$$

where $u_K|K\rangle + v_{K'}|K'\rangle$ designates an spinor which is an arbitrary coherent combination of both valleys. In the presence of this effective SU(2) symme-

try, the charged quasiparticles near $\tilde{\nu} = 1/3$ are expected to be large valley skyrmions [52, 69]. These valley skyrmions would have 1/3 of the electron charge and involve a soliton-type texture where the valley ferromagnetic order of the state described in Eq. (3.11) is locally deformed so that it points into the orthogonal spinor $v^*_{K'}|K\rangle - u^*_K|K'\rangle$ at the core of the skyrmion and it smoothly heals into the ground state spinor as one moves away from the skyrmion core.

Within the classical non-linear sigma-model (Ginzburg-Landau) description of the ferromagnetic order, the charge gap to create an arbitrarily distant pair of skyrmion quasi-electron and skyrmion quasi-hole pair can be related to the stiffness of the ferromagnetic order parameter, ρ_s, as follows,

$$\Delta^{skyrm}_{NL\sigma} = 8\pi\rho_s. \tag{3.12}$$

This formula predicts that a charge gap [48, 52, 69]:

$$\Delta^{sky}_{1/3} \approx 0.023\ e^2/\epsilon l, \tag{3.13}$$

which is expected to be reduced by a factor of approximately 5, relative to that of the usual single-component Laughlin quasi-electron and quasi-hole pairs, which is approximately $0.104e^2/\epsilon l$.

The considerable reduction of this charge gap possibly explains why there is no discernible signature of incompressibility in the measurements in suspended graphene samples [2, 14, 20, 21]. It is worth contrasting this to the behavior reported for graphene on boron nitride substrates [32]. There it

is likely that a single particle term acting as the analogue of the Zeeman coupling in the valley space, such as that described in Eq. (3.5) is present, hence breaking the remnant valley symmetry, and, if strong enough, turning the quasiparticles into conventional Laughlin quasi-electrons and quasi-holes.

At $\tilde{\nu} = 2/3$ we expect a fully spin polarized valley-singlet state of the form:

$$\Psi_{2/3} = \mathcal{A}_{K\leftrightarrow K'} \left[\Psi^{orb}_{2/3}[\{z_i\}] \left(\bigotimes_{i=1}^{N/2} |\uparrow K\rangle_i \right) \otimes \left(\bigotimes_{i=N/2+1}^{N} |\uparrow K'\rangle_i \right) \right]. \quad (3.14)$$

This state is unique and has no spontaneously broken symmetries unlike that at $\tilde{\nu} = 1/3$, and appears quite robust in experiments [14, 20, 21].

Although the ground state at $\tilde{\nu} = 2/3$ is expected to be fully spin polarized, it is possible that spin reversed quasiparticles are relevant for determining the charge gap at this fraction. In the absence of Zeeman terms, quasiparticles could lower their Coulomb energy by making flavor flips into the completely empty spinors. This is the behavior found for composite fermion wavefunctions at $\tilde{\nu} = 2/5$ [70], which we anticipate to display a similar behavior to $\nu = 2/3$ in the absence of Zeeman terms. However, a numerical study of SU(4) flavor reversed quasiparticles would be needed to quantitatively assess this scenario at $\tilde{\nu} = 2/3$. If the spin-reversed quasiparticles were found to be lower in Coulomb energy they could determine the charge gaps at low fields.

At higher fields, where the Zeeman energy dominates and penalizes

the spin-reversed quasiparticles one would recover the picture of fully spin polarized quasiparticles in the SU(2) valley space. The gap would then be [77]:

$$\Delta_{2/3} \approx 0.0784 e^2/\epsilon l. \tag{3.15}$$

These quasiparticles do not involve valley flips, since additional flips in the background of a singlet state tend to increase the Coulomb energy of the quasiparticles, contrary to the situation for polarized states as demonstrated in exact diagonalization studies [72].

3.4.2 Ordered phases for two-component states with $\tilde{\nu} \in [1, 3]$

In this section we consider the subset of incompressible states in the filling factor range $\tilde{\nu} \in [1, 3]$ that can can be understood as arising from adding quasiparticles or quasiholes in a correlated fashion to the quantum Hall ferromagnet at neutrality with $\tilde{\nu} = 2$, these states can be viewed as two-component states. The states previously discussed at $\tilde{\nu} = 4/3$ can both be understood in this fashion. At $\tilde{\nu} = 5/3$ only the two-component state with filling vector $(1, 2/3, 0, 0)$ is contained in this class. The specifics of the symmetry broken phases for these states will be discussed in the next section. A different analysis is required for the three-component state $(1, 1/3, 1/3, 0)$.

For $\tilde{\nu} \in (1, 2)$ these states would partially occupy only two spinors. The equivalent particle-hole conjugate states in $\tilde{\nu} \in (2, 3)$ fully occupy two spinors and partially occupy two other spinors. Without loss of generality we will describe only the $\tilde{\nu} \in (2, 3)$ case for which the flavor composition

is $(1, 1, \nu_3, \nu_4)$. Let us call the fully occupied spinors $|\chi_1\rangle$ and $|\chi_2\rangle$ and the partially occupied spinors $|\chi_3\rangle$ and $|\chi_4\rangle$. We assume that the spinors that minimize the energy do not have valley-spin entanglement, *i.e.* they can be written as $|\chi_i\rangle = |\mathbf{t}_i\rangle \otimes |\mathbf{s}_i\rangle \equiv |\mathbf{t}_i, \mathbf{s}_i\rangle$, where $\mathbf{t}_i$ denotes a unit vector in the valley Bloch sphere, and $\mathbf{s}_i$ denotes a unit vector in the spin Bloch sphere, in analogy with the quantum Hall ferromagnet at neutrality [38]. Given this assumption, one finds that the states which minimize the anisotropy energy, which is the expectation value of the Hamiltonian appearing Eq. (3.4), can be seperated into two classes: spin-ordered phases and valley-ordered phases. The spin ordered phases have spinors,

$$\begin{aligned} |\chi_1\rangle &= |K, \mathbf{s}_K\rangle, \quad |\chi_2\rangle = |K', \mathbf{s}_{K'}\rangle, \\ |\chi_3\rangle &= |K, -\mathbf{s}_K\rangle, \ |\chi_4\rangle = |K', -\mathbf{s}_{K'}\rangle. \end{aligned} \tag{3.16}$$

Their anisotropy energy per flux quantum computed using Eq. (2.21) can be shown to be,

$$\begin{aligned} \epsilon_a = &- V_\perp(1-\nu)\mathbf{s}_K \cdot \mathbf{s}_{K'} - V_z - V_\perp(1+\nu) \\ &- h(1-\nu_3)s^z_K - h(1-\nu_4)s^z_{K'}, \end{aligned} \tag{3.17}$$

where $\nu = \nu_3 + \nu_4$. This equation is equivalent to Eqs.(18)-(20) of Ref. [2] up to an overall constant that arises from particle-hole conjugation. Within the spin ordered phases the state that minimizes the energy depends solely on the ratio $V_\perp/h$. Three different spin ordered phases are found depending on

the value of this ratio. Without loss of generality we assume in the remainder that $\nu_3 \geq \nu_4$ and $h \geq 0$. First we have a collinear antiferromagnet (CoAFM), where the spin orientations are collinear with the Zeeman field axis, $\mathbf{s}_K = -\mathbf{e}_z$ and $\mathbf{s}_{K'} = \mathbf{e}_z$. This phase is stable for $V_\perp < 0$ and,

$$\frac{|V_\perp|}{h} \geq \frac{(1-\nu_3)(1-\nu_4)}{(1-\nu)(\nu_3-\nu_4)}, \tag{3.18}$$

and has energy $\epsilon_a = -V_z - 2\nu V_\perp - h(\nu_3 - \nu_4)$. Second we have a canted antiferromagnet (CaAFM), where the spin orientations are canted away from the Zeeman field axis in opposite directions and with different canting angles in each valley in general. This phase is stable for $V_\perp < 0$ and,

$$\frac{(1-\nu_3)(1-\nu_4)}{(1-\nu)(\nu_3-\nu_4)} \geq \frac{|V_\perp|}{h} \geq \frac{(1-\nu_3)(1-\nu_4)}{(2-\nu)(1-\nu)}, \tag{3.19}$$

the energy and canting angles of the spinors in each valley are,

$$\begin{aligned} \epsilon_a =& |V_\perp|(1+\nu) - \frac{|V_\perp|}{2}(1-\nu)\left(\frac{1-\nu_4}{1-\nu_3} + \frac{1-\nu_3}{1-\nu_4}\right) \\ & - \frac{h^2}{2|V_\perp|}\frac{(1-\nu_3)(1-\nu_4)}{(1-\nu)} - V_z, \\ s_K^z =& \frac{h(1-\nu_4)}{2|V_\perp|(1-\nu)} + \frac{|V_\perp|(1-\nu)}{2h(1-\nu_4)}\left[1 - \left(\frac{1-\nu_4}{1-\nu_3}\right)^2\right], \end{aligned} \tag{3.20}$$

and $s_{K'}^z$ can be obtained from above expression by switching labels $3 \leftrightarrow 4$. The third and last spin-ordered phase is the ferromagnet (FM), where both spins point along the Zeemann axis $\mathbf{s}_K = \mathbf{s}_{K'} = \mathbf{e}_z$, and is stable in the remaining

range of $V_\perp/h$, and has energy $\epsilon_a = -V_z - 2V_\perp - h(2-\nu)$. An important special case is when the two valleys are equally filled, *i.e.* $\nu_3 = \nu_4$. As this limit is approached the boundary to the CoAFM goes to infinity and only the CaAFM and FM phases are present. For $\nu_3 = \nu_4$ the valleys have canting angles of equal magnitude and opposite sign with respect to the Zeeman axis. Note that all transitions between the spin-ordered phases are continuous.

The second class of states, the valley ordered states, occupy spinors

$$\begin{aligned} |\chi_1\rangle &= |\mathbf{t}, \uparrow\rangle, \qquad |\chi_2\rangle = |\mathbf{t}, \downarrow\rangle, \\ |\chi_3\rangle &= |-\mathbf{t}, \uparrow\rangle, \ |\chi_4\rangle = |-\mathbf{t}, \downarrow\rangle. \end{aligned} \tag{3.21}$$

One finds two valley-ordered phases that minize the anisotropy energy. First the charge-density-wave (CDW) phase with $\mathbf{t} = \pm\mathbf{e}_z$, where the north/south poles of the Bloch sphere designate valleys K/K'. The CDW phase has energy $\epsilon_a = V_\perp(1-3\nu) - \nu V_z - h(\nu_3 - \nu_4)$. Second the Kekule-distortion (KD) phase with $t_z = 0$, and energy $\epsilon_a = V_z(1-2\nu) - 2\nu V_\perp - h(\nu_3 - \nu_4)$. The KD-CDW phase transition is first order and occurs along the line $V_\perp = V_z$. It terminates at the multicritical point $V_\perp = V_z = -h(1-\nu_3)/(2(1-\nu))$, where three phases coexist (KD-CDW-FM) for $\nu_3 > \nu_4$ and four phases coexist (KD-CDW-FM-AFM) for $\nu_3 = \nu_4$.

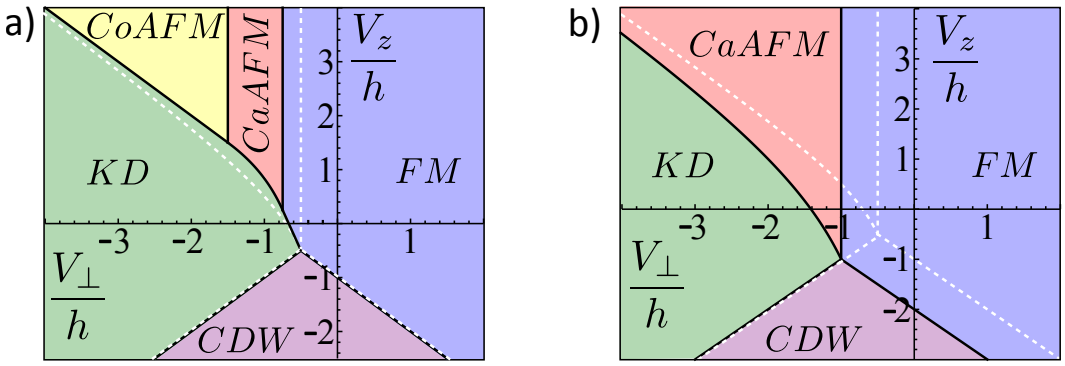

Figure 3.3: Broken symmetry phases for the state $(1, 1, 2/3, 0)$ in a), and for the state $(1, 1, 1/3, 1/3)$ in b).

3.4.3 Symmetry breaking for two-component states at $\tilde{\nu} = 4/3$ and $\tilde{\nu} = 5/3$

The anisotropic interaction has a greater impact in selecting the ground states at $\tilde{\nu} = 4/3$ and $\tilde{\nu} = 5/3$, compared to the previously discussed states at $\tilde{\nu} = 1/3$ and $\tilde{\nu} = 2/3$, which were insensitive to such short range interactions and only selected by the Zeeman term.

At $\tilde{\nu} = 4/3$ we have two candidate incompressible states, namely $(1, 1/3, 0, 0)$ and $(2/3, 2/3, 0, 0)$. To employ the results of the previous section, we perform a global particle-hole transformation into the states $(1, 1, 2/3, 0)$ and $(1, 1, 1/3, 1/3)$ respectively. An analysis of the possible ordered phases leads to the phase diagrams depicted in Fig. 3.3.

Experiments suggest canted antiferromagnetic order at $\tilde{\nu} = 2$ [79], and are consistent with $V_\perp/h \sim -10$ [2]. According to the phase diagrams in Fig. 5.1, this would imply that the $(1, 1, 2/3, 0)$ state is a collinear antiferromagnet (CoAFM) in perpendicular field measurements, whereas $(1, 1, 1/3, 1/3)$

is a canted antiferromagnet (CaAFM). We estimate that the critical field for the transition between $(1, 1, 2/3)$ and $(1, 1, 1/3, 1/3)$ states is:

$$B_c = \frac{1}{(1 - h/|V_\perp|)^2} \left(\frac{\delta\epsilon^c_{2/3}}{h} \right)^2, \tag{3.22}$$

where $\delta\epsilon^c_{2/3}$ is the Coulomb energy difference per-particle between the single component state and the singlet at $\tilde{\nu} = 2/3$ that was reported in Eq. (3.10), and all the quantities on the right hand side of this equation are understood to be evaluated at a magnetic field of 1T. In a SU(2) system like GaAs with symmetry broken only by Zeeman, the transition at $\tilde{\nu} = 2/3$ between the singlet and spin polarized states would occur at $B_c = (\delta\epsilon^c_{2/3}/h)^2$. Eq. (3.22) reduces to this expression for $h \ll |V_\perp|$ because the anisotropy energy difference between the CoAFM and CaAFM states is dominated by Zeeman energies in this limit, as can be deduced from Eq. (3.17). In graphene the ratio of Zeeman to Coulomb energies can be estimated to be

$$\frac{h}{e^2/\epsilon l} \sim 0.001\epsilon\sqrt{B[\mathrm{T}]}. \tag{3.23}$$

To account for the impact of screening at a qualitative level, we can use the RPA value of the dielectric constant of suspended graphene: $\epsilon = 1 + \pi\alpha/2 \approx 4.6$ [66]. We thus obtain the following estimate for the critical value of the perpendicular magnetic field at which the transition between the canted antiferromagnet (CaAFM) state with filling $(1, 1, 1/3, 1/3)$ into the collinear antiferromagnet (CoAFM) state with filling $(1, 1, 2/3, 0)$ occurs,

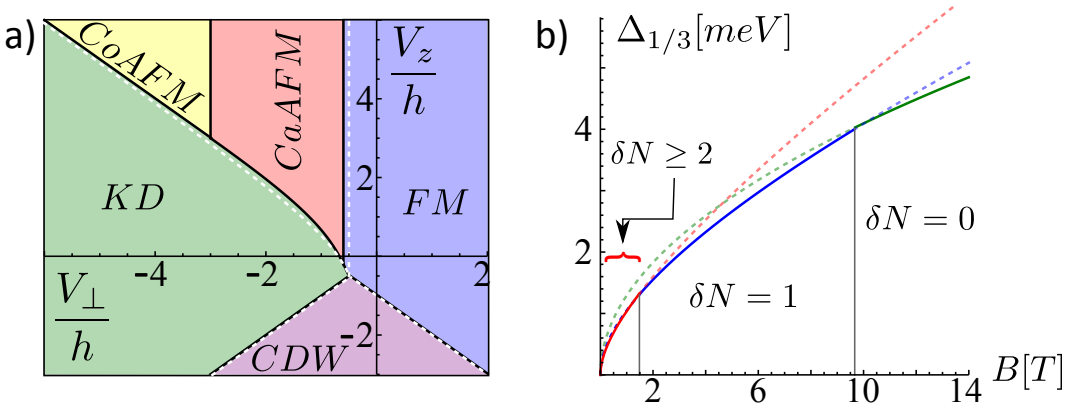

Figure 3.4: a) Broken symmetry phases for the state $(1, 1, 1/3, 0)$, b) charge gap indicating the number of spin-reversals, δN, in the quasielectron-quasihole pairs.

$$B_c = 4.7\ T \text{ for } |V_\perp|/h = 10, \tag{3.24}$$

if instead one uses $|V_\perp|/h = 5$ one gets $B_c = 6$T. These values are in agreement with the magnetic field at which a transition is observed in experiments [21]. An analysis of the gaps for the states at $\tilde{\nu} = 4/3$ indicates that the quasiparticles involve a few flavor flips, in analogy with GaAs [72].

Let us now consider the broken symmetry phases of the two component state at $\tilde{\nu} = 5/3$, whose particle-hole mirror state at $\tilde{\nu} = 7/3$ has filling vector $(1, 1, 1/3, 0)$. By applying the formulas developed in section 3.4.2 we arrive at the possible phases depicted in Fig. 3.4(a).

Let us also apply our formalism discussed in Section 2.4 to determine the charge gaps of this state. In the perpendicular field configuration the state of graphene is expected to be in the collinear antiferromagnet phase (CoAFM).

For this state there are two kinds of quasiparticles involving flavor flips. The first involves flips from the completely filled spinors. These quasiparticles have lower Coulomb energy, but considerably larger anisotropy energy and are thus likely irrelevant in experiment. We relegate the details of this discussion to Appendix C.

We will focus here on the second kind of flavor reversed quasi-particles, which involve flips between the fractionally filled and the empty spinors. In this specific case of two completely filled spinors and two fractionally filled spinors Eq. (2.25) reduces to:

$$\Delta_a = \delta N(\langle\chi_4|H_i^{HF}|\chi_4\rangle - \langle\chi_3|H_i^{HF}|\chi_3\rangle), \tag{3.25}$$

with,

$$H_i^{HF} = \sum_\sigma V_\sigma \left[\mathrm{tr}(P_i\tau_\sigma)\tau_\sigma - \tau_\sigma P_i \tau_\sigma\right] - h\sigma_z, \tag{3.26}$$

$$P_i = |\chi_1\rangle\langle\chi_1| + |\chi_2\rangle\langle\chi_2|, \tag{3.27}$$

where $\{|\chi_1\rangle, |\chi_2\rangle\}$ are the completely filled spinors, and $\{|\chi_3\rangle, |\chi_4\rangle\}$ are the fractionally filled and empty spinors in the state $(1, 1, 1/3, 0)$.

For the CoAFM state, $(1, 1, 1/3, 0)$, we can choose the completely filled spinors to be $|K, \uparrow\rangle$, $|K', \downarrow\rangle$, and the 1/3 filled spinor to be $|K', \uparrow\rangle$. The quasiparticles can lower their energy by flavor flips from the spinor, $|K', \uparrow\rangle$, into the unoccupied spinor $|K, \downarrow\rangle$. The anisotropy contribution to the gap

from Eq. (2.25) per flavor flip is simply $2h$, the conventional single spin-flip Zeeman gap. Therefore the total charge gap at $\tilde{\nu} = \{5/3, 7/3\}$ when the quasielectron-quasihole pairs involve a total of δN spin reversals is,

$$\Delta_{tot} = \Delta_{Coul}(\delta N) + 2h\delta N \tag{3.28}$$

where $\Delta_{Coul}(\delta N)$ is the contribution arising from the Coulomb energy and $2h\delta N$ is the Zeeman energy penalty for reversing spins. This is analogous to the situation of GaAs at $\tilde{\nu} = 1/3$, where one expects the quasiparticles of the Laughlin state to involve a few spin flips up to magnetic fields $\sim$ 10T [11, 15, 48, 61, 74]. Hence, it is likely that the quasiparticles of the $\tilde{\nu} = \{5/3, 7/3\}$ states in graphene involve a few spin flips as well.

Let us assess this scenario quantitatively. The conventional Coulomb gap of the Laughlin state without flavor flips is $\Delta^0_{1/3} \approx 0.1036\ e^2/\epsilon l$ [19]. The gap for a single flip corresponds to a spin-flipped quasielectron and a no-flip quasihole pair, and it is about $\Delta^1_{1/3} \approx 0.075\ e^2/\epsilon l$ [11, 15, 48, 61]. The gap for two flavor flips, $\Delta^2_{1/3}$, is known with less accuracy, but can be estimated to be lower than $\Delta^1_{1/3}$ by about $0.01\ e^2/\epsilon l$ [15, 48, 74], and it is expected to correspond to a single spin-flipped quasielectron and single spin-flipped quasihole pair. The predicted gap behavior is depicted in Fig. 3.4(b), and is in good agreement with experiment [20, 21]. Figure 3.4(b) indicates that for most of the range probed in Refs. [20, 21] the relevant quasiparticles involve a single spin flip.

3.4.4 Symmetry breaking for the three-component state at $\tilde{\nu} = 5/3$

At $\tilde{\nu} = 5/3$, in addition to the two-component Laughlin-type state described in the previuos section, there is a three component incompressible state with flavor composition $(1, 1/3, 1/3, 0)$. We will discuss in this section the possible symmetry breaking patterns that minimize the anisotropy energy of this state.

We assume again that these states have no valley-spin entanglement, and thus that the occupied spinors have the form $|\chi_i\rangle = |\mathbf{t}_i\rangle \otimes |\mathbf{s}_i\rangle \equiv |\mathbf{t}_i, \mathbf{s}_i\rangle$, where $\mathbf{t}_i$ denotes a unit vector in the valley Bloch sphere, and $\mathbf{s}_i$ denotes a unit vector in the spin Bloch sphere. With this restriction, we find *seven* phases that minimize the anisotropy energy for different values of the symmetry breaking parameters. They fill spinors: (a) $|K,\uparrow\rangle$, $|K',\downarrow\rangle$, $|K',\uparrow\rangle$; (b) $|\mathbf{t}_\perp,\uparrow\rangle$, $|-\mathbf{t}_\perp,\uparrow\rangle$, $|-\mathbf{t}_\perp,\downarrow\rangle$; (c) $|K,\uparrow\rangle, |K,\downarrow\rangle, |K',\uparrow\rangle$; (d) $|K,\mathbf{s}_1\rangle, |K',\mathbf{s}_2\rangle, |K,-\mathbf{s}_1\rangle$; (e) $|\mathbf{t},\uparrow\rangle, |K,\downarrow\rangle, |K',\downarrow\rangle$; (f) $|\mathbf{t}_\perp,\mathbf{s}_1\rangle, |-\mathbf{t}_\perp,\mathbf{s}_2\rangle, |\mathbf{t}_\perp,-\mathbf{s}_1\rangle$; (g) $|\mathbf{t}_\perp,\uparrow\rangle, |-\mathbf{t}_\perp,\uparrow\rangle, |\mathbf{t}_\perp,\downarrow\rangle$. In this listing the first spinor is understood to be fully filled and the other two to be fractionally filled, $\mathbf{t}_\perp$ is a unit vector on the equator of the valley Bloch sphere, $\mathbf{t}$ is an arbitrary unit vector on the valley Bloch sphere, and $\{\mathbf{s}_1, \mathbf{s}_2\}$ are unit vectors in the spin Bloch sphere. Any of the listed states with definite valley numbers is understood to have the $\mathbb{Z}_2$ valley interchange symmetry $K \leftrightarrow K'$, and we have listed only one of its realizations.

The anisotropy energy per flux quantum of these phases are,

$$
\begin{aligned}
&(a)\ \epsilon_a = -\frac{2}{3}(V_z + V_\perp) - h, \\
&(b)\ \epsilon_a = -\frac{1}{3}(V_z + 3V_\perp) - h, \\
&(c)\ \epsilon_a = -\frac{2}{3}V_\perp - h, \\
&(d)\ \epsilon_a = \frac{1}{12}V_\perp + \frac{1}{3}\frac{h^2}{V_\perp}, \\
&(e)\ \epsilon_a = -\frac{h}{3}, \\
&(f)\ \epsilon_a = \frac{1}{24}(V_z + V_\perp) + \frac{2}{3}\frac{h^2}{(V_z + V_\perp)}, \\
&(g)\ \epsilon_a = -\frac{1}{3}(V_z + V_\perp) - h.
\end{aligned}
\tag{3.29}
$$

Phases (d) and (f) have spins canted away from the Zeeman field. The projection of the spins along the Zeeman axis are

$$
s_z = \frac{h}{2|V_\perp|} + \frac{3|V_\perp|}{8h}, \quad s_{2z} = \frac{h}{|V_\perp|} - \frac{3|V_\perp|}{4h}. \tag{3.30}
$$

for phase (d) and

$$
\begin{aligned}
s_z &= \frac{h}{|V_z + V_\perp|} + \frac{3|V_z + V_\perp|}{16h}, \\
s_{2z} &= \frac{2h}{|V_z + V_\perp|} - \frac{3|V_z + V_\perp|}{8h}.
\end{aligned}
\tag{3.31}
$$

for phase (f).

The phase diagram obtained by comparing the energies of these states depicted in Fig. 3.5. The dashed lines in Fig. 3.5 depict the boundaries of the

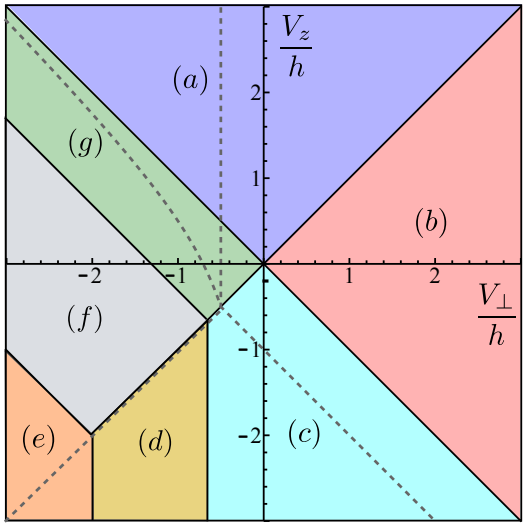

Figure 3.5: (Color online) Phase diagram of three component state $(1, 1/3, 1/3, 0)$. See text for description of the labels. The dashed lines correspond to the phase boundaries for the integer quantum Hall ferromagnet realized at neutrality [38].

ordered phases of the integer quantum Hall ferromagnet described in Ref. [38]. An important observation is that, given that the ground state of the integer quantum Hall ferromagnet is likely to be in the canted antiferromagnetic phase [79] and that $V_\perp \sim -10h$ [2], the three component state that competes with the two component Laughlin-type $(1, 2/3, 0, 0)$ collinear antiferromagnet state is likely to be in phase (a). This is true except for an extremely small region in the $V_\perp, V_z, h$ parameter space close to the boundary between the (g) and (a) phase in Fig. 3.5 (see also Fig. 3.4(a)).

Chapter 4

Quantum Hall regime in bilayer graphene

4.1 Experiments on FQHE in bilayer graphene

At the moment of writing this dissertation four experimental groups have reported the observation of FQH states in bilayer graphene [5, 39, 40, 49]. The observations are substantially distinct from each other, suggesting a special sensitivity to specific experimental conditions for bilayer graphene. This offers the potential for exploring the FQH by tunning several physical parameters. But in order to achieve control over them it is necessary to gain better understanding of the low-energy physics to be able *tame* this variability.

The observations made so far are quite rich. Reference [39] reported a FQH state at $\nu = -1/2$ and an incipient state at $\nu = -5/2$. These states have been argued to be a realization of the Moore-Read Pffafian phase [57]. If so, this would be the second instance in which this kind of non-Abelian FQH state is realized, the other one being at $\nu = 5/2$ in the 2DES of GaAs [73]. The samples in Ref. [39] were suspended and the FQH states were detected via four terminal transport measurements. Essentially all of the FQH states in this study were detected in the hole side (i.e. for a net number of electrons removed from neutral bilayer graphene), except for an incipient FQH state at $\nu = 2/3$. The

fractions observed in this study were $\{-5/2, -8/5, -4/3, -2/3, -1/2, 2/3\}$.

Reference [40] reported a FQH states occuring at $\nu = \{n+2/3, n+3/5\}$, with $n = \{-4, -2, 0, 2\}$. Remarkably a large gap of about 25meV was found at neutrality $\nu = 0$, which was present at zero magnetic field and was nearly independent of the magnetic field strength. The samples in Ref. [40] were on a boron-nitride substrate. This implies an asymmetry between bottom and top layers which could be the source of this large gap[1]. The FQH states were detected via local compressibility measurements in this study. An additional noteworthy aspect was the lack of electron-hole symmetry $\nu \to -\nu$. Although electron-hole asymmetries are commonly detected in transport measurements and are associated with extrinsic effects, the great degree of electron-hole symmetry achieved in similar compressibility measurements on monolayer graphene [20, 21] indicates that this result is not a measurement artifact.

Several authors have *incorrectly* argued this electron-hole asymmetry to naturally arise from the near degeneracy of $n = 0$ and $n = 1$ cyclotron wavefunctions in the neutral Landau level of bilayer graphene. Indeed, the properly projected interaction Hamiltonian into the neutral Landau level which includes all the leading terms in degenerate perturbation theory would contain the exchange interaction with the negative energy sea. This term produces a splitting of the $n = 0$ and $n = 1$ states, which favors $n = 1$ states, and it is

[1]Monolayer graphene samples on boron-nitride have also displayed large gaps at zero magnetic field [32, 60, 75], however, these were samples with near commensurability of the graphene and boron-nitride honeycomb lattices giving rise to moire-pattern superlattices.

necessary to restore electron-hole symmetry, as was originally pointed out by Shizuya [63]. As will be shown in this chapter one would expect this symmetry to be exact to all orders in perturbation theory, provided the original lattice model of bilayer graphene has an exact particle-hole symmetry. Therefore, it is likely that the origin of this electron-hole asymmetry is intrinsic and arises from the terms that explicitly break electron-hole symmetry in the microscopic lattice model.

More recently in Ref. [49] transport measurements were performed on bilayer graphene encapsulated in boron-nitride. The encapsulation reduces the asymmetry between top and bottom layers that is present when boron-nitride serves only as the substrate. The devices were dual-gated which allowed for an independent control of the the electron density and the interlayer displacement field in the graphene bilayer. The control over the displacement field allowed for the tunning of phase transitions between integer and fractional quantum Hall states with different layer polarizations. Similar observations were also reported in the studies of Ref. [44] for the integer quantum Hall ferromagnets of bilayer graphene.

4.2 Particle-hole symmetry in the minimal two-band model for bilayer graphene

In this section we will illustrate that particle symmetry is expected in bilayer graphene if one employs the conventional two-band model. The main purpose of this section is to illustrate that this symmetry remains in

the presence of a magnetic field, but to see it requires the proper inclusion of the exchange interaction with the negative energy which produce a splitting between the the $n = 0$ and $n = 1$ states.

We concentrate here in the study of AB stacked bilayer graphene (also known as Bernal stacked bilayer graphene). The low energy dispersion of electrons can be described within a continuum two-band model on which the sublattice low energy states reside in opposite layers [50],

$$H_K = \begin{pmatrix} u/2 & -(\pi_x - i\pi_y)^2/2m \\ -(\pi_x + i\pi_y)^2/2m & -u/2 \end{pmatrix}, \ \pi = p + eA/c, \tag{4.1}$$

where the matrix elements are in top and bottom layer/sublattice indices, u is an interlayer bias, and $H_{K'} = H_K^T$. We have also ignored the trigonal warping term. In the presence of a magnetic field the single particle spectrum is,

$$E_{nK} = u/2, \ n = 0, 1 \tag{4.2}$$

$$E_{nK} = u/2 + sign(n)\sqrt{\omega_c^2|n|(|n| - 1) + u^2/4}, \ |n| \geq 2, \tag{4.3}$$

where $n = -\infty, ..., -2, 0, 1, 2, ..., \infty$, $\omega_c = eB/mc$. The single particle states associated with these levels are:

$$\psi_{nK} = \begin{pmatrix} \phi_n \\ 0 \end{pmatrix}, \ n = \{0, 1\}, \tag{4.4}$$

$$\psi_{nK} = \begin{pmatrix} \cos(\theta_n/2) \ \phi_{|n|} \\ \sin(\theta_n/2) \ \phi_{|n|-2} \end{pmatrix}, \ n \leq -2, \quad \psi_{nK} = \begin{pmatrix} -\sin(\theta_n/2) \ \phi_{|n|} \\ \cos(\theta_n/2) \ \phi_{|n|-2} \end{pmatrix}, \ n \geq 2, \tag{4.5}$$

$$\cos(\theta_n) = \frac{u/2}{\sqrt{\omega_c^2 |n|(|n|-1) + u^2/4}}, \ \sin(\theta_n) = \frac{\omega_c \sqrt{|n|(|n|-1)}}{\sqrt{\omega_c^2 |n|(|n|-1) + u^2/4}}, \tag{4.6}$$

and the eigenvalues for the opposite valley are:

$$\psi_{nK'} = \begin{pmatrix} 0 & 1 \\ 1 & 0 \end{pmatrix} \psi_{nK}^{u \to -u}, \ E_{nK'} = E_{nK}^{u \to -u}, \tag{4.7}$$

where ϕ_n are the conventional cyclotron eigenstates for Galilean particles. Therefore the neutral landau level of bilayer graphene is eight-fold degenerate when spin is included. The single particle states would be labeled by $|n, v, s\rangle$, with $n = 0, 1$, $v = K, K'$, $s = \uparrow, \downarrow$, in addition to the intra-Landau level guiding center numbers. The sublattice degree of freedom, which in this case is equivalent to a layer index, becomes locked to the valley number in the neutral Landau level, in an analogous fashion to monolayer graphene. In this work we will focus on the properties on this neutral nearly eight-fold degenerate Landau level.

Particles will interact via two-body forces. A parameter that justifies a controlled projection onto the zero energy Landau level is the ratio of the Coulomb interaction to the cyclotron energy $\kappa = e^2/\omega_c \epsilon l$ [8, 53, 59, 64, 67]. I will describe the projected interaction Hamiltonian into the neutral Landau

level next. This follows the spirit of degenerate perturbation theory, in which the projected Hamiltonian can be argued to produce correct results in the first order in the κ expansion.

In second quantization the unprojected interaction Hamiltonian is,

$$V = \frac{1}{2} \sum_{All} v(1;2|3;4) c^{\dagger}_{n_1 v_1 m_1} c^{\dagger}_{n_2 v_2 m_2} c_{n_3 v_2 m_3} c_{n_4 v_1 m_4}. \tag{4.8}$$

Here $v(1;2|3;4)$ is a short-hand for the matrix elements of the two-body interaction in the single particle basis that diagonalizes the kinetic term in the presence of magnetic field. We are so far considering only the part of the interaction that is valley and sublattice independent.

To project the Hamiltonian is not sufficient to simply restrict all the Landau level indices to be in the neutral Landau level. To leading order in κ one must include all terms that do not involve changes in the kinetic energy of the electrons. These include the exchange interactions with the completely filled negative energy sea [67]. In the context of Galilean Landau levels these terms give rise simply a global shift of the chemical potential of the Landau level in question, and hence have a trivial role in the intra-Landau level energetics. In the present context, however, they will have the non-trivial consequence of producing different shifts to the single particle energies of the $n = 0$ and $n = 1$ orbitals [30, 63]. The projected interaction Hamiltonian is thus:

$$PVP = \bar{V} + X^{-} = \frac{1}{2} \sum_{n\in\{0,1\}} v(1;2|3;4)\ c^{\dagger}_{n_1,v_1,m_1} c^{\dagger}_{n_2,v_2,m_2} c_{n_3,v_2,m_3} c_{n_4,v_1,m_4} - \sum_{n_{1,4}\in\{0,1\},n_3\leq -2} v(3;1|3;4)\ c^{\dagger}_{n_1,v_1,m_1} c_{n_4,v_1,m_4}, \quad (4.9)$$

where the second term, X^{-}, is the aforementioned exchange field generated by the negative energy sea with $n \leq -2$, and the Hartree term vanishes because of the neutralizing background. The invariance of the completelly filled negative energy sea under magnetic translations and rotations implies that this exchange field is diagonal and independent of the intra-Landau level indices. It can be shown to have three contributions which is convenient to distinguish:

$$X^{-} = X_0 + X_1 + X_2. \quad (4.10)$$

The first contribution, X_0 reads as,

$$X_0 = -\mu_0 \sum_{n\in\{0,1\}} c^{\dagger}_{nvm} c_{nvm},\ \mu_0 = -\frac{1}{2A} \sum_q v_q \quad (4.11)$$

This contribution is the shift of the Dirac point in the presence of interactions, which is determined by the on-site Hubbard type energy $U_0 = \frac{1}{A}\sum_q v_q$. It is independent of the magnetic field and its origin can be more transparently understood in the Lattice model as I will illustrate in the next section. It produces a simple global shift of the chemical potential of no interest for the present discussion.

The second contribution, X_1, is:

$$X_1 = \mu_1 \sum (c^\dagger_{0vm} c_{0vm} + c^\dagger_{1vm} c_{1vm}) + \Delta_1 \sum (c^\dagger_{0vm} c_{0vm} - c^\dagger_{1vm} c_{1vm}), \quad (4.12)$$

$$\mu_1 = \frac{11e^2}{16\epsilon l}\sqrt{\frac{\pi}{2}}, \quad \Delta_1 = \frac{e^2}{16\epsilon l}\sqrt{\frac{\pi}{2}}. \quad (4.13)$$

This term contains the splitting between the $n = 0$, $n = 1$ orbitals, which has the effect of favoring the $n = 1$ orbitals. This term is the same as that appearing in Eq.(4.10) of Ref. [30]. We will sometimes refer to this as the Shizuya term below.

The third contribution, X_2, is:

$$X_2 = \sum \xi_n (c^\dagger_{nKm} c_{nKm} - c^\dagger_{nK'm} c_{nK'm}), \quad (4.14)$$

$$\xi_0 = -\frac{e^2}{\epsilon l} \sum_{n=2}^{\infty} \frac{\Gamma(n+1/2)}{\sqrt{2}n!} \cos(\theta_n) \ , \quad (4.15)$$

$$\xi_1 = -\frac{e^2}{\epsilon l} \sum_{n=2}^{\infty} \frac{(n-1/4)\Gamma(n-1/2)}{\sqrt{2}n!} \cos(\theta_n). \quad (4.16)$$

This term will favor $n = 0$ in one valley and $n = 1$ in the opposite valley, and would vanish when the interlayer bias vanishes $u = 0$.

Now consider a particle-hole transformation applied to Eq. (4.18), in which labels for particles are exchanged by holes in the neutral Landau level:

$$C^\dagger c^\dagger_{nvm} C = c_{nvm}. \quad (4.17)$$

The interaction hamiltonian changes into,

$$C^\dagger \bar{V} C = \bar{V} + \sum_{n\in\{0,1\}} v(3;1|3;4)\ c^\dagger_{n_1,v_1,m_1} c_{n_4,v_1,m_4} + \text{const} \tag{4.18}$$

$$C^\dagger X^- C = -X^- + \text{const} \tag{4.19}$$

therefore the particle-hole transformation generates an additional one body term and changes the sign of the exchange field with the vacuum. However, the newly generated one body term can be shown to be:

$$\sum_{n\in\{0,1\}} v(3;1|3;4)\ c^\dagger_{n_1,v_1,m_1} c_{n_4,v_1,m_4} = -2X_1 \tag{4.20}$$

Therefore,

$$C^\dagger(\bar{V} + X^-)C = \bar{V} - X_0 + X_1 - X_2 + \text{const.} \tag{4.21}$$

When the interlayer bias vanishes, $u = 0 \Rightarrow X_2 = 0$. In this case C is an exact particle-hole symmetry between $\nu \to -\nu$ in bilayer graphene, since the change of the global chemical potential from X_0 has a trivial impact in the energetics, in particular the charge gaps satisfy:

$$\Delta(\nu) = \Delta(-\nu). \tag{4.22}$$

At zero bias the swap of valleys is also an exact symmetry:

$$P^\dagger c^\dagger_{nvm} P = c_{n\bar{v}m}. \tag{4.23}$$

This is no longer a symmetry at finite bias u, and neither is C by itself. However, their product CP remains a symmetry,

$$(CP)^\dagger(\bar{V} + X^-)CP = \bar{V} - X_0 + X_1 + X_2 + \text{const.} \tag{4.24}$$

Implying an exact symmetry between electron and hole gaps in bilayer graphene at finite bias: $\Delta(\nu) = \Delta(-\nu)$. So far we have not discussed the presence of spin and the Zeeman term. In this case the operation needs to swap the spins as well in order to be a symmetry: $P^\dagger c^\dagger_{nvsm} P = c_{n\bar{v}\bar{s}m}$.

4.3 Particle-hole conjugation symmetries in the lattice

In this section we will demonstrate that the particle-hole symmetry, $\nu \to -\nu$, is as consequence of the underlying particle-hole symmetry of the microscopic lattice Hamiltonian. A crucial conclusion of the discussion in the lattice model is that the particle-hole symmetry is exact in a non-perturbative sense, and it is not restricted to a particular order of perturbation theory such as the leading order of κ which is implicitly assumed in the models of the interaction Hamiltonian projected to lowest Landau level. This is also an important difference with respect to the Landau levels in parabolic band systems like GaAs, where the particle-hole symmetry is only valid to leading order in κ. The exact lattice particle-hole symmetry has important consequences in per-

turbation theory such as the absence of certain three-body interaction terms in the neutral Landau level of monolayer [59] and bilayer graphene, which are expected to be present in GaAs.

As we will see, it is actually easier to demonstrate the particle-hole invariance in the lattice model. In particular we will find that, if the Hamiltonian is particle-hole invariant in the absence of a magnetic field, the product of particle-hole conjugation and time reversal will remain an exact symmetry in the presence of magnetic field. In other words, there is no reason to expect that a system will cease to be particle-hole symmetric by the action of a quantizing magnetic field.

4.3.1 Particle-hole symmetries of single particle terms

Consider a bipartite lattice whose hopping terms link only sites in opposite sublattices:

$$K_0 = -\sum_{ij} t_{ij} c^\dagger_{i\sigma} c_{j\sigma} \tag{4.25}$$

where i denotes lattice sites and σ spin. These lattice models include monolayer graphene without second nearest neighbor hopping, and bilayer graphene with no intralayer hopping terms between the same sublattice and no interlayer hopping terms between A and A' sites or B and B' sites. For completeness, in the remainder of this section we will deal with both cases: monolayer and bilayer graphene. Asumme t_{ij} to be real, then hermiticity implies $t_{ij} = t_{ji}$. This

Hamiltonian posseses time-reversal and particle-hole conjugation symmetries, whose action respectively is:

$$T\ zc_{i\sigma}\ T^{-1} = z^* c_{i\bar{\sigma}}, \tag{4.26}$$

$$C\ c_{i\sigma}\ C^\dagger = (-1)^{s_i} c^\dagger_{i\sigma}, \tag{4.27}$$

where z is any complex number, and $s_i = \{0, 1\}$ for sites on sublattices $\{A, B\}$ respectively (in bilayer we can think of the pairs AA' and BB' as the being in the same sublattice, i.e. $s_i = 0$ for $i \in \{A, A'\}$ and $s_i = 1$ for $i \in \{B, B'\}$). Namely we have:

$$TK_0T^{-1} = K_0, \quad CK_0C^\dagger = K_0. \tag{4.28}$$

In the pressence of a magnetic field the hoppings become complex: $t_{ij} \rightarrow t_{ij} \exp(ie/\hbar \int_{r_i}^{r_j} A(r) \cdot dl)$. Generically the magnetic field would break both symmetries separately, however, their product remains a symmetry:

$$(CT)^{-1} K_A\ CT = K_A. \tag{4.29}$$

In other words there exists a symmetry that exchanges particles and holes, namely CT, that remains intact as the magnetic field is increased provided it is a symmetry at zero field (indeed CT is a good symmetry even when the original hoppings are complex).

When there is a bias between the two sublattices an additional parity operation is needed to construct a particle-hole symmetry. The honeycomb lattice of monolayer graphene has an inversion center at the middle point of the line that joins any two nearest-neighbor carbons. This inversion swaps sublattices and it also inverts real space coordinates about such point. Let us denote by r the position of a unit cell containing two nearest neighbor carbons. Single particle states in lattice site basis can thus be labeled with r, α, σ, with $\alpha = \{A, B\}$ denoting the sublattice within a unit cell, and σ the spin. Then consider the space inversion operation,

$$P^\dagger c_{r\alpha\sigma} P = c_{-r,\bar{\alpha},\sigma}. \tag{4.30}$$

Consider a staggered sublattice potential (which gives rise to the term in Eq. (3.5)):

$$\Delta_T T_Z = \Delta_T \sum_{r\sigma} (c^\dagger_{rA\sigma} c_{rA\sigma} - c^\dagger_{rB\sigma} c_{rB\sigma}) \tag{4.31}$$

This term is odd under the action of P and C, and therefore invariant under their product CP. It is also invariant under time reversal, and hence under CPT. The kinetic term is also invariant under P, therefore the combined symmetry CPT is an exact particle-hole symmetry of the single particle Hamiltonian in the presence of magnetic field. This is also true when the Zeeman term, $\Delta_Z S_Z$, is present. Therefore:

$$(CPT)^{-1}(K_A + \Delta_T T_Z + \Delta_Z S_Z)CPT = K_A + \Delta_T T_Z + \Delta_Z S_Z \tag{4.32}$$

For bilayer graphene we can have a potential that biases the top layer with respect to bottom layer:

$$\Delta_T T_Z = \Delta_T \sum_{r\sigma} (c^\dagger_{rA\sigma} c_{rA\sigma} + c^\dagger_{rB\sigma} c_{rB\sigma} - c^\dagger_{rA'\sigma} c_{rA'\sigma} - c^\dagger_{rB'\sigma} c_{rB'\sigma}) \tag{4.33}$$

This potential is odd under the inversion about the inversion center right in the middle of the line joining the sites that are directly located on top of each other. This inversion swaps top and bottom layers and inverts real space as well,

$$P^\dagger c_{rA\sigma} P = c_{-r,B',\sigma},\ P^\dagger c_{rB\sigma} P = c_{-r,A',\sigma}. \tag{4.34}$$

T_Z is also odd under the action of C, therefore CP is a symmetry of bilayer graphene. And much like in monolayer we have an exact CPT symmetry for the single-particle Hamiltonian in the same form of Eq. (4.32).

However, in bilayer graphene, an onsite energy that distinguishes the sites that are directly on top of each other from those that are not is odd under CPT. Namely the term:

$$\Delta_U U_Z = \Delta_U \sum_{r\sigma} (c^\dagger_{rA\sigma} c_{rA\sigma} + c^\dagger_{rB'\sigma} c_{rB'\sigma} - c^\dagger_{rA'\sigma} c_{rA'\sigma} - c^\dagger_{rB\sigma} c_{rB\sigma}), \tag{4.35}$$

transfroms as:

$$(CPT)^{-1}\Delta_U U_Z CPT = -\Delta_U U_Z. \tag{4.36}$$

These terms have been argued to be present in addition to second nearest neighbor hopping terms which are also odd under CPT [35, 42, 56, 62, 81]. As we will discuss in the next section, these two kinds of terms are likely to be responsible for the particle-hole asymmetry observed in the experiments of Ref. [40].

Another term that respects the CPT symmetry is one in which a staggered potential is added to each layer:

$$\Delta_V V_Z = \Delta_V \sum_{r\sigma} (c^\dagger_{rA\sigma} c_{rA\sigma} + c^\dagger_{rA'\sigma} c_{rA'\sigma} - c^\dagger_{rB'\sigma} c_{rB'\sigma} - c^\dagger_{rB\sigma} c_{rB\sigma}), \tag{4.37}$$

namely,

$$(CPT)^{-1}\Delta_V V_Z CPT = \Delta_V V_Z. \tag{4.38}$$

In particular it is plausible that if bilayer graphene is closely aligned with a boron-nitride substrate a staggered potential acting on the bottom layer would be present. Let us for the moment ignore the lattice mismatch between graphene and boron-nitride. Then such potential would be of the form

$$V_{subs} = \Delta_{subs} \frac{U_Z + V_Z}{2}, \tag{4.39}$$

Therefore, this potential has odd and even components under the action of CPT, namely U_Z and V_Z, and will not respect this symmetry:

$$(CPT)^{-1} V_{subs} CPT = \Delta_{subs} \frac{-U_Z + V_Z}{2}. \tag{4.40}$$

This term therefore would give rise to additional particle-hole asymmetries.

We have considered several types of staggered potentials which have zero average on the full lattice. If a potential has a finite average, this can be absorbed into a global chemical potential shift, which is always odd under the CPT transformation. This however does not mean that the CPT is not a good symmetry in the presence of a chemical potential shift since the effect of such term is trivial in the energetics. In particular, if N_L is the total number of states in a finite lattice, CPT will map the number of particles as $N \to N_L - N$. Thus the fact that the global chemical potential changes sign does not alter the spectrum of the problem at a given total number of particles but simply produces a global energy shift. In particular it follows that the neutral excitation energies, i.e. those that are defined as many-body energies after subtracting the energy of the ground state of reference, are unaltered. Under the action of CPT quasi-holes will turn into quasi-electrons and viceversa, but the charge gaps would be left invariant.

4.3.2 Particle-hole symmetries of interactions terms

The full unprojected interaction Hamiltonian is independent of magnetic field. Let us start from the most general spin-independent interaction in

the lattice model:

$$V = \frac{1}{2} \sum U(ij;kl)\ c^\dagger_{i\sigma} c^\dagger_{i\sigma'} c_{k\sigma'} c_{l\sigma}. \tag{4.41}$$

Under the action of CT four terms are generated:

$$CT\ V\ (CT)^{-1} = \tag{4.42}$$

$$\frac{1}{2} \sum U(ij;kl)(-1)^{s_i+s_j+s_k+s_l}\ c^\dagger_{i\sigma} c^\dagger_{i\sigma'} c_{k\sigma'} c_{l\sigma} \tag{4.43}$$

$$- g_s \sum U(jk;ki)(-1)^{s_i+s_j}\ c^\dagger_{j\sigma} c_{i\sigma} \tag{4.44}$$

$$+ \sum U(kj;ki)(-1)^{s_i+s_j}\ c^\dagger_{j\sigma} c_{i\sigma} \tag{4.45}$$

$$+ \frac{g_s}{2} \sum [g_s U(ij;ji) - U(ij;ij)], \tag{4.46}$$

g_s is the spin degeneracy, and the only properties invoked to arrive at above result are the indistinguishability of particles $U(ij;kl) = U(ji;lk)$ and hermiticity $U(ij;kl)^* = U(lk;ji)$. The first term is a genuine interaction. The second and third are hopping terms because of lattice translational symmetry. The last term is the interaction energy of the completely filled lattice which is simply a constant.

In order for CT to be a good transformation the following condition must be satisfied:

$$U(ij;kl)(-1)^{s_i+s_j+s_k+s_l} = U(ij;kl). \tag{4.47}$$

In other words, all the non-vanishing matrix elements of $U(ij;kl)$ must have an even number of legs in each sublattice. This immediately implies a simplification of the Hartree and Fock terms: $U(jk;ki)(-1)^{s_i+s_j} = U(jk;ki)$, $U(kj;ki)(-1)^{s_i+s_j} = U(kj;ki)$. This constraint also implies that their associted effective hoppings are either between sites in the same sublattice, namely a global chemical potential shift, or hoppings that are non-vanishing starting at the second nearest neighbor distance (in the taxi-cab distance defined by t_{ij} in general, but in particular in the sense of true distance in monolayer and Bernal bilayer graphene).

Therefore, generically the new hoppings would destroy the CT symmetry. A sufficient condition to retain CT as a symmetry is that the lattice orbitals interact the way point-like objects do: $U(ij;kl) = \delta_{il}\delta_{jk}U(ij;ji)$. Under this assumption the Hamiltonian is invariant under CT up to a global chemical potential shift and an overall constant:

$$CT\ V\ (CT)^{-1} = V - \lambda N + V_{full}, \tag{4.48}$$

$$\lambda = -U(ii;ii) + g_s \sum_k U(ik;ki), \tag{4.49}$$

$$V_{full} = \frac{g_s}{2} \sum [g_s U(ij;ji) - U(ij;ij)]. \tag{4.50}$$

The chemical potentials for addition and removal of particles are: $\mu_N^+ = E_{N+1} - E_N$ and $\mu_N^- = E_N - E_{N-1}$, where E_N is the ground state energy of N particles. The charge gap is $\Delta_N = \mu_N^+ - \mu_N^-$. Among many other consequences the CT symmetry implies:

$$\mu^{+}_{N_L-N} = -\mu^{-}_{N} + \lambda, \tag{4.51}$$

$$\mu^{-}_{N_L-N} = -\mu^{+}_{N} + \lambda, \tag{4.52}$$

$$\Delta_{N_L-N} = \Delta_N. \tag{4.53}$$

where $N_L = \sum_{i\sigma} 1$ is the total number of single-particle states in the lattice.

An interesting observation is that when the system is gappless the chemical potential at neutrality is $\mu^{\Delta=0}_{N_L/2} = \lambda/2$. This is the position of the Dirac point in the presence of interactions. It is remarkable that this position depends only on the onsite Hubbard-like term after subtracting the neutralizing background energy,

$$\mu^{\Delta=0}_{N_L/2} = -\frac{U(ii;ii)}{2}. \tag{4.54}$$

This can be thought of as the binding energy of electrons to the lattice. This is the meaning of the X_0 correction described previously in the continuum model in Eq. (4.11).

Since the space inversions considered in the previous section, denoted by P, are also symmetries of the interaction Hamiltonian, it follows that, for the model of interactions here considered, CPT will be a symmetry of the full Hamiltonian provided it is a symmetry of the single-particle terms described in the previous section.

4.4 Low energy theory of bilayer graphene with explicit particle-hole symmetry breaking terms

The two previous sections have illustrated that particle-hole asymmetries between states at ν and $-\nu$, must originate from the microscopic terms in the lattice models. These terms have been recently estimated from atomistic density-functional theory-calculations in Ref. [35] which we will use to explain the particle hole asymmetries observed in bilayer graphene.

4.4.1 Two-band model with explicit particle-hole symmetry breaking terms

We begin by deriving the low energy two-band model that descends from the four-band model obtained in Ref. [35] by fitting the results of density functional with a tight-binding model that includes explicitly particle-hole symmetry breaking terms. After a dummy swap of rows and colums in Eq.(26) of Ref. [35], the four band model effective Hamiltonian for valley K is:

$$\begin{aligned} H_K^{4b} &= \begin{pmatrix} u/2 & -v_3\pi & v\pi^\dagger & -v_4\pi^\dagger \\ -v_3\pi^\dagger & -u/2 & -v_4\pi & v\pi \\ v\pi & -v_4\pi^\dagger & u/2+\Delta & t_1 \\ -v_4\pi & v\pi^\dagger & t_1 & -u/2+\Delta \end{pmatrix} \\ &= \begin{pmatrix} H_{00} & H_{01} \\ H_{10} & H_{11} \end{pmatrix}. \end{aligned} \tag{4.55}$$

where the matrix columns correspond to A, B', B, A' sites respectively. In this model the terms that break the particle hole symmetry are v_4 and Δ. $v_4 = t_4\sqrt{3}a/2\hbar \approx 4.47 \times 10^4$ m/s, is proportional to the hopping amplitude t_4

which connects the A and A' sites in opposite layers (and B and B' sites), with $a = 2.46$Åis the lattice constant of monolayer graphene [35]. $\Delta \approx 0.015$eV is an onsite energy that produces a small penalty for electrons to occupy the sites that are directly on top of each other [35]. These term thus breaks the electron-hole symmetry explicitly according to the discussion of the previous section.

Let us now construct the effective two-band model that descends from this four-band model with explicit particle-hole symmetry breaking terms. An equivalent non-linear eigenvalue problem for the projected wavefunction into the A, B' low energy sites is:

$$\left(H_{00} + H_{01}\frac{1}{E - H_{11}}H_{10}\right)\phi_0 = E\phi_0. \tag{4.56}$$

In order to turn this into a conventional eigenvalue problem we would like to set $E = 0$ in the energy denominator. To be able to do this we must resort to the approximation that we are only interested in the leading corrections to the eigenenergies in the dimensionless parameters: $(v|\pi|/t_1, v_4|\pi|/t_1, u/t_1, v_3|\pi|/t_1)$. This leads to the following eigenvalue problem:

$$\left(H_{00} - H_{01}\frac{1}{H_{11}^{u=0}}H_{10}\right)\phi_0 = E\phi_0. \tag{4.57}$$

It is important to set $u = 0$ in H_{11}. If we don't do this, we would be including some terms of order $u|v\pi|^2/t_1^3$, but not all them, since we have already neglected

terms of order u coming from the energy denominator and thus their inclusion would not be systematic. The effective low energy two-band model is therefore:

$$\begin{aligned} H_K^{2b} = &\begin{pmatrix} u/2 & 0 \\ 0 & -u/2 \end{pmatrix} - v_3 \begin{pmatrix} 0 & \pi \\ \pi^\dagger & 0 \end{pmatrix} \\ &-\frac{1}{2m_0}\begin{pmatrix} 0 & \pi^{\dagger 2} \\ \pi^2 & 0 \end{pmatrix} + \frac{1}{2m_1}\begin{pmatrix} \pi^\dagger\pi & 0 \\ 0 & \pi\pi^\dagger \end{pmatrix}, \end{aligned} \tag{4.58}$$

with:

$$\begin{aligned} \frac{1}{2m_0} &= \frac{t_1(v^2+v_4^2)+2\Delta v v_4}{t_1-\Delta^2}, \\ \frac{1}{2m_1} &= \frac{\Delta(v^2+v_4^2)+2t_1 v v_4}{t_1-\Delta^2}. \end{aligned} \tag{4.59}$$

For the K' valley we have $H_{K'}^{4b} = [H_K^{4b}(v \to -v, v_4 \to -v_4, v_3 \to -v_3)]^T$. The effective two-band hamiltonian for valley K' is therefore:

$$\begin{aligned} H_{K'}^{2b} = &\begin{pmatrix} u/2 & 0 \\ 0 & -u/2 \end{pmatrix} + v_3 \begin{pmatrix} 0 & \pi \\ \pi^\dagger & 0 \end{pmatrix} \\ &-\frac{1}{2m_0}\begin{pmatrix} 0 & \pi^{2} \\ \pi^{\dagger 2} & 0 \end{pmatrix} + \frac{1}{2m_1}\begin{pmatrix} \pi\pi^\dagger & 0 \\ 0 & \pi^\dagger\pi \end{pmatrix}. \end{aligned} \tag{4.60}$$

the Hamiltonians in the two valleys are related by: $H_{K'}^{2b} = \sigma_x H_K^{2b} \sigma_x (u \to -u, v_3 \to -v_3)$. The Hamiltonians of the valleys are exchanged by time reversal T, since $T\pi T^\dagger = -\pi^\dagger$. Therefore the product of time reversal and valley swap is a symmetry: $T\sigma_x^{KK'}$. The term that breaks explicitly the particle-hole symmetry in the two-band model is the last one parametrized by the effective mass m_1.

I have verified using perturbation theory that it is safe to neglect the trigonal warping term, *i.e.* to set $v_3 = 0$. Additionally, this term is particle-hole symmetric, so there is no qualitative or quantitave danger in neglecting it. In the presence of magnetic field we define $a = l\pi/\sqrt{2}$. The Hamiltonian reads as:

$$\begin{aligned} H_K^{2b} &\doteq \begin{pmatrix} u/2 + \omega_1 n & -\omega_0\sqrt{n(n-1)} \\ -\omega_0\sqrt{n(n-1)} & -u/2 + \omega_1(n-1) \end{pmatrix}, \\ \sigma_x^{AB'} H_{K'}^{2b} \sigma_x^{AB'} &\doteq \begin{pmatrix} -u/2 + \omega_1 n & -\omega_0\sqrt{n(n-1)} \\ -\omega_0\sqrt{n(n-1)} & u/2 + \omega_1(n-1) \end{pmatrix}, \end{aligned} \tag{4.61}$$

where the matrix in valley K has the first column associated with state $|n, A\rangle$ and the second with $|n-2, B'\rangle$, whereas the matrix in valley K' has the first column associated with state $|n, B'\rangle$ and the second with $|n-2, A\rangle$.

The eigenfunctions and energies of the neutral Landau level are therefore:

$$\begin{aligned} &H_K^{2b}|0, A\rangle = u/2|0, A\rangle,\ H_K^{2b}|1, A\rangle = (u/2 + \omega_1)|1, A\rangle, \\ &H_{K'}^{2b}|0, B'\rangle = -u/2|0, B'\rangle,\ H_{K'}^{2b}|1, B'\rangle = (-u/2 + \omega_1)|1, B'\rangle. \end{aligned} \tag{4.62}$$

We see therefore that the particle-hole symmetry breaking term ω_1, produces a small single partilce splitting between the $n = 0$ and $n = 1$ states in the neutral Landau level.

The energies of the negative and positive energy Landau levels for $n > 2$ are:

$$E^{\pm}_{nK} = \omega_1 n \pm \sqrt{\left(\frac{u+\omega_1}{2}\right)^2 + \omega_0^2\ n(n-1)}, \tag{4.63}$$

And $E^{\pm}_{nK'} = E^{\pm}_{nK}(u \to -u)$. The states associated with the negative and positive energy Landau levels are:

$$\phi^{+}_{nK} = \begin{pmatrix} \cos(\theta_n/2) \\ -\sin(\theta_n/2) \end{pmatrix},\ \phi^{-}_{nK} = \begin{pmatrix} \sin(\theta_n/2) \\ \cos(\theta_n/2) \end{pmatrix}, \tag{4.64}$$

with

$$\cos\theta_n = \frac{\left(\frac{u+\omega_1}{2}\right)}{\sqrt{\left(\frac{u+\omega_1}{2}\right)^2 + \omega_0^2 n(n-1)}}, \tag{4.65}$$

$$\sin\theta_n = \frac{\omega_0\sqrt{n(n-1)}}{\sqrt{\left(\frac{u+\omega_1}{2}\right)^2 + \omega_0^2 n(n-1)}}. \tag{4.66}$$

The states at valley K' can be obtained from formulae above by replacing $u \to -u$.

4.4.2 Interaction with negative energy sea in the presence of explicit particle-hole symmetry-breaking terms

Let us now revisit the interaction with the negative energy sea in the presence of explicit particle-hole symmetry-breaking terms. The exchange potential generated by valley K can be written as:

$$\hat{X}^{-}_{K} = -\frac{1}{A}\sum_{q} v_q e^{iq\cdot\hat{r}}\ \hat{P}^{-}_{K}\ e^{-iq\cdot\hat{r}}, \tag{4.67}$$

with $\hat{P}_-^K$ the projector into the occupied negative energy sea of valley K:

$$\hat{P}_K^- = \sum_{n\geq 2,m} |\phi_{nmK}^-\rangle\langle\phi_{nmK}^-|. \tag{4.68}$$

Because the interaction conserves valley at its vertices there will not be intervalley exchange potential, and a completely analogous expression for the intravalley exchange potential for valley K' would hold. When acting on the neutral Landau level, Eq. (4.67) can be written as:

$$\hat{X}_K^- = \hat{X}_{0K} + \hat{X}_{1K} + \hat{X}_{2K}, \tag{4.69}$$

where $\hat{X}_{0K}$ is binding energy of the Dirac point (namely the UV divergent term that depends only on the onsite Hubbard type term) and $\hat{X}_{1K}$ is the exchange interaction with the negative energy sea, which sometimes we refer to as the Shizuya term:

$$\hat{X}_{0K} + \hat{X}_{1K} = -\frac{1}{2A}\sum_q v_q e^{iq\cdot\hat{r}} \left(\sum_{n\geq 2} \hat{P}_{nAK}\right) e^{-iq\cdot\hat{r}}. \tag{4.70}$$

More explicitly one has,

$$\hat{X}_{0K} = -\frac{U_0}{2}(\hat{N}_{0K} + \hat{N}_{1K}), \tag{4.71}$$

$$\hat{X}_{1K} = \eta_0\hat{N}_{0K} + \eta_1\hat{N}_{1K}, \tag{4.72}$$

$$\eta_0 = \frac{3}{4}\sqrt{\frac{\pi}{2}}\frac{e^2}{\epsilon l},\ \eta_1 = \frac{5}{8}\sqrt{\frac{\pi}{2}}\frac{e^2}{\epsilon l},\ U_0 = \frac{1}{A}\sum_q v_q \tag{4.73}$$

where $\hat{N}_{0K}/\hat{N}_{1K}$ is the number of electrons in the neutral Landau level with $n = 0/n = 1$ cyclotron wave-functions[2].

$\hat{X}_{2K}$ is the correction to the Shizuya term arising from the presence of the interlayer bias:

$$\hat{X}_{2K} = \frac{1}{2A} \sum_q v_q e^{iq\cdot\hat{r}} \left(\sum_{n\geq 2} \cos\theta_n \ \hat{P}_{nAK} \right) \ e^{-iq\cdot\hat{r}}, \tag{4.74}$$

in both expressions above $\hat{P}_{nAK} = \sum_m |nmAK\rangle\langle nmAK|$, where m is an intra Landau level label.

More explicitly the bias dependent exchange potential with the negative energy sea can be shown to be,

$$\hat{X}_{2K} = \xi_{0K}\hat{N}_{0K} + \xi_{1K}\hat{N}_{1K}, \tag{4.75}$$

$$\xi_{0K} = \frac{e^2}{\epsilon l} \sum_{n=2}^{\infty} \frac{\Gamma(n+1/2)}{2\sqrt{2}n!} \cos\theta_n, \tag{4.76}$$

$$\xi_{1K} = \frac{e^2}{\epsilon l} \sum_{n=2}^{\infty} \frac{(n-1/4)\Gamma(n-1/2)}{2\sqrt{2}n!} \cos\theta_n. \tag{4.77}$$

For large n: $\Gamma(n+1/2)/n! \to 1/\sqrt{n}$, and $(n-1/4)\Gamma(n-1/2)/n! \to 1/\sqrt{n}$. Therefore since:

[2]In the notation of Eq. (4.10) we had $\eta_0 = \mu_1 + \Delta_1$ and $\eta_1 = \mu_1 - \Delta_1$.

$$\cos\theta_n \to \frac{1}{n}\left(\frac{u+\omega_1}{2\omega_0}\right), \text{ for } n\to\infty, \tag{4.78}$$

for any finite ω_0 the sums in Eqs. (4.76) and (4.77) are absolutely convergent. In the zero field limit (*i.e.* $\omega_{0,1}=0$): $\theta_n = 0,\ \forall n$, and hence the individual sums are divergent. However the product of $e/\epsilon l$ times the divergent sum remains finite. In fact, using the approximation:

$$\sum_{n=2}^{\infty}\frac{\Gamma(n+1/2)}{n!}\frac{1}{\sqrt{1+\epsilon^2 n(n-1)}}\approx \frac{1}{\epsilon}\int_{2\epsilon}^{\infty}\frac{\Gamma(x/\epsilon+1/2)}{(x/\epsilon)!}\frac{dx}{\sqrt{1+x(x-\epsilon)}}\approx \frac{1}{\sqrt{\epsilon}}\frac{8}{\sqrt{\pi}}\Gamma(5/4)^2\approx\frac{3.708}{\sqrt{\epsilon}}, \tag{4.79}$$

where $\epsilon\equiv 2\omega_0/|u+\omega_1|$. By performing numerically the sums at small ϵ, above constant is found to be ≈ 3.70 (this just to double check the approximations capture the leading divergence in the limit $\epsilon\to 0$). This implies that ξ_{0K} and ξ_{1K} have the following limit as $B\to 0$,

$$\xi_{0K}^{B\to 0}=\xi_{1K}^{B\to 0}=sign(u)\ \frac{e^2\sqrt{m_0|u|}}{\epsilon}\frac{2}{\sqrt{\pi}}\Gamma(5/4)^2 \approx 0.92\ sign(u)\ \frac{e^2\sqrt{m_0|u|}}{\epsilon}. \tag{4.80}$$

therefore this predicts an enhancement between the intervalley gap which will be relevant in explaining the large gap $\nu=0$ found in the experiments of

Ref. [40]. It is not surprinsing that an enhancement to the gap at $\nu = 0$ exists at zero field since the putative band structure is gapped at finite u and there should be a finite exchange correction to such gap. It would be interesting to compare this value to that enhancement, and to further examine the meaning and validity of the term here found.

Since $\xi_{0K}^{B\to 0} \to \xi_{1K}^{B\to 0}$ as $B \to 0$, it is also interesting to determine how their splitting vanishes as $B \to 0$. Indeed using the identity: $\Gamma(n + 1/2) = (n - 1/2)\Gamma(n - 1/2)$, one can verify that:

$$sign(\xi_{1K} - \xi_{0K}) = sign(u + \omega_1),\ \forall B, \tag{4.81}$$

and one finds that sums that determine this spliting remain absolutely convergent even in the limit $B \to 0$, and are given by:

$$\xi_{1K}^{B\to 0} - \xi_{0K}^{B\to 0} = sign(u)\frac{1}{8}\sqrt{\frac{\pi}{2}}\frac{e^2}{\epsilon l}. \tag{4.82}$$

It is remarkable that the limit of this splitting is independent of the magnitude of u. Note that this term *exactly equals* the Shizuya term, $\eta_0 - \eta_1$, in magnitude. Therefore, for $u > 0$, the Shizuya splitting tends to be doubled in the valley/layer that is energetically favored by the interlayer bias, while it tends to be completely canceled in the valley/layer that is unfavored by the bias.

This exact balance is a consequence of the limiting form for the valley valence band states:

$$\phi_{nK}^{-B\to 0} = \begin{pmatrix} 0 \\ 1 \end{pmatrix}, \ \forall n \geq 2, u > 0, \tag{4.83}$$

$$\phi_{nK'}^{-B\to 0} = \begin{pmatrix} 1 \\ 0 \end{pmatrix}, \ \forall n \geq 2, u > 0, \tag{4.84}$$

Which is completely different with the case in which the term $|u + \omega_1|$ is set to zero from the start:

$$\phi_{nK}^{-} = \frac{1}{\sqrt{2}} \begin{pmatrix} 1 \\ 1 \end{pmatrix}, \ \forall n \geq 2, B > 0 \tag{4.85}$$

$$\phi_{nK'}^{-} = \frac{1}{\sqrt{2}} \begin{pmatrix} 1 \\ 1 \end{pmatrix}, \ \forall n \geq 2, B > 0. \tag{4.86}$$

In other words, the limits $B \to 0$ and $u \to 0$ yield different states for the valence Dirac sea when taken in different orders, and hence their associated exchange potentials differ.

Table 4.1 summarizes the different energy scales of the effective two-band model that includes explicit particle hole-symmetry breaking. The explicit particle-hole symmetry breaking energy scale, $\hbar\omega_1$, appears much smaller than the Coulomb energy scale which dictates the strength of the exchange interaction with vacuum and hence of the terms that attempt to restore particle-hole symmetry. On this note, one could naively expect that the particle-hole symmetry will be present. However, as we will see in the next section there is a substantial reduction of the Coulomb energy scale from screening that in turn reduces the vacuum exchange term substantially, making it smaller than

Table 4.1: Relevant energy scales for bilayer graphene in the quantum Hall regime obtained from parameters in Ref [35].

m_0/m_e	0.044
m_1/m_e	0.301
$\hbar\omega_0$	$2.6meVB$[T]
$\hbar\omega_1$	$0.38meVB$[T]
$\mu_B B$	$0.058meVB$[T]
e^2/l	$56meV\sqrt{B[T]}$

the explicit particle-hole symmetry-breaking scale at typical magnetic fields where the quantum Hall effect is observable.

4.5 Gaps at integer fillings for the screened Coulomb interaction

It is recognized that the effects of screening are more pronounced in bilayer than in monolayer graphene in the quantum Hall regime [25, 57, 65]. We have developed a systematic discussion of static screening in bilayer which is presented in Appendix B. In this section, we will employ the approximate analytic expressions obtained in Section B.5, which are able to describe the screening over a wide range or wavevectors, to compute the expected charge gaps at integer fillings in the presence of an interlayer bias. As we shall see the computed gaps are in very good agreement with those measured in Ref. [40].

4.5.1 Gap at $\nu = -3$

Let us assume without loss of generality that $u > 0$ so that valley K' is filled first. Generically if there exists a single particle term that favors the

$n = 1$ states over the $n = 0$ states, such as the exchange interaction with the negative energy sea described in Eqs. (4.71)-(4.73), the ground state at $\nu = -3$ would a coherent combination of $n = 0$ and $n = 1$ states [30]. Therefore, the criterion for the stability of ground state occupying the spinor $|K' \uparrow n = 0\rangle$ is that the effective single-particle energy of the $n = 1$ state is larger than that of the $n = 0$ states. This energy contains contributions from the exchange interaction with the negative sea as well as the explicit particle-hole symmetry breaking splitting described in Eqs. (4.62). The criterion for the ground state to be the completely filled spinor $|K' \uparrow n = 0\rangle$ can therefore be written as:

$$\omega_1 + \xi_{1K'} - \xi_{0K'} + \eta_1 - \eta_0 \geq 0. \tag{4.87}$$

Where $\xi_{1K'}$, $\xi_{0K'}$, η_1, η_0 are the contributions from the exchange interaction with the negative energy sea described in Section 4.4.2, but with the bare Coulomb interaction replaced by the screened Coulomb interaction from Eq. (B.2). Figure 4.1 plots this energy difference for typical parameters that simulate the conditions of the experiment in Ref. [40]. This figure makes evident that the screening reduces so much the total contribution from the exchange energy with the negative energy sea that the dominant term is the explicit single particle splitting ω_1 which favors the $n = 0$ states. As a consequence we expect that the ground state at $\nu = -3$ is the completely filled flavor $|K' \uparrow n = 0\rangle$ in Ref. [40].

The charge gap at $\nu = -3$ is therefore associated with a hole in $|K' \uparrow n = 0\rangle$ and an electron in $|K' \uparrow n = 1\rangle$ [1, 6], and it is:

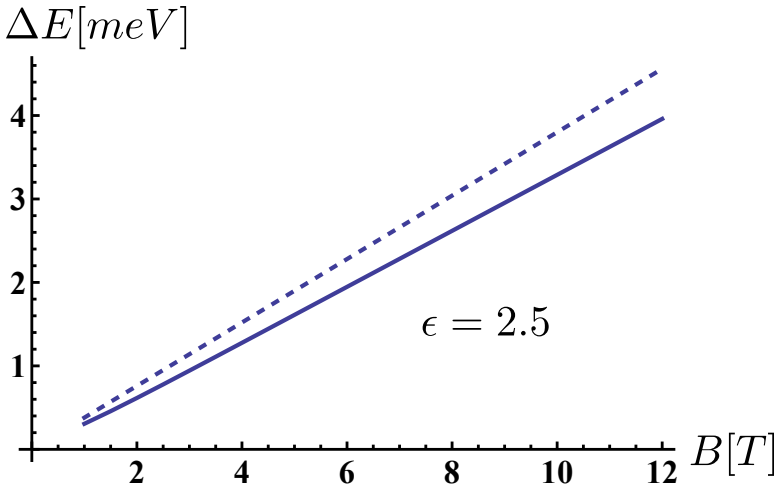

Figure 4.1: The solid line is the single particle energy difference between $n = 0$ and $n = 1$ states in the K' valley. We chose an extrinsic dielectric constant that is the average of vacuum $\epsilon = 1$ and that of boron nitride $\epsilon \approx 4$, and an interlayer bias of $u = 10$meV. The dashed line is the single particle splitting arising from the explicit symmetry breaking energy $\hbar\omega_1$.

$$\Delta_{-3} = \Delta_{odd}^{Coul} + \omega_1 + \xi_{1K'} - \xi_{0K'} + \eta_1 - \eta_0. \tag{4.88}$$

where Δ_{odd}^{Coul} is the contribution of the exchange interaction of the electron and the hole at odd integers which reads as:

$$\Delta_{odd}^{Coul} = \int \frac{d^2q}{(2\pi)^2} v_q^{sc} (|F_{00}(q)|^2 - |F_{10}(q)|^2). \tag{4.89}$$

where $F_{n'n}(q)$ are the usual parabolic band form factors (see *e.g.* Eq. C(21) in Ref. [67]).

4.5.2 Gap at $\nu = -2$

The ground state is expected to occupy spinors $|K' \uparrow n = 0\rangle, |K' \uparrow n = 1\rangle$ [1, 6]. The lowest energy gap is associated with a hole in $|K' \uparrow n = 1\rangle$ and an electron in $|K' \downarrow n = 0\rangle$, and it is:

$$\Delta_{-2} = \Delta_{even}^{Coul} + \Delta_z - \omega_1 - \xi_{1K'} + \xi_{0K'} - \eta_1 + \eta_0. \tag{4.90}$$

where $\Delta_z = g\mu_B B$ is the Zeeman gap, and the Coulomb gap at even integers is:

$$\Delta_{even}^{Coul} = \int \frac{d^2q}{(2\pi)^2} v_q^{sc} (|F_{11}(q)|^2 + |F_{10}(q)|^2). \tag{4.91}$$

4.5.3 Gap at $\nu = -1$

The ground state is expected to occupy spinors $|K' \uparrow n = 0\rangle, |K' \uparrow n = 1\rangle, |K' \downarrow n = 0\rangle$. The lowest energy gap is associated with a hole in $|K' \downarrow n = 0\rangle$ and an electron in $|K' \downarrow n = 1\rangle$, and it has the same expression as that at $\nu = -3$ appearing in Eq. (4.88). It must be borne in mind however that the screened interactions are slightly different by virtue of the fact the polarizability of both states is slightly different, as described in Appendix B.

4.5.4 Gap at $\nu = 0$

The ground state is expected to occupy spinors $|K' \uparrow n = 0\rangle, |K' \uparrow n = 1\rangle, |K' \downarrow n = 0\rangle, |K' \downarrow n = 1\rangle$. The lowest energy gap is associated with a hole

in $|K' \downarrow n=1\rangle$ and an electron in $|K \uparrow n=0\rangle$, and it is:

$$\Delta_0 = \Delta_{even}^{Coul} + u - \Delta_z - \omega_1 - \xi_{1K'} + \xi_{0K} - \eta_1 + \eta_0. \tag{4.92}$$

The large gap in the experiments of Ref. [40] is pressumably arising from a large single particle bias $u \sim 10meV$ which is further enhanced by exchage.

4.5.5 Gap at $\nu = 1$

In analogy with $\nu = -3$, the ground state is expected to occupy spinors $|K' \uparrow n=0\rangle, |K' \uparrow n=1\rangle, |K' \downarrow n=0\rangle, |K' \downarrow n=1\rangle, |K \uparrow n=0\rangle$, whenever the following condition is met:

$$\omega_1 + \xi_{1K} - \xi_{0K} + \eta_1 - \eta_0 \geq 0. \tag{4.93}$$

This condition is met at any field because of the previously discussed propertis in section 4.4.2 that the Shizuya term, $\eta_1 - \eta_0$, is nearly canceled at low fields by the exchage term arising from the presence of a finite layer bias, and the property described in Eq. (4.81) that $\xi_{1K} - \xi_{0K} > 0$. I have also verified numerically the condition remains true in the case of the screened interactions.

The lowest energy gap is associated with a hole in $|K \uparrow n=0\rangle$ and an electron in $|K \uparrow n=1\rangle$, and it is:

$$\Delta_1 = \Delta_{odd}^{Coul} + \omega_1 + \xi_{1K} - \xi_{0K} + \eta_1 - \eta_0. \tag{4.94}$$

4.5.6 Gap at $\nu = 2$

The ground state spinors are: $|K' \uparrow n = 0\rangle, |K' \uparrow n = 1\rangle, |K' \downarrow n = 0\rangle, |K' \downarrow n = 1\rangle, |K \uparrow n = 0\rangle, |K \uparrow n = 1\rangle$. The lowest energy gap is associated with a hole in $|K \uparrow n = 1\rangle$ and an electron in $|K \downarrow n = 0\rangle$, and it is:

$$\Delta_{-2} = \Delta_{even}^{Coul} + \Delta_z - \omega_1 - \xi_{1K} + \xi_{0K} - \eta_1 + \eta_0. \tag{4.95}$$

4.5.7 Gap at $\nu = 3$

The ground state spinors are: $|K' \uparrow n = 0\rangle, |K' \uparrow n = 1\rangle, |K' \downarrow n = 0\rangle, |K' \downarrow n = 1\rangle, |K \uparrow n = 0\rangle, |K \uparrow n = 1\rangle, |K \downarrow n = 0\rangle$. The lowest energy gap is associated with a hole in $|K \downarrow n = 0\rangle$ and an electron in $|K \downarrow n = 1\rangle$, and it has the same expression as that at $\nu = 1$.

Figure 4.2 depicts all the gaps with parameters suitable for experiment [40] and there is overall good quantitative agreement.

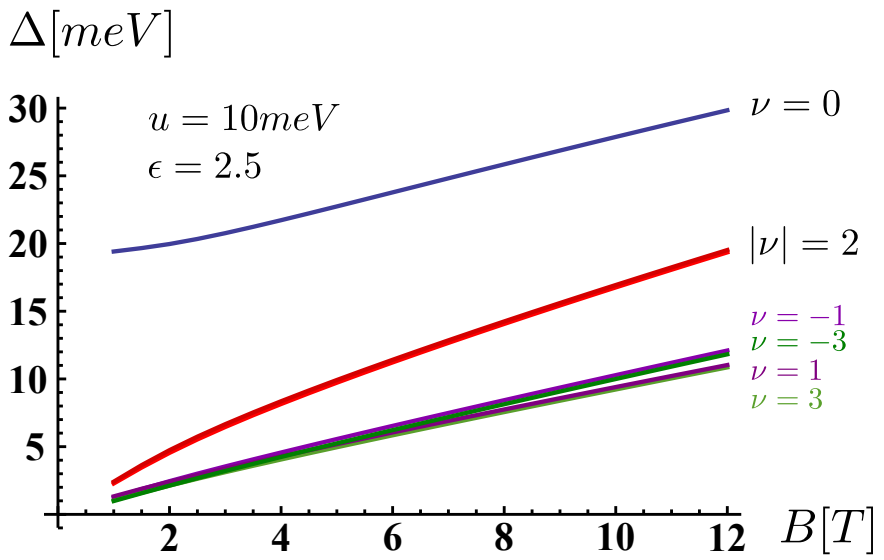

Figure 4.2: Predicted gaps at integer fillings in the neutral Landau level of bilayer graphene for an interlayer bias of $u = 10$meV and surrounding medium with dielectric constant $\epsilon = 2.5$ which is the approximate value for a boron nitride substrate. These gaps include the effects of exchange interactions with the negative energy sea, screening at the level of static RPA, and explicit particle-hole symmetry breaking terms, as described in the text.

Chapter 5

Fractional quantum Hall states with $n = 0/n = 1$ coherence in bilayer graphene

In this chapter we will put aside the question of the size and origin of the term that splits the $n = 0$ and $n = 1$ orbitals and take it as a given parameter. We will explore the ground states as a function of this parameter. For simplicity we will consider many body states created within a fixed valley and spin flavor and explore tendency to form states with coherence between the $n = 0$ and $n = 1$ orbitals. The possiblity of creating states with strong coherence between the $n = 0$ and $n = 1$ cyclotron indices has no analogue in GaAs, therefore it holds the possibility of bringing novel quantum Hall behaviour to life in bilayer graphene.

5.1 General mapping formula for two-point correlation functions from $n = 0$ LL into coherent $n = 0/n = 1$ LLs

Imagine a "ferromagnetic" many-body state with coherence between $n = 0$ and $n = 1$ cyclotron quantum numbers described by a spinor $\zeta = \binom{u}{v}$ of the form,

$$|\Psi\rangle_\zeta = \Psi(b_1^\dagger, ..., b_N^\dagger) \prod_i (u + v a_i^\dagger)|\mathrm{O}\rangle, \tag{5.1}$$

where b and a are lowering operators of the guiding center and cyclotron quantum numbers respectively and Ψ is a fully antisymmetric polynomial of N coordinates.

Consider the operator that measures the conditional probability density for finding a particle at position r_2 given that another is at r_1

$$G(r_1, r_2) = \sum_{i \neq j} \delta^2(r_1 - r_i)\delta^2(r_2 - r_j) \tag{5.2}$$

Decomposing the coordinates into guiding center c, and mechanical momentum π variables: $r = c + l^2 z \times \pi$, $\pi = p + eA/c$. One finds the projected operator into the coherently rotated Landau level to be:

$$G_\zeta(r_1, r_2) = \frac{1}{A^2} \sum_{q_1, q_2} e^{iq_1 \cdot r_1 - iq_2 \cdot r_2} F_\zeta(q_1) F_\zeta(-q_2) \sum_{i \neq j} e^{iq_1 \cdot c_i - iq_2 \cdot c_j} \tag{5.3}$$

Where $F_\zeta(q)$ is the form factor of the rotated LL:

$$F_\zeta(q) = (u^* \langle 0| + v^* \langle 1|) e^{-il^2 z \cdot q \times \pi} (u|0\rangle + v|1\rangle). \tag{5.4}$$

This expression is easily evaluated using Eq.(C21) from [67],

$$F(q, \zeta) = F_0(q) \Big[1 - \frac{q^2}{2} \sin^2(\theta/2) + i \frac{q}{\sqrt{2}} \sin\theta \sin(\phi_q + \phi) \Big], \tag{5.5}$$

with $\zeta = \binom{\cos\theta/2 e^{i\phi/2}}{\sin\theta/2 e^{-i\phi/2}}$, $F_0(q) = e^{-q^2l^2/4}$ (the form factor of the usual $n = 0$ LL), and ϕ_q is the angle of the vector q.

Assuming the state is translationally invariant, one finds the expectation of G_ζ to be

$$\langle G_\zeta(r)\rangle_\Psi = \frac{1}{A}\sum_q e^{-iq\cdot r}|F_\zeta(q)|^2 s_\Psi(q) \tag{5.6}$$

Where s_Ψ is the guiding center structure factor which encapsulates the "intrinsic" density correlations of Ψ in a LL independent manner: $s_\Psi(q) = 1/A\sum_{i\neq j}\langle\sum_{i\neq j} e^{iq_1\cdot c_i - iq_2\cdot c_j}\rangle_\Psi$.

By suitably choosing the y-axis, so that $q_y = q\sin(\phi_q + \phi)$, it is easy to express $\langle G_\zeta(r)\rangle_\Psi$ in terms of $\langle G_0(r)\rangle_\Psi$, namely the correlation function one would have for the conventional $n = 0$ LL, when $\theta = 0$. Combining Eqs. (5.6) and (5.5), this relation is easily seen to be,

$$\langle G_\zeta(r)\rangle_\Psi = \left[\left(1 + \frac{1}{2}\sin^2(\theta/2)\nabla^2\right)^2 - \frac{1}{2}\ \sin^2\theta\ \partial_y^2\right]\langle G_0(r)\rangle_\Psi \tag{5.7}$$

The conventional two-point correlation function for a homogeneous state of density n is given by: $g(r) = n^2\langle G_\zeta(r)\rangle_\Psi$. Thus, above equation maps the two-point correlation functions of given wavefunction in the $n = 0$ LL into its analogue in the coherent $n = 0/n = 1$ LL.

The interaction energy per particle (subtracting neutralizing background contribution) is:

$$\frac{V}{N} = \frac{n}{2}\int d^2r\ v(r)(g(r)-1) \tag{5.8}$$

5.2 Laughlin state with coherence between $n = 0/n = 1$

Slater determinants with coherence between $n = 0$ and $n = 1$ at $\nu = 1$ have been explored in Refs. [6, 30]. Here we will consider the case of the Laughlin state with coherence between $n = 0$ and $n = 1$ at $\nu = 1/3$. These states have an XY order with ferroelectric behavior [6] and also nematic characteristics as will be clear from the shape of their two-point correlation function.

The two-point correlation function of the Laughlin state has been widely studied. A useful parametrization is [23]:

$$g(r) = 1 - e^{-r^2/2} + \sum_{l=1}^{\infty} \frac{2c_l}{(2l-1)!}\Big(\frac{r^2}{4}\Big)^{2l-1} e^{-r^2/4} \tag{5.9}$$

I will use the coefficients c_l from Table I of Ref. [24]. Fig 5.1 illustrates the two-point correlations in the usual $n = 0$ and $n = 1$ LL. Fig 5.2 illustrates the anisotropic two-point correlations in a ferroelectric-nematic Laughlin state with $n = 0/n = 1$ coherence.

The energy per particle is,

$$\epsilon(\theta) = \frac{\nu e^2}{l_0}(\epsilon_0 + \epsilon_1 \cos\theta + \epsilon_2 \cos 2\theta), \tag{5.10}$$

It interesting to note that the dependence on θ is general: the energy

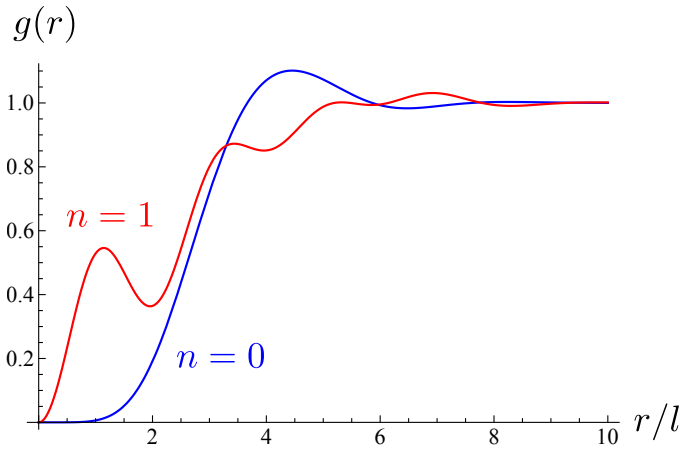

Figure 5.1: Two-point function for the Laughlin state in the $n = 0$ (blue) and $n = 1$ (red) LLs.

of any state is a quadratic polynomial of $\cos\theta$. Therefore knowing its value at 3 specific angles would determine the whole function (unfortunately, one usually knows only two angles $\theta = 0$ and $\theta = \pi$ for well-studied states). The values of the coefficients for the Laughlin state are,

$$\epsilon_0 = -1.07781, \tag{5.11}$$

$$\epsilon_1 = -0.12583, \tag{5.12}$$

$$\epsilon_2 = -0.02165, \tag{5.13}$$

Imagine there is an additional Zeeman-like term with a contribution to the energy per particle of the form $\frac{e^2}{l}\epsilon_z \cos\theta$, which tends to favor $n = 1$ LL, like that generated from the exchange interaction with the vacuum which we discussed previously. The angle that minimizes the energy of the Laughlin

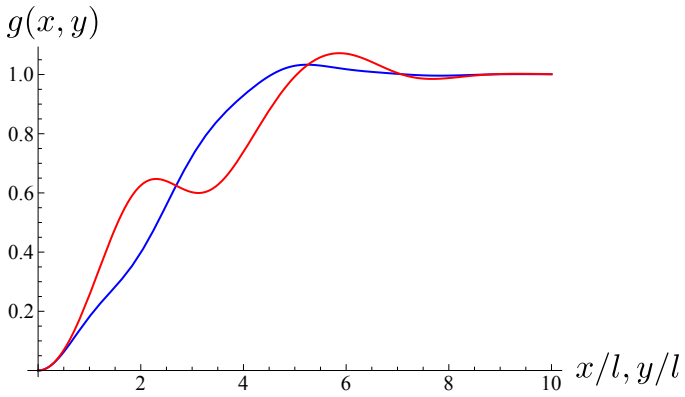

Figure 5.2: Two-point function for the ferroelectric/nematic Laughlin state with equal mixing of $n = 0$ and $n = 1$ (i.e. $\theta = \pi/2$) along the y-axis (blue) and x-axis (red).

state is depicted in Fig. 5.3. The critical Zeeman value where coherence starts being energetically favorable is,

$$\epsilon_{z,crit} = \nu(4\epsilon_2 - \epsilon_1) \approx 0.0130718. \tag{5.14}$$

The prefactor ν is not a notational artifact and suggests that the critical Zeeman to destabilize states of lower filling fractions is smaller. This is a consequence of the exchange-correlation energy per particle having an overall decrease with total density (see e.g. the n prefactor in Eq. (5.8)).

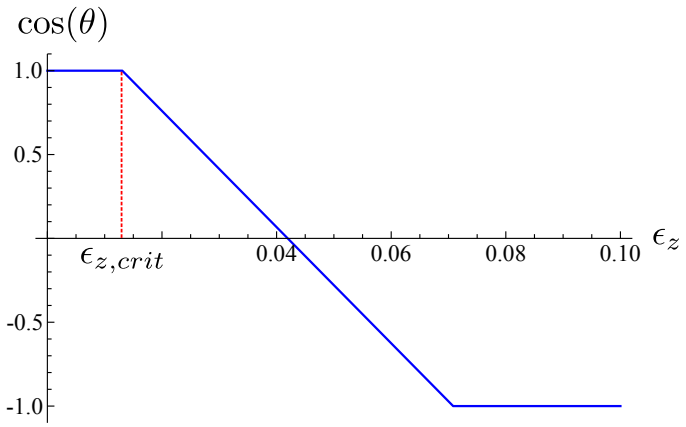

Figure 5.3: Optimal orientation of ferroelectric/nematic Laughlin state for a Zeeman-like term, ϵ_z, favoring the $n = 1$ orbital.

Appendices

Appendix A

Flavor flip quasiparticles for the Laughlin type state at $\tilde{\nu} = 7/3$ involving the completely filled flavors[1]

As discussed in the main text the two-component Laughlin type state at $\tilde{\nu} = 5/3$, *i.e.* $(1, 2/3, 0, 0)$ is not the ground state in the absence of symmetry breaking terms, and instead the three component state $(1, 1/3, 1/3, 0)$ has lower Coulomb energy. This statement also applies at $\tilde{\nu} = 7/3$ because of the global particle-hole symmetry. We therefore expect the state $(1, 2/3, 2/3, 0)$ to have lower Coulomb energy than $(1, 1, 1/3, 0)$. However, sufficiently strong Zeeman or $V_\perp$ anisotropy terms will make $(1, 1, 1/3, 0)$ have lower energy. We believe that the state observed in experiments on suspended graphene samples in graphene is likely the $(1, 1, 1/3, 0)$ state. For $V_\perp < 0$ and $|V_\perp| > 3h$ the phase that minimizes the anisotropy energy of $(1, 1, 1/3, 0)$ is the collinear antiferromagnet as explained in the first section of this supplement. This collinear antiferromagnetic Laughlin-like state is likely the one realized in the experiments of Refs. [20, 21].

We would like to determine what type of quasiparticles give rise to

[1] This Appendix is based on Ref. [68], all authors in this reference contributed equally to this work.

the charge gap of this state. These quasiparticles will generally involve flavor flips. There are two types of flavor flips which is convenient to distinguish. The first kind is more easily conceptualized for the state $(1, 1, 1/3, 0)$. For the collinear antiferromagnetic order the completely filled spinors can be chosen to be $|K \uparrow\rangle$ and $|K' \downarrow\rangle$. The neutral quasiparticle-quasihole pairs can involve flips from the 1/3 filled spinor, i.e. $|K' \uparrow\rangle$, into the empty spinor $|K \downarrow\rangle$. The anisotropy energy contribution to this gap reduces simply to the Zeeman gap, $2h$, per flavor-flip. In particular, as discussed in the text, the flavor flipped quasi-electron and no flip quasi-hole are expected to be the lowest energy excitations for most of the magnetic field range explored in Refs. [20, 21]. The gap associated with these excitations is expected to be $\Delta^1_{1/3} = 0.075e^2/\epsilon l + 2h$, where the Coulomb energy has been extracted from exact diagonalization studies extrapolated to the thermodynamic limit [15, 48, 61, 74].

A second kind of quasiparticle-quasihole pair associated with the state $(1, 1, 1/3, 0)$, would involve flavor flips from either of the completely filled spinors into the 1/3 filled spinor. Quasiparticles involving a flip from one of the completely filled spinors into the completely empty spinor would have an associated Coulomb gap $\sqrt{\pi/2}e^2/\epsilon l$, which is considerably larger than those here considered and hence unlikely to be lowest energy charged excitations. These quasiparticles are more easily conceptualized in the particle-hole mirror state $(1, 2/3, 0, 0)$, where they appear as involving flavor flips from the 2/3 filled spinor into the completely empty ones. For $(1, 2/3, 0, 0)$ if we choose the completely filled spinor to be $|K \uparrow\rangle$, the partially filled spinor

would be $|K' \downarrow\rangle$ in the collinear antiferromagnetic phase. Since there are two completely empty spinors, there are two-types of flavor flips. In the first one we remove an electron from $|K' \downarrow\rangle$ and place it into $|K' \uparrow\rangle$. Applying Eq. (3.25) from the main text one finds that these quasiparticles would have a gap $\Delta^1_{2/3} \approx 0.051e^2/\epsilon l - 2(V_\perp + h)$. For the second type of flavor flip we remove an electron from $|K' \downarrow\rangle$ and place it into $|K \downarrow\rangle$, these quasiparticles would have a gap $\Delta^1_{2/3} \approx 0.051e^2/\epsilon l + 2V_z$. We have obtained the Coulomb gap for a quasiparticle-quasihole pair involving a single flavor flip from the exact diagonalization studies of Ref. [72], which are not extrapolated to thermodynamic limit and thus might contain finite size effects. Reference [72] found that the charged gap for a single spin-flip is associated with a single spin-flip quasielectron and a no spin-flip quasihole. Note that in the absence of symmetry breaking terms these quasi-particles are expected to have lower energy than those discussed in the previous paragraph. We believe this is a natural explanation for the finding in Ref. [58] that there is an intermediate regime in which the lowest energy excitations of the Laughlin like state $(1, 1, 1/3)$ involve flips from the completely filled spinors.

However, it is unlikely that the latter quasiparticles play a role at magnetic fields where the FQHE is observable. The reason is the relatively large anisotropy energy cost they involve. The critical fields at which the two types of charge gaps of the second kind of flavor flipped quasiparticle equals the first kind are,

$$
\begin{aligned}
B_c &= \left[\frac{0.024e^2}{(2|V_\perp| - 4h)\epsilon l}\right]^2, \\
B_c &= \left[\frac{0.024e^2}{2V_z\epsilon l}\right]^2,
\end{aligned}
\tag{A.1}
$$

where the quantities in the right side are understood to be evaluated at 1T. For the first critical field one obtains, $B_c = 0.1$T for $V_\perp = -10h$. One obtains $B_c = 0.74$T for $V_\perp = -5h$. The second critical fields is expected to be even smaller because the stability of collinear antiferromagnetic states requires $V_z \geq |V_\perp|$.

Appendix B

Screening in bilayer graphene with and without magnetic fields

In this appendix we will compute the static density response function χ_q of bilayer graphene within the two-band and four-band models. The need to consider both models stems from the fact that the screening of charge fluctuations at a length scale r will depend on the available electron-hole excitations that have total momentum $q \sim r^{-1}$. Therefore, a proper account of the screening of the short-range behavior of the interactions requires the account of particle-hole excitations of large total momentum. Thus the screening of short range components will be dictated by large momentum and high energy virtual electron-hole pairs requiring us to go beyond the two-band model.

We will distinguish three different regimes of screening: (i) a long wavelength screening for $q \ll \max(l^{-1}, \sqrt{mu})$ where χ_q vanishes quadratically due to the absence of zero energy particle-hole excitations associated with cyclotron and/or interlayer bias gap. In this regime the interactions remain essentially unscreened because of the gap. (ii) An intermediate-wavelength screening $\max(l^{-1}, \sqrt{mu}) \ll q \ll t_1/v$, where the screening function is essentially constant, $\chi_q \approx \frac{m \ln 2}{\pi}$, due to finite density of states in the two-band model at

neutrality. (iii) A short-wavelength screening $t/v \ll q \ll 1/a$, where the screening is effectively that of two-decoupled graphene layers $\chi_q \approx \frac{q}{8v}$, and t is the interlayer hopping amplitude in bilayer graphene. (Formulae just described don't contain spin-valley multiplicity factor). We will also derive approximate formulae that interpolate the three regimes reproducing exactly their asymptic behavior, which are used to compute the gaps discussed in section 4.5.

B.1 When is it OK to use statically screened RPA?

The static density response function of a non-interacting fermion system is in general[1]:

$$\chi_q = \frac{2}{A} \sum_{e,h} \frac{|\langle e,h|n_{-q}|0\rangle|^2}{E_e + E_h} \tag{B.1}$$

where e and h label electron and hole states added to a reference ground state $|0\rangle$, $E_e + E_h$ is the excitation energy of the electron-hole pair state $|e,h\rangle$, and $n_{-q} = \sum_i e^{iq\cdot r_i}$ is the density operator.

Static screening is typically a reasonable description of the effective interactions for integer quantum Hall ferromagnets provided that the non-interacting cyclotron gaps are much larger than the interaction induced gaps. This is because the density response is well approximated by the static value for frequencies smaller than the non-interacting cyclotron gaps: $\chi(q,\omega) \approx$

[1]The only assumption is inversion symmetry of the density response $\chi_q = \chi_{-q}$.

$\chi(q, \omega = 0)$ for $\omega \ll \Delta_0$. When this condition is satisfied, we expect that the effective screened interaction is well described by:

$$v_q^{sc} = \frac{v_q}{1 + v_q \chi_q}. \tag{B.2}$$

The integer quantum Hall ferromagnetic gaps are typically dominated by the short range components of the interactions, because they are predominantly determined by the zero relative angular momentum Haldane pseudopotential. Therefore the gaps will be determined by the behavior of the interactions for $q \gtrsim l^{-1}$, where l is the magnetic length. This is why the sole inclusion of the short range corrections to the interactions in monolayer graphene produces a typically good description of its integer quantum Hall ferromagnetism.

The form of the dielectric function at increasingly large momentum becomes less and less sentitive to low frequency corrections, therefore the short range behavior of the screened interaction is better described by static screening as compared to its long range behavior. Since the short range part of the interaction dominates the integer quantum Hall ferromagnetism physics, this is another reason to justify the use of static screening for the purposes of estimating the gaps at integer fillings.

B.2 Large q behavior: four band model without magnetic field

Let us consider the 4-band model with the minimal features that are needed to describe short-wavelengths $q \gtrsim t/v$:

$$H_K^{4b} = \begin{pmatrix} 0 & 0 & vp^* & 0 \\ 0 & 0 & 0 & vp \\ vp & 0 & 0 & t \\ 0 & vp^* & t & 0 \end{pmatrix}, \tag{B.3}$$

the matrix columns correspond to A, B', B, A' sites respectively. The following unitary transformation is convenient:

$$\begin{aligned} U_p \; H_K^{4b} \; U_p^\dagger &= \begin{pmatrix} 0 & t_{AB} \\ t_{AB} & 0 \end{pmatrix}, \\ t_{AB} &= \begin{pmatrix} t & v|p| \\ v|p| & 0 \end{pmatrix}, \\ U_p &= \begin{pmatrix} 0 & 0 & 0 & 1 \\ e^{i\phi_p} & 0 & 0 & 0 \\ 0 & 0 & 1 & 0 \\ 0 & e^{-i\phi_p} & 0 & 0 \end{pmatrix}. \end{aligned} \tag{B.4}$$

From it we get:

$$
\begin{aligned}
&U_p\ (H_K^{4b})^2\ U_p^\dagger = \begin{pmatrix} t_{AB}^2 & 0 \\ 0 & t_{AB}^2 \end{pmatrix}, \\
&t_{AB}^2 = (vp)^2 + t^2/2 + m_p \hat{m}_p \cdot \sigma, \\
&m_p = \sqrt{(t/2)^2 + (vp)^2}, \\
&\hat{m}_p = \cos\theta_p \hat{z} + \sin\theta_p \hat{x}, \\
&\cos\theta_p = t/(2m_p),\ \sin\theta_p = vp/(2m_p).
\end{aligned}
\tag{B.5}
$$

From this representation we obtain the spectrum:

$$
\begin{aligned}
|p, s_1 s_2\rangle &\doteq \frac{1}{\sqrt{2}} U_p^\dagger \begin{pmatrix} \phi_{s_2} \\ s_1 \phi_{s_2} \end{pmatrix}, \\
E_{s_1 s_2} &= s_1 t/2 + s_1 s_2\ m_p.
\end{aligned}
\tag{B.6}
$$

where $s_{1,2} = \{+, -\}$, and:

$$
\phi_+ = \begin{pmatrix} \cos\theta_p/2 \\ \sin\theta_p/2 \end{pmatrix},\ \phi_- = \begin{pmatrix} -\sin\theta_p/2 \\ \cos\theta_p/2 \end{pmatrix}. \tag{B.7}
$$

When momentum is a good quantum number we have:

$$
n_{-q} = \sum_{p\alpha} c_{p+q,\alpha}^\dagger c_{p,\alpha}, \tag{B.8}
$$

with α denoting the sublattice index. In this case, Eq. (B.1) reduces to:

$$
\chi_q = \frac{2}{A} \sum_{p,ss'} \frac{|\langle p+q, s_1 s_2 | p, s_1' s_2' \rangle|^2}{E_{p+q,s_1 s_2} - E_{p,s_1' s_2'}} n_{p,s_1' s_2'} (1 - n_{p+q,s_1 s_2}) \tag{B.9}
$$

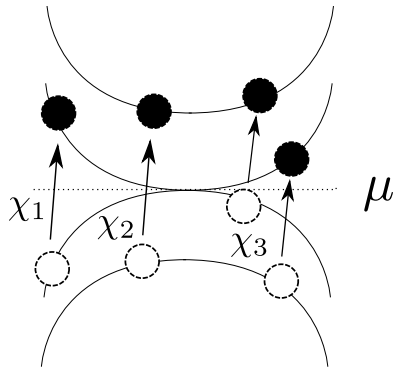

Figure B.1: Particle hole excitations contribution to screening in the four band model.

where the factor $n_{p,s_1's_2'}(1 - n_{p+q,s_1s_2})$ enforces that $p+q, s_1s_2$ and $p, s_1's_2'$ are electron and hole states respectively. There are four particle-hole excitations in the four-band model for a neutral system, depicted in Fig. B.1. The first excitation from near-valence to near-conduction we denote by χ_1:

$$\chi_1 = \int \frac{d^2p}{(2\pi)^2} \frac{(m_p + t/2)(m_{p+q} + t/2)\sin^2(\phi_p - \phi_{p+q})}{2m_p m_{p+q}(m_p + m_{p+q} - t)}. \tag{B.10}$$

The second excitation from far-valence to far-conduction we denote by χ_2, and satisfies $\chi_2 = \chi_1|_{t\to -t}$. Finally, the contributions from far-valence to near-conduction and near-valence to far-conduction are identical to each other and we denote their sum by χ_3,

$$\chi_3 = \int \frac{d^2p}{(2\pi)^2}\left[\frac{(m_p - t/2)(m_{p+q} + t/2) + (m_p + t/2)(m_{p+q} - t/2)\cos^2(\phi_p - \phi_{p+q})}{m_p m_{p+q}(m_p + m_{p+q})} - \frac{2v^2 p\cdot(p+k)}{m_p m_{p+q}(m_p + m_{p+q})}\right], \tag{B.11}$$

The behavior of these functions at small q is,

$$\begin{aligned}
\chi_1 &\approx \frac{t}{v^2}\frac{\ln 2}{2\pi} \approx m\ \frac{\ln 2}{\pi}, \\
\chi_2 &\approx \frac{q^2}{t}\left[\frac{1-\ln 2}{8\pi} + \mathcal{O}(vq/t)\right], \\
\chi_3 &\approx \frac{q^2}{t}\left[\frac{1}{12\pi} + \mathcal{O}(vq/t)\right],
\end{aligned} \tag{B.12}$$

The large q behavior of these functions is:

$$\begin{aligned}
\chi_1 &\approx \frac{q}{v}\left[\frac{4-\pi}{8\pi} + \mathcal{O}(t/vq)\right], \\
\chi_2 &\approx \frac{q}{v}\left[\frac{4-\pi}{8\pi} + \mathcal{O}(t/vq)\right], \\
\chi_3 &\approx \frac{q}{v}\left[\frac{3\pi-8}{8\pi} + \mathcal{O}(t/vq)\right], \\
\chi_1 + \chi_2 + \chi_3 &\approx \frac{q}{8v}\left[1 + \mathcal{O}(t/vq)\right].
\end{aligned} \tag{B.13}$$

The last result coincides with twice the dielectric function for monolayer graphene for a single spin and valley, as expected.

B.3 Intermediate q behavior: two-band model without magnetic field

Let us consider the two-band model with finite interlayer bias:

$$\begin{aligned} H_K^{2b} &= \begin{pmatrix} u/2 & -p^{*2}/2m \\ -p^2/2m & -u/2 \end{pmatrix} = \mu_p \hat{\mu}_p \cdot \sigma, \\ \mu_p &= \sqrt{(u/2)^2 + (p^2/2m)^2}, \end{aligned} \tag{B.14}$$

where $m = t/2v^2$. And the spectrum is:

$$\begin{aligned} |p,+\rangle &\doteq \begin{pmatrix} e^{i\phi_p}\cos\vartheta_p/2 \\ -e^{-i\phi_p}\sin\vartheta_p/2 \end{pmatrix}, \\ |p,-\rangle &\doteq \begin{pmatrix} e^{i\phi_p}\sin\vartheta_p/2 \\ e^{-i\phi_p}\cos\vartheta_p/2 \end{pmatrix}, \\ E_{ps} &= s\mu_p,\ \cos\vartheta_p = \frac{u/2}{\mu_p},\ \sin\vartheta_p = \frac{p^2/2m}{\mu_p}, \end{aligned} \tag{B.15}$$

with $s = \pm$ denoting the conduction and valence bands.

In the two-band model there is only one type of particle-hole excitations which are the analogue of the χ_1 term discussed in the four-band model. We label this term as χ_1 as well:

$$\chi_1 = \int \frac{d^2p}{(2\pi)^2} \frac{\mu_p\mu_{p+q} - (u/2)^2 - (p^2/2m)((p+q)^2/2m)\cos(2\phi_p - 2\phi_{p+q})}{\mu_p\mu_{p+q}(\mu_p + \mu_{p+q})}. \tag{B.16}$$

The small and large q behaviors of this function are:

$$\chi_1 \approx \frac{q^2}{u}\left[\frac{1}{3\pi} + \mathcal{O}\left(\frac{q^2}{mu}\right)\right],$$
$$\chi_1 \approx m\left[\frac{\ln 2}{\pi} + \mathcal{O}\left(\frac{mu}{q^2}\right)\right]. \tag{B.17}$$

For $u = 0$, the integral can be performed analytically for any q. For this it is particularly convenient to use Elliptic coordinates: $p_x = \frac{q}{2}(\cosh\mu\cos\nu - 1)$, $p_y = \frac{q}{2}\sinh\mu\sin\nu$, $\nu \in [-\pi, \pi[$, $\mu \in [0, \infty)$. The value of the density response is:

$$\chi_1(q) = m\frac{\ln 2}{\pi},\ \forall q. \tag{B.18}$$

The result above is remarkable. A convetional parabolic 2DEG has a static reponse of the form:

$$\chi_{2DEG}(q) = \frac{m}{2\pi}\left[1 - \theta(q - 2k_F)\frac{\sqrt{q^2 - 4k_F^2}}{q}\right]. \tag{B.19}$$

Hence, short-range components of the interaction $r \ll k_F^{-1}$, remain unscreened. In contrast in bilayer graphene the vanishing gap between valence and conduction band produces a density response function that is independet of wavevector throughout the range of applicability of the two-band model $q \ll t/v$.

B.4 Small q behavior: two-band model with magnetic field

In the presence of a magnetic field the two band model Hamiltonian is:

$$H_K^{2b} \doteq \begin{pmatrix} u/2 & -\omega_0\sqrt{n(n-1)} \\ -\omega_0\sqrt{n(n-1)} & -u/2 \end{pmatrix}, \tag{B.20}$$

where the matrix has the first column associated with state $|n, A\rangle$ and the second with $|n-2, B'\rangle$. For valley K' the first column associated with state $|n, B'\rangle$ and the second with $|n-2, A\rangle$, and $u \to -u$.

The eigenfunctions and energies of the neutral Landau level are:

$$H_K^{2b}|0, A\rangle = u/2|0, A\rangle,\ H_K^{2b}|1, A\rangle = u/2|1, A\rangle, \tag{B.21}$$

The energies of the negative and positive energy Landau levels for $n \geq 2$ are:

$$E_n^{\pm} = \pm\mu_n,\ \mu_n = \sqrt{(u/2)^2 + \omega_0^2\ n(n-1)}, \tag{B.22}$$

The eigen-states are:

$$\phi_n^+ = \begin{pmatrix} \cos(\theta_n/2) \\ -\sin(\theta_n/2) \end{pmatrix},\ \phi_n^- = \begin{pmatrix} \sin(\theta_n/2) \\ \cos(\theta_n/2) \end{pmatrix}, \tag{B.23}$$

with

$$\cos\theta_n = \frac{u/2}{\mu_n},\ \sin\theta_n = \frac{\omega_0\sqrt{n(n-1)}}{\mu_n}. \tag{B.24}$$

The states at valley K' can be obtained from formulae above by replacing $u \to -u$.

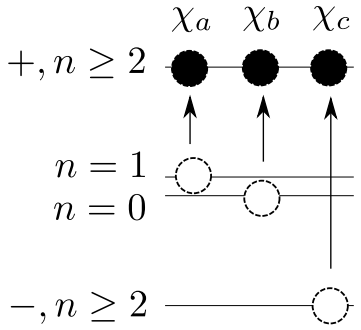

Figure B.2: Particle hole excitations contributing to screening in the two-band model with a magnetic field.

Equation (B.1) in the presence of the magnetic field reduces to:

$$\chi_q = \frac{1}{\pi l^2} \sum_{ab} \frac{|\langle a|e^{iq\cdot\hat{z}\times\pi}|b\rangle|^2}{E_a - E_b} n_b(1 - n_a), \tag{B.25}$$

where a and b are the single particle eigenstates just described.

The small q behavior of the screening function will depend on which cyclotron states are filled in the neutral Landau level. Let us consider in detail the case in which the neutral Landau level is completely filled. We will later relate the results at different fillings to these.

Figure B.2 illustrates three kinds of particle-hole excitations whose explicit forms are:

$$\chi_a(q,u) = \frac{1}{2\pi l^2} \sum_{n\geq 2} \frac{\mu_n + u/2}{\mu_n(\mu_n - u/2)} |F_{n1}(q)|^2, \tag{B.26}$$

$$\chi_b(q,u) = \frac{1}{2\pi l^2} \sum_{n\geq 2} \frac{\mu_n + u/2}{\mu_n(\mu_n - u/2)} |F_{n0}(q)|^2, \tag{B.27}$$

$$\chi_c(q,u) = \frac{1}{4\pi l^2}\sum_{n,n'\geq 2}\left[\frac{(\mu_{n'}+u/2)(\mu_n-u/2)|F_{n'n}|^2+(\mu_{n'}-u/2)(\mu_n+u/2)|F_{n'-2,n-2}|^2}{\mu_n\mu_{n'}(\mu_n+\mu_{n'})}\right.$$
$$\left.-\frac{2\omega_0^2\sqrt{n(n-1)n'(n'-1)}|F_{n',n}||F_{n'-2,n-2}|}{\mu_n\mu_{n'}(\mu_n+\mu_{n'})}\right], \tag{B.28}$$

where $|F_{n'n}(q)|$ are the usual parabolic band form factors as defined in Eq. C(21) in Ref. [67]. χ_c is an even function: $\chi_c(q,u) = \chi_c(q,-u)$.

For χ_a and χ_b the small q behavior is:

$$\begin{aligned}
\chi_a &\approx \frac{q^2}{2\pi}\frac{\mu_2+u/2}{\mu_2(\mu_2-u/2)}+\mathcal{O}(q^4),\\
\chi_b &\approx \mathcal{O}(q^4),\\
\chi_c &\approx \frac{q^2}{2\pi}\sum_{n\geq 2}\frac{n[\mu_{n+1}\mu_n-(u/2)^2-\omega_0^2(n^2-1)]}{\mu_n\mu_{n+1}(\mu_n+\mu_{n+1})}+\mathcal{O}(q^4).
\end{aligned} \tag{B.29}$$

Let us label the coefficient of the q^2 term in χ_a as:

$$\gamma_a(u) \equiv \frac{\mu_2+u/2}{\mu_2(\mu_2-u/2)},\ \chi_a \approx \frac{q^2\gamma_a}{2\pi}. \tag{B.30}$$

The coefficient of the q^2 term in χ_c can be very well approximated by the following form:

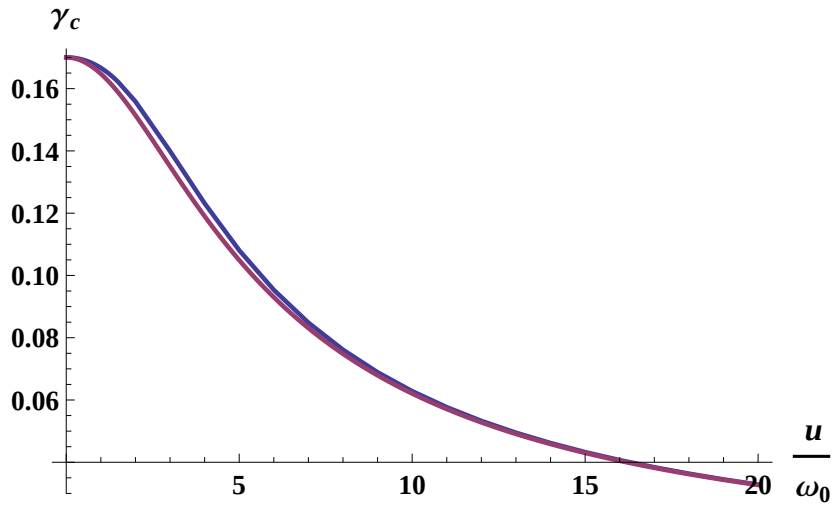

Figure B.3: Coefficient γ_c in the small-q expansion: $\chi_c = \frac{\gamma_c q^2}{2\pi\omega_0}$. The blue curve is the exact value and the purple is the approximation described in Eq. (B.31)

$$\gamma_c(u) \equiv \sum_{n\geq 2} \frac{n[\mu_{n+1}\mu_n - (u/2)^2 - \omega_0^2(n^2-1)]}{\mu_n\mu_{n+1}(\mu_n+\mu_{n+1})} \approx \frac{1}{\sqrt{(a\omega_0)^2+(bu)^2}},\ a \approx 5.881,\ b = \frac{3}{2}. \tag{B.31}$$

where a and b are obtained from the $u \to 0$ and $\omega_0 \to 0$ limits of the infinite sum in question. Figure B.3 illustrates this behavior.

Another class of particle-hole excitations that are available at odd integer fillings are those from $n = 0$ to $n = 1$. In the four-band model of Eq. (B.3) $n = 0$ and $n = 1$ are degenerate and hence, these transitions would have a zero energy. However once the particle-hole symmetry breaking terms are included these states are split by the energy ω_1 as described in Eq. (4.62). These transitions will produce a contribution to the density susceptibility of

the form:

$$\chi_d = \frac{1}{\pi l^2}\frac{|F_{10}(q)|^2}{\omega_1} \approx \frac{q^2}{2\pi\omega_1} + \mathcal{O}(q^4) \tag{B.32}$$

We are now in a position to obtain the screening function for any filling factor of the neutral Landau level. Because the interactions do not flip spin or valleys the total density susceptibility are additive:

$$\chi = \sum_{\sigma,v} \chi_{\sigma v} \tag{B.33}$$

where σ runs over spins and $v = K, K'$. The susceptibilities at different fillings can be related to the functions $\chi_a, \chi_b, \chi_c, \chi_d$ discussed above as follows:

$$\begin{aligned}
\chi^{-1}_{\sigma,K}(q,u) &= \chi_a(q,-u) + \chi_b(q,-u) + \chi_c(q,u) \\
\chi^{0}_{\sigma,K}(q,u) &= \chi_a(q,-u) + \chi_b(q,u) + \chi_c(q,u) + \chi_d(q,u) \\
\chi^{1}_{\sigma,K}(q,u) &= \chi_a(q,u) + \chi_b(q,u) + \chi_c(q,u)
\end{aligned} \tag{B.34}$$

Where the superscripts $-1, 0, 1$ denote the filling of the corresponding spin-valley flavor, namely -1 stands for $n = 0$ and $n = 1$ empty, 0 stands for $n = 0$ occupied and $n = 1$ empty, and 1 stands for $n = 0$ and $n = 1$ occupied. The susceptibilities for valley K' can be obtained from those above by changing $u \to -u$ in the right-hand-side of the equations. Figure B.4 illustrates the particle-hole transitions and the different contributions to the formulae (B.34).

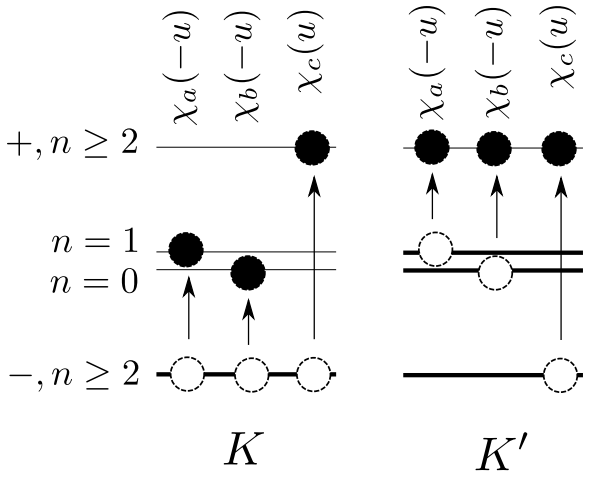

Figure B.4: Left: particle hole transitions contributing to screening to valley K when $n = 0$ and $n = 1$ are empty. Left: particle hole transitions contributing to screening to valley K' when $n = 0$ and $n = 1$ are full.

B.5 Closed approximate forms for all q

For the four-band model we want an expression that reduces to $\frac{t \ln 2}{2\pi v^2}$ for $q \ll t/v$, and asymptotes to $\frac{q}{8v}$ for $q \gg t/v$. A natural choice for a function that interpolates between such asymptotic behavior is:

$$[\chi_{4b}(q;\eta)]^\eta = \left(\frac{q}{8v}\right)^\eta + \left(\frac{t \ln 2}{2\pi v^2}\right)^\eta, \tag{B.35}$$

where η can be seen as a fitting parameter. Figures B.5 and B.6 illustrate that $\eta = 3$ provides a very good fit.

For the two-band model we want an expression that reduces to $\frac{\gamma q^2}{2\pi}$, for $q \ll \sqrt{m/\gamma} \ll t/v$, and that asymptotes to the χ_{4b} expression for $\sqrt{m/\gamma} \ll q \ll t/v$. This is naturally accomplished by the following function:

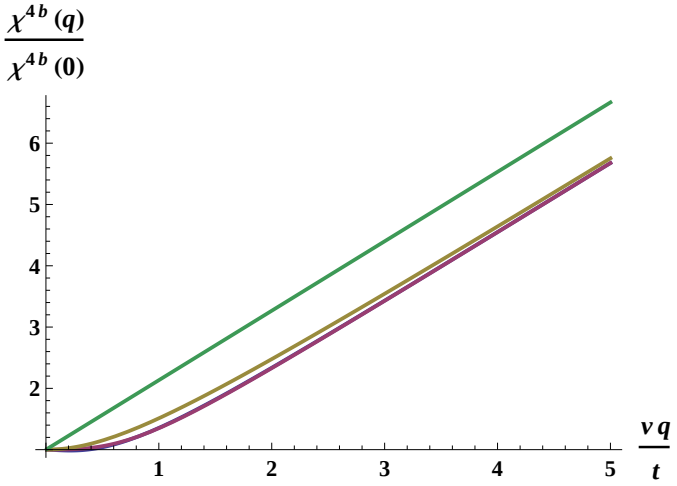

Figure B.5: Screening in four-band model: blue is the sum $\chi_1+\chi_2+\chi_3$, purple, yellow and green are the approximate forms with $\eta = \{3, 2, 1\}$ respectively.

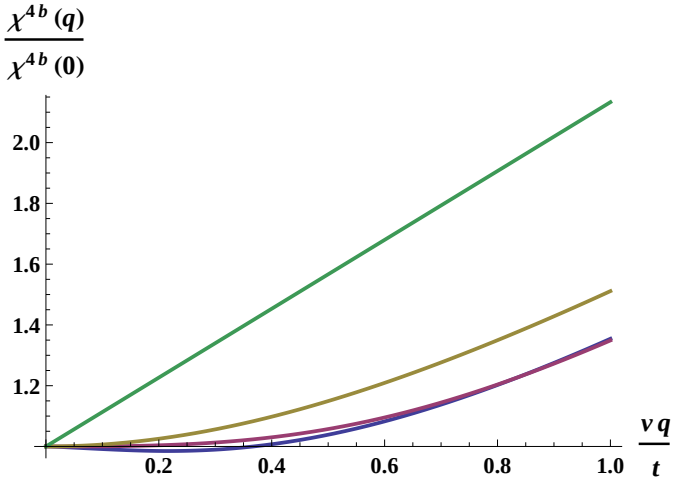

Figure B.6: Screening in four-band model: blue is the sum $\chi_1+\chi_2+\chi_3$, purple, yellow and green are the approximate forms with $\eta = \{3, 2, 1\}$ respectively.

$$\frac{1}{[\chi(q;\xi,\eta)]^{\xi}} = \frac{1}{\left(\frac{\gamma q^2}{2\pi}\right)^{\xi}} + \frac{1}{[\chi_{4b}(q;\eta)]^{\xi}}. \tag{B.36}$$

where ξ is another fitting parameter. $\chi(q;\xi,\eta)$ is an approximate form that describes the screening from long range to short range components all the way down to the order of the lattice constant where the four-band model ceases to be valid. Although it correctly fits the short distance $q \gg t/v$ and the longer range distances $q \ll \sqrt{m/\gamma}$, it does not capture the intermediate oscillatory behavior displayed on scales $q \sim \sqrt{m/\gamma}$, which is particularly pronounced when $u/\omega_0 \gtrsim 1$. This is illustrated in Figs. B.7. This produces an understimation of screening in the intermediate wavelength regime. Hence predictions with the approximate forms will effectively describe slightly stronger interaction strengths. If we happen to find small gaps with these approximate forms, the use of the full screening functions would only produce even smaller ones.

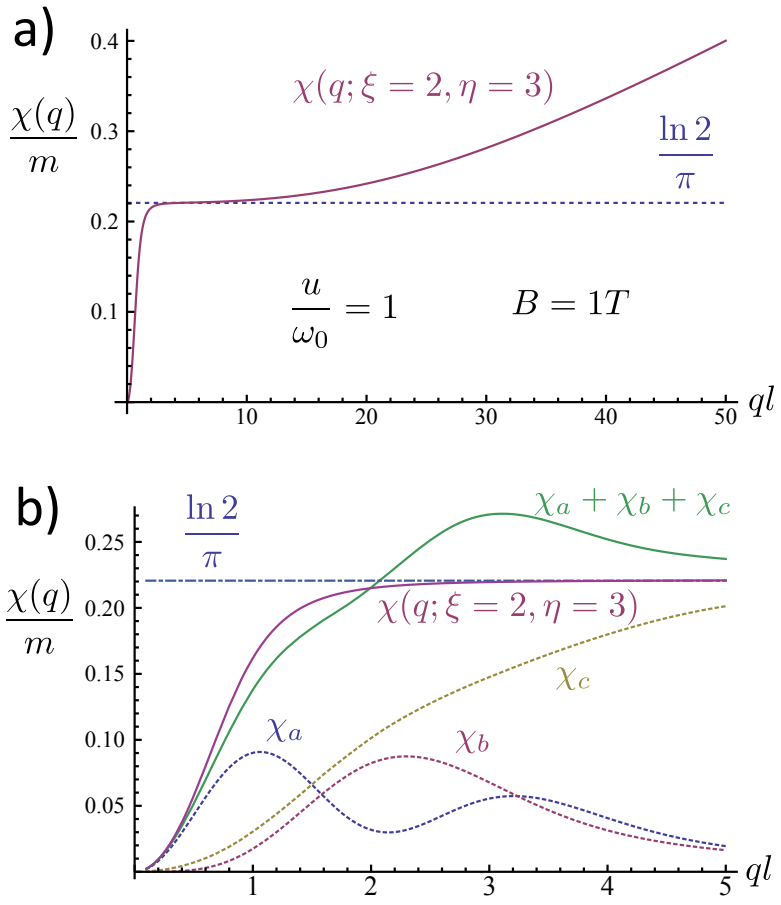

Figure B.7: Static polarizability function of bilayer graphene χ_q. (a) Illustratres clearly the the three regimes of screening. For small q the polarizability vanishes due to the cyclotron and interlayer bias gaps. At intermediate q the function is flat, as one expects from the two band model due to its finite density of states and semimetallic behavior. At large q the function becomes linear in q as one expects for two decoupled graphene monolayers. (b) Detail of the behavior at small q. The green curve is the exact density response function computed within the two-band model in the presence of an interlayer bias and magnetic field, and the purple curve is the approximate expression obtained from Eq. (B.36).

Appendix C

Effective low energy theory in the two-band model

In our discussion of bilayer graphene we have not included the possible short-range interactions allowed by the lattice symmetries which break the SU(4) spin-valley invariance as we did for monolayer graphene. We discuss these terms in this appendix and demonstrate that they do not produce a splitting of the $n = 0$ and $n = 1$ states as the Coulomb interaction with the negative energy sea does.

C.1 Symmetries of Bloch wavefuntions at K, K' points

The lattice of bilayer graphene has a D_{3d} point symmetry. In addition it is invariant under the translations by Bravais lattice vectors $n\mathbf{a}_1 + n'\mathbf{a}_2$. At neutrality there are *four* degenerate eigenstates which are four Bloch wavefunctions that can be denoted by $u_{AK}(r), u_{\tilde{B}K}(r), u_{AK'}(r), u_{\tilde{B}K'}(r)$. This eigenstates must form a "multiplet" of all the symmetries of the Hamiltonian, namely the action of the symmetry operators acting on any of these wavefunctions is closed within the subspace spanned by the wavefunctions themselves.

Following Ref. [45] we write the column vector

$$u = (u_{AK}(r), u_{\tilde{B}K}(r), u_{\tilde{B}K'}(r), -u_{AK'}(r))^{\mathrm{T}}$$
$$\equiv (u_{\bar{A}K}(r), u_{\bar{B}K}(r), u_{\bar{A}K'}(r), u_{\bar{B}K'}(r))^{\mathrm{T}}. \quad \text{(C.1)}$$

Let us denote the Pauli matrices in valley as ρ and those in the $\bar{A}\bar{B}$ indices as τ. Then the D_{3d} is composed of $2\pi/3$ rotations around the z-axis centered on any carbon atom, denoted by $\hat{C}_3$ which transforms the Bloch wavefunctions as [3, 7, 45]:

$$\hat{C}_3 u = e^{i\frac{2\pi}{3}\tau_z} u. \quad \text{(C.2)}$$

The other operations that belong to the D_{3d} symmetry are a reflection about the y-axis of Fig.1 in Ref [45], labeled $\hat{R}_h$, and a reflexion about the x-axis composed by an inversion about the plane that swaps the top and bottom layers, labeled $\hat{R}_v$. Their action on Bloch wavefunctions is,

$$\hat{R}_h u = \tau_y \rho_y u, \quad \text{(C.3)}$$
$$\hat{R}_v u = \tau_x \rho_z u, \quad \text{(C.4)}$$

the two operations correspond simply to swaping the valleys and swaping the sublattices respectively. Finally the translations act as,

$$T_{a_1} u = e^{iK\cdot a_1 \rho_z} u = e^{i\frac{2\pi}{3}\rho_z} u, \quad \text{(C.5)}$$

C.2 Low energy theory of bilayer graphene

A continuous theory can be constructed by writing all short range interactions that are allowed by the symmetried of the lattice. In the spirit of $k \cdot p$ we expand the low energy single-particle states using as basis the Bloch wavefunctions of the high-symmetry points:

$$u_k(r) = \frac{e^{ik\cdot r}}{\sqrt{A}} \sum_{v,l} c_{vl}(k) u_{vl}(r), \tag{C.6}$$

where $v = K, K'$ and $l = \bar{A}, \bar{B}$. The coefficients $c_{vl}(k)$ are the components of the spinors in the low energy theory.

Let us now consider the most general form of sort-ranged interactions that are consistent with the symmetries of the Lattice. The discrete rotational symmetry $\hat{C}_3$ implies sublattice conservation (in the bar indices basis but not the original one), the discrete translational symmetry T_{a_1} implies valley conservation, and the mirror symmetries R_h and R_v imply invariance under swapping $K \leftrightarrow K'$, and $\bar{A} \leftrightarrow \bar{B}$ respectively. These constraints allow for *nine* types of short ranged interaction, one of which is the SU(4) valley/subalttice independent delta function, and the other *eight* can be separated into two classes: *three* "g_z-type" interactions, which differentiate intra/inter valley/sublattice interactions but don't flip these degrees of freedom, and five "$g_\perp$-type" interactions that produce flips of valley/sublattice while conserving the total valley/sublattice numbers.

Any of these interactions can be written in first quantization in the form

$$V_{12} = \hat{v}(v_1, l_1; v_2, l_2)\delta(r_1 - r_2), \tag{C.7}$$

where $\hat{v}(v_1, l_1; v_2, l_2)$ is a two-body matrix acting on valley and sublattice degrees of freedom. The three "g_z-type" interactions have the following $v's$:

$$\hat{v}_{0z} = g_{0z}\tau_{z1}\tau_{z2}, \tag{C.8}$$

$$\hat{v}_{z0} = g_{z0}\rho_{z1}\rho_{z2}, \tag{C.9}$$

$$\hat{v}_{zz} = g_{zz}\rho_{z1}\tau_{z1}\tau_{z2}\rho_{z2}, \tag{C.10}$$

The five "$g_\perp$-type" interactions have the following $v's$:

$$\hat{v}_{0\perp} = g_{0\perp}\tau_{\perp 1} \cdot \tau_{\perp 2}, \tag{C.11}$$

$$\hat{v}_{\perp 0} = g_{\perp 0}\rho_{\perp 1} \cdot \rho_{\perp 2}, \tag{C.12}$$

$$\hat{v}_{z\perp} = g_{z\perp}\tau_{\perp 1} \cdot \tau_{\perp 2}\rho_{z1}\rho_{z2}, \tag{C.13}$$

$$\hat{v}_{\perp z} = g_{\perp z}\rho_{\perp 1} \cdot \rho_{\perp 2}\tau_{z1}\tau_{z2}, \tag{C.14}$$

$$\hat{v}_{\perp\perp} = g_{\perp\perp}\rho_{\perp 1} \cdot \rho_{\perp 2}\tau_{\perp 1} \cdot \tau_{\perp 2}, \tag{C.15}$$

C.3 Projection into neutral Landau level and exchange interaction with negative energy sea

Once projected into the zero energy Landau level these interactions will get regrouped into a few terms. The usual g_z and $g_\perp$ we have been considering in monolayer graphene will appear and in particular: $g_z = g_{z0} + g_{zz}$, $g_\perp = g_{\perp 0} + g_{\perp z}$, as pointed out in Refs. [36, 38]. One might expect these interactions to contribute to the exchange potential with the negative energy sea, much like the Coulomb potential discussed in the main text.

However, as we will demonstrate next, because these interactions are all short range it turns out that they will not produce a splitting between the $n = 0$ and $n = 1$ like the Coulomb interaction does. Let us label the single particle eigenstates by three labels $|v, n, m\rangle$, where $v = \{K, K'\}$, $n = \{-\infty, ..., -2, 0, 1, 2, ..., \infty\}$ labels the Landau levels of bilayer, and $n = 0$, $n = 1$ form the neutral Landau level, and m is the intra-Landau level guiding center number. Another complete single particle basis is $|v, l, r\rangle$ where $l = \{\bar{A}, \bar{B}\}$, and $|r\rangle$ is a position eigenstate.

Consider for the moment a more general symmetry breaking interaction between particles i and j of the form:

$$ {}_i\langle v_1 l_1 r|_j\langle v_2 l_2 r'|v_{ij}|v_3 l_3 r'\rangle_j|v_4 l_4 r\rangle_i = \tag{C.16} $$

$$ V(v_1 l_1, v_2 l_2; v_3 l_3, v_4 l_4)\ v(r - r') \tag{C.17} $$

The exchange potential generated by the negative energy sea level $n_2 \leq -2$, on the states in the $n = 0$, $n = 1$ levels can be written in general as,

$$\hat{X}_{v_2 n_2} = -\sum_{l_2, l_2'} \int dr dr' V(vl, v_2 l_2; v'l', v_2 l_2') v(r - r') \tag{C.18}$$

$$\times P_{v_2 n_2}(l_2 r, l_2' r') |vlr\rangle\langle v'l'r'| \tag{C.19}$$

Where P_{v_2, n_2} is the density matrix of the occupied level:

$$P_{v_2 n_2}(l_2 r, l_2' r') = \langle v_2 l' r' | \Big(\sum_{m_2} |v_2, n_2, m_2\rangle\langle v_2, n_2, m_2| \Big) |v_2 l_2' r'\rangle. \tag{C.20}$$

Invariance under magnetic translations implies that the density matrix at coincident points $r = r'$ is independent of position $P_{v_2 n_2}(l_2 r, l_2' r) = P_{v_2 n_2}(l_2, l_2')$. Thus when the interaction is a delta function, $v \to \delta$, the exchange becomes independent of position,

$$\hat{X}_{v_2 n_2} = -\sum_{l_2, l_2'} V(vl, v_2 l_2; v'l', v_2 l_2') P_{v_2 n_2}(l_2, l_2') |vl\rangle\langle v'l'|, \tag{C.21}$$

thus short-range interactions are unable to produce a splitting of the orbital degree of freedom of the neutral Landau level.

Appendix D

Haldane pseudo-potentials for $n = 0$ and $n = 1$ cyclotron pseudo-spin

Consider the basis of two-body states for spin-1/2 particles projected into the $n = 0$ LL

$$\Psi^{1,-1}_{M,m} = \frac{B^{\dagger M} b^{\dagger m}}{\sqrt{M!m!}} |0\downarrow, 0\downarrow\rangle \tag{D.1}$$

$$\Psi^{1,0}_{M,m} = \frac{B^{\dagger M} b^{\dagger m}}{\sqrt{M!m!}} \frac{\sigma_1^+ + \sigma_2^+}{\sqrt{2}} |0\downarrow, 0\downarrow\rangle \tag{D.2}$$

$$\Psi^{1,1}_{M,m} = \frac{B^{\dagger M} b^{\dagger m}}{\sqrt{M!m!}} \sigma_1^+ \sigma_2^+ |0\downarrow, 0\downarrow\rangle \tag{D.3}$$

$$\Psi^{0,0}_{M,m} = \frac{B^{\dagger M} b^{\dagger m}}{\sqrt{M!m!}} \frac{\sigma_1^+ - \sigma_2^+}{\sqrt{2}} |0\downarrow, 0\downarrow\rangle \tag{D.4}$$

Where $\Psi^{S,S_z}_{M,m}$ is a state with spin of magnitude S, projection S_z, center of mass angular momentum M and relative angular momentum m, and $\sigma^+ = (\sigma_x + i\sigma_y)/2$. Thus for spinless particles, by imagining the cyclotron quantum number as a pseudo-spin, we can label the states of two particles constrained to occupy the $n = 0$ and $n = 1$ LL as,

$$\Psi^{1,-1}_{M,m} = \frac{B^{\dagger M} b^{\dagger m}}{\sqrt{M!m!}} |00,00\rangle \tag{D.5}$$

$$\Psi^{1,0}_{M,m} = \frac{B^{\dagger M} b^{\dagger m}}{\sqrt{M!m!}} \frac{a_1^\dagger + a_2^\dagger}{\sqrt{2}} |00,00\rangle \tag{D.6}$$

$$\Psi^{1,1}_{M,m} = \frac{B^{\dagger M} b^{\dagger m}}{\sqrt{M!m!}} a_1^\dagger a_2^\dagger |00,00\rangle \tag{D.7}$$

$$\Psi^{0,0}_{M,m} = \frac{B^{\dagger M} b^{\dagger m}}{\sqrt{M!m!}} \frac{a_1^\dagger - a_2^\dagger}{\sqrt{2}} |00,00\rangle \tag{D.8}$$

A convenient basis for finding the matrix elements of the Coulomb interaction is the center of mass and relative coordinates basis,

$$\Phi_{M,m,N,n} = \frac{B^{\dagger M} b^{\dagger m}}{\sqrt{M!m!}} \frac{A^{\dagger N} a^{\dagger n}}{\sqrt{N!n!}} |00,00\rangle \tag{D.9}$$

where $A = (a_1 + a_2)/\sqrt{2}$, $a = (a_1 - a_2)/\sqrt{2}$. In this basis the interaction is almost diagonal (only three indices specify non-vanishing matrix elements),

$$\langle \Phi_{M',m',N',n'} | v(r_1 - r_2) | \Phi_{M,m,N,n} \rangle = \tag{D.10}$$

$$\delta_{M'N',MN} \delta_{m'-n',m-n} v(n'm', nm) \tag{D.11}$$

For an analytic expression of $v(n'm', nm)$ see Eq.(C6) in [67]. The pseudo-spin basis of Eqs. (D.5)-(D.8), relates to the latter basis as follows,

$$\Psi^{0,0}_{M,m} = \Phi_{M,m,0,1}, \tag{D.12}$$

$$\Psi^{1,-1}_{M,m} = \Phi_{M,m,0,0}, \tag{D.13}$$

$$\Psi^{1,0}_{M,m} = \Phi_{M,m,1,0}, \tag{D.14}$$

$$\Psi^{1,1}_{M,m} = \frac{1}{\sqrt{2}}(\Phi_{M,m,2,0} - \Phi_{M,m,0,2}), \tag{D.15}$$

The interaction can be decomposed into Haldane pseudo-potential matrices. The states $\Psi^{1,0}_{M,m}$ are completely decoupled from the remainder because they are the only ones with center of mass kinetic energy $N = 1$. Since the remaining states all have projection into states with center of mass kinetic energy $N = 0$, there will be off-diagonal matrix elements of the interaction between them. Thus the interaction can be separated into two pieces, one piece is diagonal and projects into the $N = 1$ states:

$$v^1 = \sum_m v^1_m |\Psi^{1,0}_{M,m}\rangle\langle\Psi^{1,0}_{M,m}| \tag{D.16}$$

and the other piece has the structure of 3×3 matrices and projects into the remaining states with $N = 0$ components,

$$v^0 = \sum_m \begin{pmatrix} |\Psi^{1,1}_{M,m+1}\rangle & |\Psi^{0,0}_{M,m}\rangle & |\Psi^{1,-1}_{M,m-1}\rangle \\ -- & -- & -- \\ -- & -- & -- \end{pmatrix} \tag{D.17}$$

The notation above simply specifies the states labeling the columns of the matrix (same order for the rows). For $m = 0$ the last colum/row

is understood to be absent (the matrix is 2×2). The total interaction is $v = v^0 + v^1$. For fermions (bosons) m in Eq. (D.16) is restricted to be odd (even), and in Eq. (D.17) to be even (odd).

Let me now discuss the interpretation of the different states, compare them with the spinful case and list some of the relevant pseudopotentials (restricted to fermions).

For $m = 0$ in Eq. (D.17) we have 2×2 matrix with states: $\Psi^{1,1}_{M,1}$ ($\nu \sim 1$ polarized into the $n = 1$ LL) and $\Psi^{0,0}_{M,0}$ ($\nu \sim 2$ singlet of $n = 0$ and $n = 1$ LL), with the following pseudo-potentials,

$$v^0_0 = \begin{pmatrix} 0.42 & -0.11 \\ -0.11 & 0.44 \end{pmatrix} \xrightarrow{SU(2)} \begin{pmatrix} 0.44 & 0 \\ 0 & 0.87 \end{pmatrix} \tag{D.18}$$

The symbol $\xrightarrow{SU(2)}$ indicates the values the pseudopotentials have for the conventional real spin case, listed for comparison.

For $m = 1$ from v^1 we have the state $\Psi^{1,0}_{M,1}$ ($\nu \sim 1$ polarized along the equator of the $n = 0/n = 1$ pseudo-spin Bloch sphere, i.e. nematic-like)

$$v^1_1 = 0.44 \xrightarrow{SU(2)} 0.44 \tag{D.19}$$

The fact that the pseudo-potential coincides with that of the usual spin case is no accident, and it can be verified that all the Haldane pseudopotentials associated with v^1 are identical to those of the conventional $n = 0$ LL.

For $m = 2$ in Eq. (D.17) we have states: $\Psi^{1,1}_{M,3}$ ($\nu \sim 1/3$ polarized into the $n = 1$ LL), $\Psi^{0,0}_{M,2}$ ($\nu \sim 2/5$ singlet of $n = 0$ and $n = 1$ LL, i.e. a pseudo-spin Halperin state or un-projected composite fermion state at 2/5), and $\Psi^{1,-1}_{M,1}$ ($\nu \sim 1$ polarized into $n = 0$ LL) with the following pseudo-potentials,

$$v_2^0 = \begin{pmatrix} 0.32 & -0.12 & -0.07 \\ -0.12 & 0.39 & -0.11 \\ -0.07 & -0.11 & 0.44 \end{pmatrix} \xrightarrow{SU(2)} \begin{pmatrix} 0.28 & 0 & 0 \\ 0 & 0.33 & 0 \\ 0 & 0 & 0.44 \end{pmatrix} \tag{D.20}$$

For $m = 3$ in Eq. (D.16) we have the state $\Psi^{1,0}_{M,3}$ ($\nu \sim 1/3$ polarized nematic state) with the following pseudo-potential,

$$v_3^1 = 0.28 \xrightarrow{SU(2)} 0.28 \tag{D.21}$$

For $m = 4$ in Eq. (D.17) we have states: $\Psi^{1,1}_{M,5}$ ($\nu \sim 1/5$ polarized into the $n = 1$ LL), $\Psi^{0,0}_{M,4}$ ($\nu \sim 2/9$ singlet of $n = 0$ and $n = 1$ LL), and $\Psi^{1,-1}_{M,3}$ ($\nu \sim 1/3$ polarized into $n = 0$ LL, i.e the conventional Laughlin state) with the following pseudo-potentials,

$$v_2^0 = \begin{pmatrix} 0.22 & -0.06 & -0.02 \\ -0.06 & 0.26 & -0.05 \\ -0.02 & -0.05 & 0.28 \end{pmatrix} \xrightarrow{SU(2)} \begin{pmatrix} 0.22 & 0 & 0 \\ 0 & 0.24 & 0 \\ 0 & 0 & 0.28 \end{pmatrix} \tag{D.22}$$

The chemical potential jump at 1/3 for spinless electrons is controlled by the difference between V_3 (0.28) and V_1 (0.44). For spinful electrons the jump is controlled by the difference between V_3 (0.28) and V_2 (0.33), and hence

it is substantially reduced. A more elaborate guess for chemical potential jumps for $n = 0/n = 1$ pseudo-spins would require some correction for the fact that the wavefunctions made from $n = 0$ and $n = 1$ LL's have slighlity different sizes (i.e. different densities), however ignoring this for the time being, and neglecting the off-diagonal Haldane pseudopotentials, we can imagine the chemical potential jump at 1/3 to be roughly controlled by the difference of the expectation values of Coulomb for $\Psi^{1,-1}_{M,3}$ (0.28) and $\Psi^{0,0}_{M,2}$ (0.39). This reduced jump, which is comparable to the conventional case of spinful electrons could be important in understanding the missing fractions in Ref. [40].

Bibliography

[1] D. A. Abanin, S. A. Parameswaran, and S. L. Sondhi. Charge $2e$ skyrmions in bilayer graphene. *Phys. Rev. Lett.*, 076802, **103** (2009).

[2] D. A. Abanin, B. E. Feldman, A. Yacoby, and B. I. Halperin. Fractional and integer quantum hall effects in the zeroth landau level in graphene. *Phys. Rev. B*, 115407, **88** (2013).

[3] I. L. Aleiner, D. E. Kharzeev, and A. M. Tsvelik. Spontaneous symmetry breaking in graphene subjected to an in-plane magnetic field. *Phys. Rev. B*, 195415, **76** (2007).

[4] J. Alicea and M. P. A. Fisher. Graphene integer quantum hall effect in the ferromagnetic and paramagnetic regimes. *Phys. Rev. B*, 075422, **74** (2006).

[5] W. Bao, Z. Zhao, H. Zhang, G. Liu, P. Kratz, L. Jing, J. Velasco, D. Smirnov, and C. N. Lau. Magnetoconductance oscillations and evidence for fractional quantum hall states in suspended bilayer and trilayer graphene. *Phys. Rev. Lett.*, 246601, **105** (2010).

[6] Y. Barlas, R. Côté, K. Nomura, and A. H. MacDonald. Intra-landau-level cyclotron resonance in bilayer graphene. *Phys. Rev. Lett.*, 097601, **88** (2008).

[7] D. M. Basko. Theory of resonant multiphonon raman scattering in graphene. *Phys. Rev. B*, 125418, **78** (2008).

[8] W. Bishara and C. Nayak. Effect of landau level mixing on the effective interaction between electrons in the fractional quantum hall regime. *Phys. Rev. B*, 121302, **80** (2009).

[9] K. I. Bolotin, F. Ghahari, M. D. Shulman, H. L. Stormer, and P. Kim. Observation of the fractional quantum hall effect in graphene. *Nature*, 196, **462**, (2009).

[10] A. H. Castro Neto, F. Guinea, N. M. R. Peres, K. S. Novoselov, and A. K. Geim. The electronic properties of graphene. *Rev. Mod. Phys.*, 109, **81** (2009).

[11] T. Chakraborty, P. Pietiläinen, and F. C. Zhang. Elementary excitations in the fractional quantum hall effect and the spin-reversed quasiparticles. *Phys. Rev. Lett.*, 130, **57** (1986).

[12] S. C. Davenport. *Multicomponent Fractional Quantum Hall Effects*. PhD thesis, University of Oxford, 2013.

[13] S. C. Davenport and S. H. Simon. Spinful composite fermions in a negative effective field. *Phys. Rev. B*, 245303, **85** (2012).

[14] C. R. Dean, A. F. Young, P. Cadden-Zimansky, L. Wang, H. Ren, K. Watanabe, T. Taniguchi, P. Kim, J. Hone, and K. L. Shepard. Multicomponent fractional quantum hall effect in graphene. *Nature Physics*, 693, **7** (2011).

[15] A. F. Dethlefsen, R. J. Haug, K.l Výborný, O. Certík, and A. Wójs. Transport gap in a $\nu = 1/3$ quantum hall system: A probe for skyrmions. *Phys. Rev. B*, 195324, **74** (2006).

[16] R. R. Du, A. S. Yeh, H. L. Stormer, D. C. Tsui, L. N. Pfeiffer, and K. W. West. Fractional quantum hall effect around $\nu = 3/2$: Composite fermions with a spin. *Phys. Rev. Lett.*, 3926, **75** (1995).

[17] X. Du, I. Skachko, F. Duerr, A. Luican, and E. Y. Andrei. Fractional quantum hall effect and insulating phase of dirac electrons in graphene. *Nature*, 192, **462** (2009).

[18] J. P. Eisenstein and A. H. MacDonald. Bose-einstein condensation of excitons in bilayer electron systems. *Nature*, 691, **432** (2004).

[19] G. Fano, F. Ortolani, and E. Colombo. Configuration-interaction calculations on the fractional quantum hall effect. *Phys. Rev. B*, 2670, **34** (1986).

[20] B. E. Feldman, B. Krauss, J. H. Smet, and A. Yacoby. Unconventional sequence of fractional quantum hall states in suspended graphene. *Science*, 1196, **337** (2012).

[21] B. E. Feldman, A. J. Levin, B. Krauss, D. A. Abanin, B. I. Halperin, J. H. Smet, and A. Yacoby. Fractional quantum hall phase transitions and four-flux states in graphene. *Phys. Rev. Lett.*, 076802, **111** (2013).

[22] F. Ghahari, Y. Zhao, P. C.-Zimansky, K. Bolotin, and P. Kim. Measurement of the $\nu = 1/3$ fractional quantum hall energy gap in suspended graphene. *Phys. Rev. Lett.*, 046801, **106** (2011).

[23] S. M. Girvin. Anomalous quantum hall effect and two-dimensional classical plasmas: Analytic approximations for correlation functions and ground-state energies. *Phys. Rev. B*, 558, **30** (1984).

[24] S. M. Girvin, A. H. MacDonald, and P. M. Platzman. Magneto-roton theory of collective excitations in the fractional quantum hall effect. *Phys. Rev. B*, 2481, **33** (1986).

[25] E. V. Gorbar, V. P. Gusynin, and V. A. Miransky. Energy gaps at neutrality point in bilayer graphene in a magnetic field. *JETP letters*, 314, **91** (2010).

[26] F. D. M. Haldane. Fractional quantization of the hall effect: A hierarchy of incompressible quantum fluid states. *Phys. Rev. Lett.*, 605, **51** (1983).

[27] F. D. M. Haldane. *The quantum Hall effect*, volume 1. Springer-Verlag New York, 1987.

[28] F. D. M. Haldane and E. H. Rezayi. Finite-size studies of the incompressible state of the fractionally quantized hall effect and its excitations. *Phys. Rev. Lett.*, 237, **54** (1985).

[29] B. I. Halperin. Theory of the quantized hall conductance. *Helvetica Physica Acta*, 75, **56** (1983).

[30] R. Hegde. *Interactions and Quantum Hall Effects in Graphene Multilayers*. PhD thesis, University of Texas at Austin, 2013.

[31] I. F. Herbut. Theory of integer quantum hall effect in graphene. *Phys. Rev. B*, 165411, **75** (2007).

[32] B. Hunt, J. D. Sanchez-Yamagishi, A. F. Young, M. Yankowitz, B. J. LeRoy, K. Watanabe, T. Taniguchi, P. Moon, M. Koshino, P. Jarillo-Herrero and R. C. Ashoori. Massive dirac fermions and hofstadter butterfly in a van der waals heterostructure. *Science*, 1427, **340** (2013).

[33] J. K Jain. *Composite fermions*. Cambridge University Press, 2007.

[34] J. Jung and A. H. MacDonald. Theory of the magnetic-field-induced insulator in neutral graphene sheets. *Phys. Rev. B*, 235417, **80** (2009).

[35] J. Jung and A. H. MacDonald. Accurate tight-binding and continuum models for the π bands of bilayer graphene. *arXiv preprint arXiv:1309.5429*, 2013.

[36] M. Kharitonov. Antiferromagnetic state in bilayer graphene. *Phys. Rev. B*, 195435, **86** (2012).

[37] M. Kharitonov. Edge excitations of the canted antiferromagnetic phase of the $\nu = 0$ quantum hall state in graphene: A simplified analysis. *Phys. Rev. B*, 075450, **86** (2012).

[38] M. Kharitonov. Phase diagram for the $\nu = 0$ quantum hall state in monolayer graphene. *Phys. Rev. B*, 155439, **85** (2012).

[39] D.-K. Ki, V. I. Falko, D. A. Abanin, and A. Morpurgo. Observation of even denominator fractional quantum hall effect in suspended bilayer graphene. *Nano letters*, 2135, **14** (2014).

[40] A. Kou, B. E. Feldman, A. J. Levin, B. I. Halperin, K. Watanabe, T. Taniguchi, and A. Yacoby. Electron-hole asymmetric integer and fractional quantum hall effect in bilayer graphene. *Science*, 55, **345** (2014).

[41] I. V. Kukushkin, K. v. Klitzing, and K. Eberl. Spin polarization of composite fermions: Measurements of the fermi energy. *Phys. Rev. Lett.*, 3665, **82** (1999).

[42] A. B. Kuzmenko, I. Crassee, D. van der Marel, P. Blake, and K. S. Novoselov. Determination of the gate-tunable band gap and tight-binding parameters in bilayer graphene using infrared spectroscopy. *Phys. Rev. B*, 165406, **80** (2009).

[43] R. B. Laughlin. Anomalous quantum hall effect: An incompressible quantum fluid with fractionally charged excitations. *Phys. Rev. Lett.*, 1395, **50** (1983).

[44] K. Lee, B. Fallahazad, J. Xue, D. C. Dillen, K. Kim, T. Taniguchi, K. Watanabe, and E. Tutuc. Chemical potential and quantum hall ferromagnetism in bilayer graphene. *Science*, 58, **345** (2014).

[45] Y. Lemonik, I. Aleiner, and V. I. Fal'ko. Competing nematic, antiferromagnetic, and spin-flux orders in the ground state of bilayer graphene. *Phys. Rev. B*, 245451, **85** (2012).

[46] A. H. MacDonald. Introduction to the Physics of the Quantum Hall Regime. *arXiv preprint arXiv:cond-mat/9410047*, (1994).

[47] A. H. MacDonald, H. A. Fertig, and L. Brey. Skyrmions without sigma models in quantum hall ferromagnets. *Phys. Rev. Lett.*, 2153, **76** (1996).

[48] A. H. MacDonald and J. J. Palacios. Magnons and skyrmions in fractional hall ferromagnets. *Phys. Rev. B*, R10171, **58** (1998).

[49] P. Maher, L. Wang, Y. Gao, C. Forsythe, T. Taniguchi, K. Watanabe, D. Abanin, Z. Papic, P. Cadden-Zimansky, J. Hone, P. Kim, and C. R. Dean. Tunable fractional quantum hall phases in bilayer graphene. *Science*, 61, **345** (2014).

[50] E. McCann and V. I. Fal'ko. Landau-level degeneracy and quantum hall effect in a graphite bilayer. *Phys. Rev. Lett.*, 086805, **96** (2006).

[51] J. W. McClure. Diamagnetism of graphite. *Phys. Rev.*, 666, **104** (1956).

[52] K. Moon, H. Mori, Kun Yang, S. M. Girvin, A. H. MacDonald, L. Zheng, D. Yoshioka, and S.-C. Zhang. Spontaneous interlayer coherence in double-layer quantum hall systems: Charged vortices and kosterlitz-thouless phase transitions. *Phys. Rev. B*, 5138, **51** (1995).

[53] G. Murthy and R. Shankar. Hamiltonian theory of the fractional quantum hall effect: Effect of landau level mixing. *Phys. Rev. B*, 245309, **65** (2002).

[54] C. Nayak, S. H. Simon, A. Stern, M. Freedman, and S. Das Sarma. Non-abelian anyons and topological quantum computation. *Rev. Mod. Phys.*, 1083, **80** (2008).

[55] K. Niemelä and P. Pietiläinen, and T. Chakraborty. Spin transitions in the fractional quantum hall systems. *Physica B: Condensed Matter*, 1716, **284** (2000).

[56] J. Nilsson, A. H. Castro Neto, F. Guinea, and N. M. R. Peres. Electronic properties of bilayer and multilayer graphene. *Phys. Rev. B*, 045405, **78** (2008).

[57] Z. Papic and D. A. Abanin. Topological phases in the zeroth landau level of bilayer graphene. *Phys. Rev. Lett.*, 046602, **112** (2014).

[58] Z. Papic, M. O. Goerbig, and N. Regnault. Atypical fractional quantum hall effect in graphene at filling factor 1/3. *Phys. Rev. Lett.*, 176802, **105** (2010).

[59] M. R. Peterson and C. Nayak. More realistic hamiltonians for the fractional quantum hall regime in gaas and graphene. *Phys. Rev. B*, 245129, **87** (2013).

[60] L. A. Ponomarenko, R. V. Gorbachev, G. L. Yu, D. C. Elias, R. Jalil, A. A. Patel, A. Mishchenko, A. S. Mayorov, C. R. Woods, J. R. Wallbank, M. Mucha-Kruczynski, B. A. Piot, M. Potemski, I. V. Grigorieva, K. S. Novoselov, F. Guinea, V. I. Falko, and A. K. Geim. Cloning of dirac fermions in graphene superlattices. *Nature*, 594, **497** (2013).

[61] E. H. Rezayi. Reversed-spin excitations of the fractionally quantized hall effect from finite-size calculations. *Phys. Rev. B*, 5454, **36** (1987).

[62] K. Shizuya. Renormalization and cyclotron resonance in bilayer graphene with weak electron-hole asymmetry. *Phys. Rev. B*, 075409, **84** (2011).

[63] K. Shizuya. Structure and the lamb-shift-like quantum splitting of the pseudo-zero-mode landau levels in bilayer graphene. *Phys. Rev. B*, 045431, **86** (2012).

[64] S. H. Simon and E. H. Rezayi. Landau level mixing in the perturbative limit. *Phys. Rev. B*, 155426, **87** (2013).

[65] K. Snizhko, V. Cheianov, and S. H. Simon. Importance of interband transitions for the fractional quantum hall effect in bilayer graphene. *Phys. Rev. B*, 201415, **85** (2012).

[66] I. Sodemann and M. M. Fogler. Interaction corrections to the polarization function of graphene. *Phys. Rev. B*, 115408, **86** (2012).

[67] I. Sodemann and A. H. MacDonald. Landau level mixing and the fractional quantum hall effect. *Phys. Rev. B*, 245425, **87** (2013).

[68] I. Sodemann and A. H. MacDonald, Broken SU(4) symmetry and the fractional quantum hall effect in graphene. *Phys. Rev. Lett.*, 126804, **112** (2014).

[69] S. L. Sondhi, A. Karlhede, S. A. Kivelson, and E. H. Rezayi. Skyrmions and the crossover from the integer to fractional quantum hall effect at small zeeman energies. *Phys. Rev. B*, 16419, **47** (1993).

[70] C. Toke and J. K. Jain. Multi-component fractional quantum hall states in graphene: SU(4) versus SU(2). *Journal of Physics: Condensed Matter*, 235601, **24** (2012).

[71] D. C. Tsui, H. L. Stormer, and A. C. Gossard. Two-dimensional magnetotransport in the extreme quantum limit. *Phys. Rev. Lett.*, 1559, **48** (1982).

[72] K. Výborný, A. F. Dethlefsen, R. J. Haug, and A. Wójs. Charge-spin excitations of the ising-type fractional quantum hall ferromagnets. *Phys. Rev. B*, 045407, **80** (2009).

[73] R. Willett, J. P. Eisenstein, H. L. Störmer, D. C. Tsui, A. C. Gossard, and J. H. English. Observation of an even-denominator quantum number in the fractional quantum hall effect. *Phys. Rev. Lett.*, 1776, **59** (1987).

[74] A. Wójs and J. J. Quinn. Spin excitation spectra of integral and fractional quantum hall systems. *Phys. Rev. B*, 045323, **66** (2002).

[75] C. R. Woods, L. Britnell, A. Eckmann, G. L. Yu, R. V. Gorbachev, A. V. Kretinin, J. Park, L. A. Ponomarenko, M. I. Katsnelson, Yu. N. Gornostyrev, Yu. N. Gornostyrev, K. Watanabe, T. Taniguchi, C. Casiraghi, H. J. Gao, A. K. Geim, K. S. Novoselov. Commensurate-incommensurate transition for graphene on hexagonal boron nitride. Nature Physics, 451, **10** (2014).

[76] X. G. Wu, G. Dev, and J. K. Jain. Mixed-spin incompressible states in the fractional quantum hall effect. *Phys. Rev. Lett.*, 153, **71** (1993).

[77] X. C. Xie, Y. Guo, and F. C. Zhang. Fractional quantum hall effect with spin reversal. *Phys. Rev. B*, 3487, **40** (1989).

[78] K. Yang, S. Das Sarma, and A. H. MacDonald. Collective modes and skyrmion excitations in graphene $su(4)$ quantum hall ferromagnets. *Phys. Rev. B*, 075423, **74** (2006).

[79] A. F. Young, J. D. Sanchez-Yamagishi, B. Hunt, S. H. Choi, K. Watanabe, T. Taniguchi, R. C. Ashoori, and P. Jarillo-Herrero. Tunable symmetry breaking and helical edge transport in a graphene quantum spin hall state. *Nature*, 528, **505** (2014).

[80] A. F. Young, C. R. Dean, L. Wang, H. Ren, P. Cadden-Zimansky, K. Watanabe, T. Taniguchi, J. Hone, K. L. Shepard, and P. Kim. Spin and valley quantum hall ferromagnetism in graphene. *Nature Physics*, 550, **8** (2012).

[81] L. M. Zhang, Z. Q. Li, D. N. Basov, M. M. Fogler, Z. Hao, and M. C. Martin. Determination of the electronic structure of bilayer graphene from infrared spectroscopy. *Phys. Rev. B*, 235408, **78** (2008).